Sr ISOTOPE, MAJOR AND TRACE ELEMENTAL MOBILITY OF CENTRAL GANGA ALLUVIAL PLAIN

Ph.D THESIS

by

PRIYANKA SINGH

DEPARTMENT OF EARTH SCIENCES
INDIAN INSTITUTE OF TECHNOLOGY ROORKEE
ROORKEE- 247667, INDIA
APRIL, 2017

Sr ISOTOPE, MAJOR AND TRACE ELEMENTAL MOBILITY OF CENTRAL GANGA ALLUVIAL PLAIN

A THESIS

Submitted in partial fulfilment of the requirements for the award of the degree

of

DOCTOR OF PHILOSOPHY

in

EARTH SCIENCES

by

PRIYANKA SINGH

DEPARTMENT OF EARTH SCIENCES
INDIAN INSTITUTE OF TECHNOLOGY ROORKEE
ROORKEE- 247667, INDIA
APRIL, 2017

©INDIAN INSTITUTE OF TECHNOLOGY ROORKEE, ROORKEE- 2017
ALL RIGHTS RESERVED

INDIAN INSTITUTE OF TECHNOLOGY ROORKEE
ROORKEE

CANDIDATE'S DECLARATION

I hereby certify that the work which is being presented in the thesis entitled "**Sr ISOTOPE, MAJOR AND TRACE ELEMENTAL MOBILITY OF CENTRAL GANGA ALLUVIAL PLAIN**", in partial fulfilment of the requirements for the award of the Degree of Doctor of Philosophy and submitted in the Department of Earth Sciences of the Indian Institute of Technology Roorkee is an authentic record of my own work carried out during a period from July, 2011 to April 2017, under the supervision of Dr. Sandeep Singh, Professor, Department of Earth Sciences, Indian Institute of Technology Roorkee, Roorkee.

The matter presented in the thesis has not been submitted by me for the award of any other degree of this or any other Institution.

(PRIYANKA SINGH)

This is to certify that the above statement made by the candidate is correct to the best of my knowledge.

Dated: _____

(Sandeep Singh)
Supervisor

Abstract

In northern part of Indian sub-continent, Indo-Ganga-Brahmaputra Plain forms the largest alluvial plain in the world which has been formed due to Himalayan orogeny. The sediments deposited in the foreland basin are from the Himalayan as well as from the craton regions. The center part of the Indo-Ganga-Brahmaputra Plain is widely known as the Ganga Alluvial Plain (GAP) which covers an area of about 250,000 km^2 and located between longitudes 77ºE to 88ºE and latitudes 30ºN to 24ºN. The Gomati River (a tributary of the Ganga River) drains the Ganga Alluvial Plain and derives its sediments from weathering of alluvial deposits under monsoon controlled sub-tropical climate. The present study mainly aims at major, trace and rare earth element geochemistry along with Sr isotopic ratio study of the Central Ganga Alluvial Plain within Gomati River Basin. For this purpose four sampling sites were chosen and samples were collected for further processing and geochemical analysis. One set of mica-rich bedload and normal bedload sediments was collected from each site. The normal and mica-rich bedload sediments along with separated minerals (muscovite, biotite and feldspar) were analyzed for element geochemistry to obtain following objectives:

1. To look at the mobility of major and trace element during chemical weathering processes in Ganga Alluvial Plain (GAP).
2. To constrain the source of $^{87}Sr/^{86}Sr$ isotopic ratios in Ganga Alluvial Plain (GAP).

Chapter 1 contains a brief introduction of weathering of sediments and minerals in fluvial environment, mica minerals, rare earth elements and Strontium isotope. It also reports previous studies related to weathering processes and elemental mobility phenomenon. This introductory chapter provides a framework for the study.

Study area begins with Chapter 2, which presents background information of Ganga Alluvial Plain. The Gomati River originates within the Ganga Alluvial Plain (GAP) and its basin experiences a humid sub-tropical climate. Weathering products in the Ganga Alluvial Plain are transported by the Gomati River as dissolved, bedload and suspended load. The Gomati River sediments act as weathering products of the Ganga Alluvial Plain having its ultimate sediment source in the Himalayan region. The mineralogy of bedload sediments is mainly composed of quartz, followed by plagioclase, alkali feldspar and mica. Average mineral composition of the river sand consists of quartz (55%), rock fragments (19%), muscovite (15%), K-feldspar (8%), biotite (2%) and plagioclase (1%).

Chapter 3 addresses analytical techniques and methods applied to accomplish this study. Sediment samples of mica-rich bedload and normal bedload were collected from four sampling sites- Naimeserayan Haidergarh, Sultanpur and Chandwak. Minerals - muscovite, biotite and feldspar were separated from bedload sediments with the help of Isodynamic separator. After dissolution, samples were analyzed by ICP-MS. Sr isotopic analysis was done using Thermal Ionisation Mass Spectrometer (TIMS) TRITON T1. The analysis of mica grains has been done with the help of Scanning Electron Microscope with attached Energy Dispersive X-Ray (EDX) Spectrometer.

Chapter 4 report the results generated from the geochemical analysis of bedload sediments along with associated silicate minerals-biotite, muscovite and feldspar. Biotite has higher percentage of MgO & $FeO_{(t)}$ than muscovite and feldspar. Muscovite has higher percentage of Al_2O_3 & K_2O and feldspar has higher percentage of CaO & Na_2O. Biotite has higher concentration of trace elements- As, Co, Cr, Cu, Li, Ni, Rb, V, Zn than muscovite and feldspar. Muscovite has higher concentration of Ba, Sr than biotite and feldspar. In the normal bedload sediments, total-REE concentration (ΣREE), light-REE concentration (LREE) and heavy-REE concentration (HREE) are 92.1–323.1 ppm, 83.7–302.1 ppm and 7.8–21.0 ppm, respectively. Ce is the most abundant of the ΣREE compositions. The decreasing order of ΣREE concentration in common silicate minerals is biotite > muscovite > feldspar. Chondrite-normalised REE patterns of the river sediments show a strong LREE enrichment, relatively flat HREE, weak positive Gd anomaly and absence of prominent negative Eu-anomaly. In associated minerals, positive Eu-anomaly was shown by feldspar and muscovite, whereas negative Eu-anomaly by biotite. Biotite differs from feldspar and muscovite in REE enrichment and positive Gd-anomaly. The most characteristic sign of chemical alteration of biotite in the normal bedload sediments is its consistent downstream REE depletion. Microanalysis of grain of biotite mineral shows depletion of element from core to marginal edge.

Chapter 5 deals with the discussion of generated dataset and focuses on the distribution of bedload sediments along with associated silicate minerals- biotite, muscovite and feldspar to understand the mobility of major, trace and rare earth elements in Ganga plain. Biotite show enrichment in Al_2O_3, P_2O_5, FeO, MgO, MnO,TiO_2 and depletion in Na_2O, K_2O, CaO relative to UCC. Muscovite show enrichment in Al_2O_3, P_2O_5, and depletion in Na_2O, K_2O, FeO, MnO, CaO. Except for CaO, and TiO_2, all other major elements are depleted in Feldspar relative to UCC. Bedload Sediments are enriched in CaO and TiO_2 and depleted in Al_2O_3, $FeO_{(t)}$, MgO ,MnO, Na_2O, P_2O_5 relative to UCC. Biotite shows enrichment in As, Co, Cs, Cr, Cu, Ga, Li, Ni, Pb, Rb, V and Zn and Muscovite show enrichment in As, Ba, Co, Cs, Cr, Cu, Ga, Li, Ni,

Pb, Rb, V and Zn relative to UCC. Feldspar show enrichment in As and other trace elements are depleted. Bedload sediments are enriched in As, Cs, Ga, Li, Rb, and Se relative to UCC. Bivariant plots were plotted to find out association and source of elements. In sediments, K_2O shows positive correlation with Al_2O_3, indicating the common mineral sources in mica minerals and Mg shows strong positive correlation with Al_2O_3, K_2O, CaO, and $FeO_{(t)}$, indicating the common mineral sources in plagioclase and mica minerals. Significant positive correlation of Ba with K_2O and Al_2O_3 favours its association with K-aluminosilicates. Weathering influences the spatial variability in ΣREE content in biotite of the bedload sediments. The ΣREE concentrations in biotite of the normal bedload sediments decrease from 471 ppm to 142 ppm with downstream suggesting the release of REE through the intensive chemical weathering of easily weatherable biotite. On the other hand, total REE concentration in biotite of the mica-rich bedload sediments increased markedly with downstream from 375 ppm to 1445 ppm due to secondary deposition on the mineral's surface. Biotite has lower $^{87}Sr/^{86}Sr$ and lower Sr content in sediments of Gomati River Basin. The Sr isotopic ratio is increasing from Biotite to Muscovite to sediments in Gomati River Basin. Lower values of Sr may be due to relative increase in carbonate weathering or due to dilution of Sr concentration due to increase in water discharge. Elevated $^{87}Sr/^{86}Sr$ ratios of the Gomati River throughout post-monsoon season demonstrate that the interaction among the GAP sediments increased the Sr-influx after monsoon season. Chapter 6 introduces the conclusion derived from the results and discussion of present study.

This study provides major, trace and rare earth element geochemistry of bedload sediments of Gomati river along with associated silicate minerals-biotite, muscovite and feldspar to evaluate their usefulness in weathering studies. Major and trace element distribution in the weathering products is controlled by mineral sorting during transportation and deposition. REE geochemistry has utility for understanding the impacts of biotite weathering process and its significance in REE mobilization in the Gomati River Basin under its humid sub-tropical climatic condition. Gomati river water and biotite have lower values of Sr isotopic ratio while muscovite and sediments have higher Sr isotopic ratios. At Ramnagar cliff, a marked correlation between climate and Sr isotopic ratios is noted indicating the influence of climate over Sr isotopic concentration. At Behta nadi cliff section, Sr isotopic values are increasing from bottom to top of the facies revealing that Sr ratio is increasing within the Ganga Alluvial Plain. Higher Sr isotopic ratios of the Gomati River are due to chemical weathering of alluvial material present within the Ganga Alluvial Plain.

Acknowledgements

I would like to express my profound gratitude to my supervisor Prof. Sandeep Singh, Department of Earth Sciences, Indian Institute of Technology - Roorkee, for his invaluable guidance, vital encouragement and continuous support. I am grateful for his timely suggestions, unconditional help and expert guidance throughout my research and thesis writing.

Besides my supervisor, I would like to thank the rest of my thesis committee: Prof. A. K. Sen, Department of Earth Sciences; Prof. A. K. Singh, Department of Chemistry and Dr. Biplab Bhattacharya, Department of Earth Sciences for their insightful comments and encouragement. I am also grateful to the members of my committee for their patience and support, in overcoming numerous obstacles I have been facing during my research.

My sincere thank also goes to Prof. A. K. Choudhary, Institute Instrumentation Centre (IIC), for providing access to the laboratory facilities. His precious support helps me a lot in conducting this research. I am also thankful to Poornima Ma'am of IIC for help in making standards and in learning the basics of sample dissolution.

I also offer my sincere thanks to Prof. D. C. Srivastava and Prof. A. K. Saraf, the present and former Heads of the Department, respectively for providing all the necessary facilities and administrative support during the course of research work.

I take this opportunity to thank Prof. Munendra Singh, Department of Geology, University of Lucknow for helping in field work and for providing suggestion regarding research. A special vote of thanks to my seniors – Dr. D. K. Jigyasu and Late Rohit Kuvar whose encouragement and support has helped me to accomplish my work successfully.

Nevertheless, I am also thankful to Mr. Nair, Mr. Rishiraj, Mr. Bheem and other non-teaching staff of the department for their generous help in many ways during my Ph.D. work. In addition, I would like to express my gratitude to the staff of Institute Instrumentation Centre (IIC).

I would like to thank my friends and fellow doctoral students- Neethu, Pragya, Sumedha, Dr. Sugandha for their feedback, of course friendship and for all the fun we have had in these years. I thank my fellow lab mate- Rimpi for the stimulating discussions and for maintaining friendly atmosphere in lab. I would also like to thank my friends Dr. Jyoti, Dr. Harshita,

Mahima from other institutions for encouraging me throughout the journey and keeping immense faith in me.

I am also grateful to God for giving me hope in bad times and providing strength and true spirits in me.

Last but not the least; I would like to thank my family. I feel short to express my feelings towards my parents, sister, brother, sister-in-law and nieces- Anushka, Asmita for their love and moral support, which has been a constant source of inspiration for me.

Priyanka Singh

Table of Contents

List of Figures

List of Tables

Chapter 1 Introduction

1.1 Background

The planet earth contains valuable records of sediment yield history along with elemental mobility. The elemental mobility gives us insight into provenance of sediments, their transport path vis-a-vis different processes involved. The elements are transported mainly in association with particular phase. Weathering breaks down minerals and rocks by physical and chemical actions and the resulting particulate and dissolved materials are transported from continent to ocean by rivers. Climate is an important element which controls the geochemical environment of weathering processes and also has an overriding influence upon the weathering products (Nagell, 1962). The degree of weathering increases with mean annual temperature and precipitation. Temperature manages the rate of chemical weathering reactions and precipitation provides an aqueous medium and moisture for ion exchange for these reactions (Loughnan, 1969). Physical and chemical weathering processes control the evolution of the earth's surface, shaping landscapes; determine nutrients to ecosystems and regulating global chemical cycles. The products of chemical weathering of a drainage basin are transported in three different forms: bedload sediments, solid-suspended load and dissolved load (figure 1.1). The significance of bedload sediments and solid-suspended load is not so direct because it corresponds to the transport of particles produced during chemical weathering as well as physical weathering. The dissolved load represents the products of chemical weathering. Chemical weathering processes determine the flux of dissolved materials carried by rivers and act as the major component of the element cycling of the earth's surface (Martin & Whitfield, 1983).

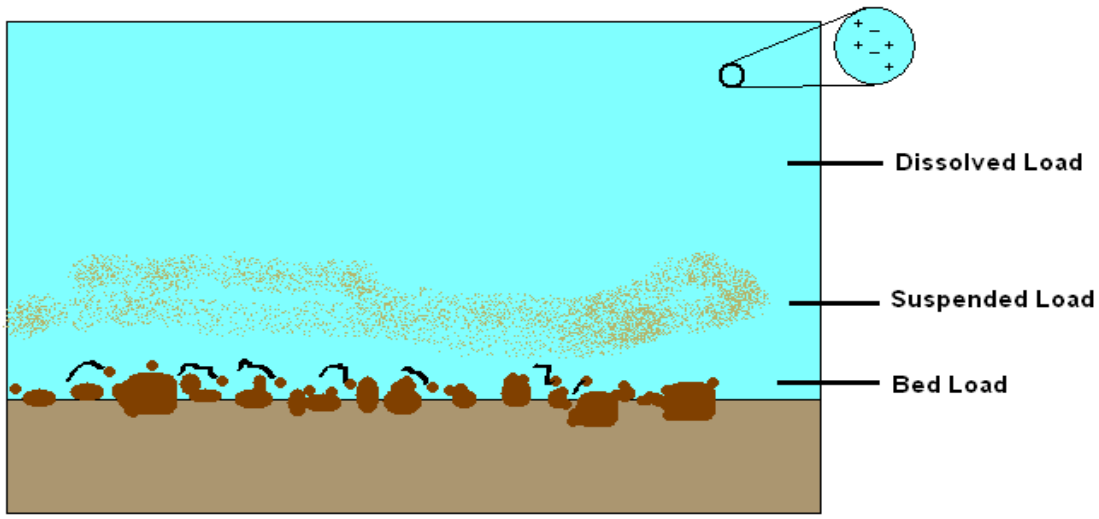

Figure 1.1 A schematic diagram of different types of sediment load (https://en.wikipedia.org/ wiki /Stream load).

Weathering in the source area affects the composition of sedimentary rocks and also paves ground for the genesis of sedimentary rocks by dislodging the mineral grains from the parent rocks for erosion and sedimentation processes. Chemical weathering have pronounced effect on the composition of silicate rocks, where large cations (Rb, Sr) remain fixed in the weathered residue in preference to smaller cations such as Na, Ca, K, which are selectively leached (Nesbitt et al., 1980). These chemical trends are generally transferred to the sedimentary record (Nesbitt and Young, 1982; Wronkiewicz and Condie, 1987) and thus provide a useful tool for monitoring source area weathering conditions. Ca, Na and K are largely removed from the feldspar during weathering, so the abundance of these elements with respect to resistant elements can be used as a measure of the extent of chemical weathering. Stronger chemical weathering is generally associated with the warm and humid climates, whilst more arid climate is generally associated with relatively weak chemical weathering. Relationship between climate and the degree of rock weathering have shown that high rainfall corresponds to the increase loss of labile mineral and higher CIA values in the resulting sediments (Basu, 1981; James et al., 1981; Suttner et al., 1981; Dutta and Suttner, 1986; Girty, 1991; White and Blum, 1995). Higher temperatures significantly enhance the rate of mineral decomposition and the potential for minerals such as plagioclase and potassium feldspar to undergo hydrolysis. Generally, the chemical weathering of rocks leads to a quick removal of alkali and alkaline earth elements; whereas Si, Fe and Al are retained as a residual deposit. Aluminium is considered as an immobile element and occurs in soils as bauxite (Jigyasu et al., 2015).

The chemical weathering of minerals is a fundamental process in the geological cycle of elements. The interactions between minerals and water play an important role in geochemical processes i.e., soil formation, elemental mobility, bio-mineralization and nutrient availability etc (Putins and Ruiz-Agudo, 2013). The study of chemical weathering processes of minerals in natural system is essential to estimate the release of various elements into solution. Many common rock-forming minerals weather at significantly different rates. Thus differential weathering of minerals gives rise to a range of geochemical and isotopic signatures in the weathered sediments. These signatures in suspended and bed sediments remain largely intact when they are ultimately displaced from the catchment areas and transported downstream in a river system (Rengarajan and Sarin, 2004). Wilson (2004) studied the weathering processes of primary rock forming minerals, products and rates in detail. The weathering product may be closely related to the primary mineral, both compositionally and structurally. The natural susceptibility of mineral to weathering is related to overall chemical composition and structure, as well as the distribution and density of defects, dislocation and exsolution features and often

control the progress of weathering reactions. Olivine is replaced during the early stages of weathering and consequently is normally not found to any great extent in soils, except under unusual circumstances (Delvigneetal., 1979). During mineral weathering, olivine transforms to ortho-pyroxenes and serpentines. Pyroxene and amphibole are also weathered in a similar way as olivine and form clay minerals. Feldspar mineral weathering mainly takes place at structural defects, particularly at the boundary of twinned and untwined domains, firstly altered to amorphous minerals. These minerals later crystallized to sheet silicates like illite and montmorillonite. Biotite weathers very easily and may progress to advanced stages even at the base of the weathering profile and is the potential source of potassium in soils. Muscovite is often extremely resistant to weathering and may persist unaltered to the top of the weathering profile. Muscovite has been found to dissolve congruently, but two orders of magnitude slower than the biotite (Wilson, 2004).

It has been established that the Himalaya shed their weathered product into the Ganga Alluvial Plain (GAP) which has been recycled, after a gap of time, to Bay of Bengal (Jigyasu et al., 2016). Sediments of the GAP show much higher weathering index as compared to the sediments shed by the Himalaya (Singh, 2004). A river is continually picking up and dropping solid particles of rock and soil from its bed throughout its length. Alluvium is formed by the sediments deposited by a river. The alluvium in the Indo- Gangetic Plain belongs to Quaternary period. It was eroded from the Himalayas by the rivers. These alluvial deposits consist of clay, loam, silt etc. and are divided into the older alluvium and the newer alluvium. The older alluvium is called bhangar and is present in the ground above the flood level of the rivers. Khaddar or newer alluvium is confined to the river channels and their flood plains. The Indo-Gangetic Plain is a foreland basin and closely linked to the tectonic development of the Himalayas. The plain is morphologically characterized by alluvial rivers, lakes, small streams, aeolian ridges etc. The sediment eroded from the Himalaya comes to the Ganga Alluvial Plain (GAP), where it is stored for over a reasonable time. Part of this sediment is preserved to make alluvial deposits of the plain, and part has been recycled to the Bay of Bengal. The Gomati River flows along the great alluvial plain which is of Pleistocene- Holocene origin. Gomati River, which has a source from ground water, is perennial with medium discharge and low sediment load (Singh, 2009). The discharge is very high during strong monsoon season. The Gomati River redistributes the primary weathered sediments of the Ganga Alluvial Plain (GAP) derived from the Himalaya. Sediments of the Ganga Alluvial Plain (GAP) show much higher weathering indices than the sediments coming from the Himalayan source (Singh, 2004). In the Ganga River Basin, monsoon climate controls the weathering pattern of the GAP as well as

physical and chemical fluxes. The weathering products also demonstrated a progressive incomplete alteration in the alluvial sequence. The sediment load supplied to the channel and water discharge controls the geometry and pattern of the river channel. Rainfall is directly responsible for the increase in water budget of the basin, so its discharge is mainly controlled by climate (Singh et al., 2010). Physical weathering in the Himalayan region is very prominent releasing huge amount of sediment load to the Ganga River. The concentration of various elements in the dissolved load of the Ganga River at Rishikesh is less than that of the Gomati River (Chakrapani, 2005). On the other side, chemical weathering of the Ganga Alluvial Plain is significant, primarily due to high content of porous, mica rich silty sediments (Singh et.al. 1999).

Minerals in bedload sediments of the Gomati River include quartz, feldspar, mica (muscovite and biotite) along with hornblende, garnet, epidote, tourmaline, kyanite etc. as heavy minerals (Kumar and Singh, 1978). In channel deposits, mica minerals (biotite and muscovite) get concentrated as bedload sediments during decreasing discharge condition because of their large grain size and flaky character. These mica-rich bedload sediment contain a relatively higher percentage of mica (>50 to 80%) compared to normal bedload sediments. The mica proportion in bedload deposit sediments of the Ganga Alluvial Plain is reported as high as 30%.

1.2 Mica

The mica minerals are the most easily weatherable mineral and belong to the most important OH- bearing silicates on Earth. The mica minerals are sheet silicates (phyllosilicate), commonly characterized by platy morphology and perfect basal cleavage, which are consequence of their layered atomic structure (Deer et al., 1978). The mineral group is chemically and geochemically complex and composed of some 41 species and seven mineral series (Rieder et al., 1998). Biotite and muscovite are the most familiar representative rock forming minerals belonging to mica group. Biotite is essentially a ferromagnesian mineral series (mafic, dark coloured) with compositional affinity to other ferromagnesian minerals like olivine, pyroxene and amphiboles; whereas muscovite is an aluminosilicate (felsic, light coloured) with compositional affinity to feldspar, feldspathoids and quartz. Biotite is a trioctahedral mica whereas muscovite is a diotahedral mica. Trioctahedral micas have complex crystal structure; hence they incorporate a large number of elements of different ionic sizes by a variety of isomorphic substitution (Tischendorf et al., 2001). The paragenesis of mica-group minerals encompasses a broader range of whole-rock and fluid compositions, temperature, pressure, and redox state depending upon prevailing geological environment. Mica is a

phyllosilicate mineral and consists of octahedral (o-layer) sheet sandwich between two identical tetrahedral (t-layer) sheets producing the characteristic t–o–t layer. The mica minerals have the general formula $AR^{2-3}\ G_{1-0}\ T_4\ O_{10}\ X_2$, where A is an interlayered cation (K, Na, Ca, Ba, Cs, NH_4); R is an octahedral layered cation (Al, Mg, Fe^{2+}, Fe^{3+}, Li, Ti, Mn^{2+}, Mn^{3+}, Zn, Cr, V, Na); G is a vacancy in the octahedral layer; T is a tetrahedral layer cation (Si, Al, Fe^{3+}, Be, B); O is oxygen; and X is an anion (legand) not bonded to T (OH, F, Cl, O, S) (Deer et al., 2003). In biotite tetrahedral sheets are occupied by Si and Al, whereas the octahedral sheets are usually inhabited by Fe, Mg and other cations. The interlayer site is typically resided by K (Deer et al., 1966). Significant concentrations of elements occurring in the mica minerals are Si, Al, Fe, Ti, Mn, Cr, V, Mg, K, Na, Rb and Ca etc. (Tischendorf et al., 2007). Mobilization of trace elements from the octahedral layer of mica structure to the river water of the alluvial plain is a complex natural process. Microscopic study of the core and margin of biotite grain indicate that along the margins silicate structure is broken during the chemical weathering and elements are being removed into their dissolved phase (Jigyasu et al., 2014). The main source of elements in the Gomati river water is essentially considered to be biotite mineral of the alluvial plain sediments. Mica minerals can play considerable role in understanding of trace-elements mobility in the Ganga Alluvial Plain. The study of chemical weathering processes of minerals in natural system is essential to estimate the release of various elements into solution. Therefore it is important to study the chemical weathering of various minerals of the sediments, release of major and trace elements, transfer of these elements into river water.

Biotite is a phyllo- (layer) silicate mineral and consists of octahedral (o-layer) sheet sandwich between two identical tetrahedral (t-layer) sheets producing the characteristic t-o-t layer (figure 1.2). Biotite quickly weathers in to secondary minerals by solid-state alteration and dissolution processes (Banfield and Eggleton, 1988). Dissolution processes take place by replacement of K at interlayer site, oxidation of Fe in octahedral sheet, movement of other cations from octahedral sheet into solution and neutralization of OH groups by H (Feldman et al., 1991). Mica minerals particularly biotite is prone to chemical weathering and releases large amount of major and trace elements to be moved into solution (Price and Velbel, 2014). The chemical change in biotite can be written as follow (Dong et al., 1998):

$$K_{0.65}(Al_{1.10}Ti_{0.15}Fe_{0.50}Mg_{0.55})(Si_{3.20}\ Al_{0.80})O_{10}(OH)_2 + 8H^+ = (Al_{1.71}Fe_{0.31}Ti_{0.03})Si_2o_5(OH)_4 + 0.65K^+ + 0.19Al^{3+} + 0.55Mg^{2+} + 0.19Fe^{2+} + 0.12Ti^{4+} + 1.2Si^{4+} + 3H_2O$$

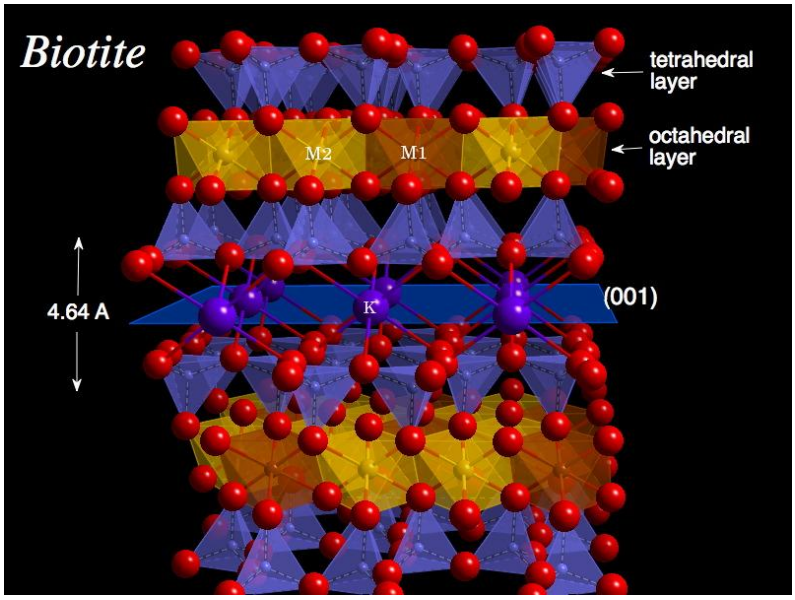

Figure 1.2 Structure of biotite showing t-o-t layer (http://theteachersinstitute.org/sites/default/ files/ Carambo, %20Cristobal%20-%20unit.pdf).

Muscovite is common di-octahedral mica with wide variety of elemental substitutions (figure 1.3), which may result in disorder and complexities within the structure and hence influence ideality of structural formula (Benincasa et al., 2003).

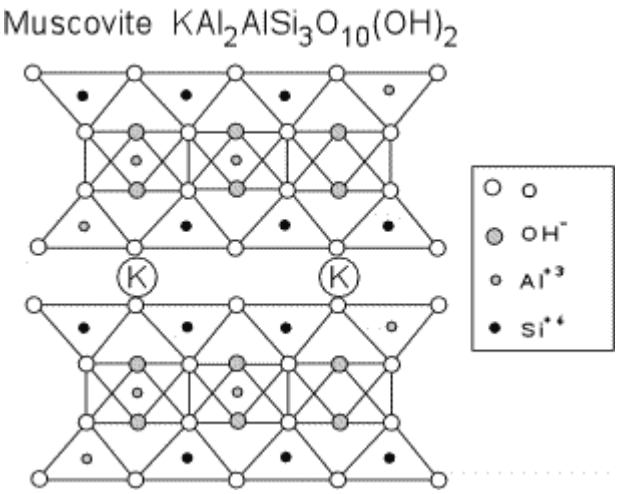

Figure 1.3 Structure of muscovite showing t-o-t layer (http://www.tulane.edu/~sanelson/eens 211/weathering&clayminerals.htm)

1.3 REEs

Rare earth elements (REEs) form lanthanide series from La to Lu. Rare earth elements in river sediments are widely used as valuable indicators for the determination of sediment sources, chemical evolution of the continental crust and weathering processes in drainage

basins (Goldstein and Jacobsen, 1988; Nesbitt et al., 1990; Holser, 1997; Vital et al., 1999; Kumar et al., 2007). REEs show similar behaviour in the environment as they have similar chemical properties and have a tendency to exist together naturally (Henderson, 1984; Tyler, 2004; Hu et al., 2006). REEs are generally mobilized under acidic condition and have tendency to be adsorbed on particles when the pH is neutral or alkaline. The REE show a unique behavior during chemical weathering and can also be adsorbed by minerals during weathering processes (Bau, 1999). Due to their low solubility and relative immobility in the upper crust, REEs undergo little geochemical fractionation during weathering processes. In recent years, many publications dealing with distribution and geochemistry of REE from various rivers have emerged (Zhu et al., 1997; Singh, 2009; Sultan et al., 2009; Antonina et al., 2013; Foley et al., 2013; Li et al., 2013).

Sholkovitz (1995) studied the chemistry of rare earth elements (REE) in rivers and estuaries and claimed that the concentration and fractionation of REEs dissolved in river waters are highly pH dependent and REEs are fractionated during the formation of weathering products from parent rocks. Johannesson and Xiaoping (1997) reviewed the geochemistry of rare earth elements in natural terrestrial waters and proposed that processes like; solution complexion, surface adsorption along with weathering control the behaviour and concentrations of REEs in natural waters. Ramesh et al. (2000) studied the distribution of rare earth elements in sediments of Himalayan River System and suggested that the distribution of REE is mainly controlled by physical weathering process in the Himalayan River sediments. The distribution of REE shows an almost uniform pattern due to high level of terrigenous mixing in the bed sediments. Singh and Rajamani (2001) studied the REE geochemistry of sediments from Kaveri floodplains and concluded that mineral titanite has controlled the REE chemistry of these sediments and REEs in these clastic sediments could be present as surface coatings on grains, in addition to heavy and clay minerals. Rengarajan and Sarin (2004) studied the distribution of REEs in the Yamuna and the Chambal Rivers and examined that Yamuna River sediments depict strong HREE enrichment and a positive Eu anomaly whereas the Chambal River samples show significant LREE enrichment and Eu enrichment. Ross et al. (1995) analyzed the REEs in sediments of upper Manso River, Rio Negro, Argentina and concluded that grain size is not a determining factor in the REE concentrations. Li et al. (2009) studied rare earth elements in the sediments of Yarlung Tsangbo (Upper Brahmaputra River), southern Tibetan plateau and supported that grain size influences the REE concentrations of the Yarlung Tsangbo sediments. The <63μm fraction of the sediment has higher REE concentrations and different REE patterns compared to the <20 μm fraction due to the contribution of some REE-

enriched heavy minerals. Song and Choi (2009) studied the REE characteristics of fine grained sediments from major rivers around the Yellow Sea and observed that LREE and MREE are enriched in the Korean river sediments while Chinese river sediments show only MREE enrichment. This could be due to climatic influence.

REE may be concentrated in specific minerals of the sediments and it is important to understand the REE pattern in individual minerals of sediment. Therefore, in the present study REE pattern in biotite, muscovite and feldspar mineral has been attempted along with bedload sediments of Gomati River.

1.4 Sr isotope

Radiogenic isotopes are used to investigate the physical and chemical erosion processes in river basins. Particularly Sr isotope is used for chemical weathering studies. Sr is a divalent cation that readily substitutes for Ca^{2+} in carbonates, sulphates, feldspars and other rock forming minerals. Like Ca^{2+}, it participates in water-rock reactions, and is a minor component of most groundwaters. Sr isotopes have proven to be a useful indicator of water-rock interaction and as a tracer for groundwater movement and the origin of salinity (Shand et al., 2009).

Increasing Sr flux in ocean since last 40 million years always fascinated scientist and largely been attributed to rise in Himalayas and weathering of Himalayan rocks (Singh et al., 2010). Several studies have identified that Himalayan Rivers are the potential source for steady increase of marine Sr isotopic budget. The influx has always been attributed to present day exposure of the Himalaya within Tethyan Sedimentary Sequences, Higher Himalayan Crystallines, Lesser Himalayan Sedimentary Sequences and Siwalik ranges. The Ganga – Brahmaputra river system are main contributors towards the increase in marine $^{87}Sr/^{86}Sr$ isotopic ratio. The increase in marine Sr since Himalayan collision is a result of drainage of material by the Ganga, the Brahmaputra, the Yamuna and the Indus River system which follows the southern slope of Himalayas and drain in to ocean (Edmond, 1992; Krishnaswami et al., 1992; Raymo and Ruddiman, 1998; English et al., 2000; Karim and Veizer, 2000; Bickle et al., 2001; Dalai et al., 2003, Singh et al., 2010). The Sr flux to the ocean has been attributed to either silicate weathering (Galy et al., 1999) or carbonate weathering (English et al., 2000). However the silicate weathering is more responsible for Sr contribution as compared to carbonate weathering. Data suggested that the rivers draining the Himalayan along its southern slopes have higher Sr concentration with $^{87}Sr/^{86}Sr$ isotopic ratio - 0.7236 (Harris, 1995), however, the major rivers on the global scale have an average of 0.7111 (Palmer and Edmond, 1989, 1992; Harris, 1995; Galy et al., 1999).

The Gomati River, an important tributary of Ganga River, is one of the rivers which are originating from the Ganga Alluvial Plain (GAP). The river recycles the Himalayan derived sediments and transport its weathering products into the Ganga River and finally to Bay of Bengal. The Gomati River water has dissolved Sr concentrations 375 μg/l, which is more than five times higher than the world's average of river water (70 μg/l) and nearly three times higher than the Ganga river water in the Himalayas (130 μg/l). The $^{87}Sr/^{86}Sr$ isotopic ratios reported are also higher than global average runoff (0.7119) and to modern seawater (0.7092) values (Singh et al., 2010). The Sr isotopic data from the Gomati River and lakes occurring within the Gomati River Basin, which does not have any inflow from the Himalayan region, indicate that the ratios are higher as compared to the Himalayan River (Singh et al., 2010). This Sr isotopic ratio from the Indo-Gangetic plain is higher because of the fact that the material deposited within the Indo-Gangetic Plain is derived from the Himalayan rocks which were exposed at the earlier dates, and indicate that the materials have source from the area of higher Sr isotopic ratios. Singh et al. (2010) interpreted the variation in Sr isotopic ratios during pre-monsoon and post-monsoon season is due to monsoonal erosion of the GAP into the Gomati River. This indicates that the interaction within the GAP sediments increased the Sr-influx after monsoon season. It has also been established that GAP plays an important role in contribution of Sr-influx to the ocean. Hydrogeochemical processes operating in the Ganga Alluvial Plain (GAP) has significant geochemical linkage between the Himalayas as source and the Bay of Bengal as sink and, therefore, should be emphasized in interpretation of elemental mobility, cycling and budgets of the Ganga Fluvial System (Singh et al., 2008). Singh et al. (2006) studied the Sr isotope in Brahmaputra river water and sediments and concluded that the Brahmaputra has less radiogenic Sr (~0.72) compared to the Ganga (~0.73) but the flux of Sr is similar in both rivers. Tripathi et al. (2013) studied Sr isotope characteristics of Indo-Gangetic Plain sediments to constrain their sources and concluded that sediments of the Ganga–Yamuna and Satluj systems have high $^{87}Sr/^{86}Sr$ (>0.75) values, characteristics of Higher Himalayan Crystallines. However, sediments of the Ghaggar River and the Thar Desert have distinctly lower $^{87}Sr/^{86}Sr$ (<0.75) values derived from the Sub-Himalayan sediments. The isotope geochemistry of the Indo-Gangetic Plain sediments indicates the shifting of the Yamuna River from Thar Desert to the Ganga domain and indicated that the paleo-Yamuna river must have flowed to the south of the paleo-Ganga course but to the north of its present day Yamuna course (Tripathi et al., 2013).

The contribution made by minerals in the Ganga Alluvial Plain (GAP) has been neglected so far, therefore, present investigation was undertaken to obtain a preliminary data on Sr flux from mineral phases within the Ganga Alluvial Plain through analysis of $^{87}Sr/^{86}Sr$ isotopic ratios.

1.5 Geochemical mobility

In chemical weathering processes, geochemical reactions dealing with mineral-water interactions are controlled by the mineralogy of earth surface and reflect the mobility of elements. This mineral-water interactions effect the regulation of climate and the distribution of life on the earth. The mobility of major elements is controlled by equilibrium with solid phases in which they are present. An element may be highly soluble in acidic, reducing conditions but very insoluble under alkaline, oxidizing conditions, due to changes in chemical form. The positive and negative charged species of elements are most strongly absorbed under alkaline and acidic conditions, respectively. Mineral surfaces are generally negatively charged under alkaline conditions; whereas positively charged under acidic conditions. The mobility of geochemical elements also affects the availability of nutrients in the biosphere of the earth system. The geochemical mobility can be described quantitatively in terms (i) percent change, (ii) depletion/enrichment and (iii) mobility index. Their detail descriptions are as follows:

1.5.1 Percent change

Kronberg et al. (1987) studied the mobility of alkaline and alkali earth elements during weathering by percent change. It is a measure of element mobility relative to K. It is calculated as follows:

$$\textbf{Percent change} = [(Rs - Rp)/Rp] \times 100$$

Where R is the relative concentration of elements with respect to K in sample (s) and parent rock (p).

1.5.2 Percent Depletion/Enrichment

The perent depletion/percent enrichment of an element in sediments is a measure of its loss (or gain) from the parent rocks due to chemical weathering and subsequent mobilization. Canfield (1997) calculated percent depletion or enrichment by using the following relation:

$$\textbf{Percent depletion/ percent enrichment} = [\{(X/Al)_{Sediments} - (X/Al)_{UCC}\}/(X/Al)_{UCC}] \times 100$$

Where X = Na, K, Ca, Mg, Ba, Sr, etc and $(X/Al)_{UCC}$ is the element to Al ratio in parent rock. The $(X/Al)_{Sediments}$ is the element to Al ratio in weathered rock or sediments.

1.5.3 Mobility index

The abundances of elements in rivers depends both on their abundances in the continental crust and their mobility during weathering and transport. In order to depict the element mobility

trend of elements, dissolved concentrations (Cw) are normalized to those of the upper continental crust (Cc), and all normalized concentrations are compared to the value for Na. A number of very different processes contribute to the occurrence of elements in river water as dissolved load. Gaillardet et al., (2003) proposed a classification of element mobility based on concentration of elements in the dissolved load of river water on the basis of this approach.

$$\text{Mobility index} = Cw/Cc$$

Where Cw and Cc refers to the concentration of elements in river water and in upper continental crust, respectively.

The elemental mobility was classified as high, moderate, non-mobile and immobile elements (Gaillardet et al., 2003). The highly mobile element has mobility indexes greater than that of Na. The moderately mobile elements have mobility indexes ~10 times less than that of Na. The non-mobile elements have mobility index 10-100 times less than that of Na. The immobile elements have mobility indexes more than 100 times lower than that of Na.

1.6 Previous studies

Element mobility is of fundamental importance to understand the weathering processes and the water-rock interaction. Element mobility in the water-rock interaction processes in various geological settings is of increasing interest to the scientific community. The subject itself was studied by several researchers in different parts of the world due to the availability of more sophisticated technical equipment for measuring elemental concentrations. Various studies have been carried out all over the world which deals with weathering processes and elemental mobility (table 1.1).

Middleburg et al. (1988) studied the mobility of major, minor and trace elements during the weathering of the Portuguese granitic rocks and concluded that Ca, Na, K, Sr, Ba, Rb, Mg and Si are mobile elements derived mainly from leachable minerals such as feldspar, mica and apatite; whereas Zr, Fe, Al, and rare earth elements are immobile elements and are either concentrated in resistant phases or strongly adsorbed by secondary minerals. Weijden and Weijden (1995) studied the mobility of major, minor, some trace elements and rare-earth elements during weathering of granitoids in central portugal and proposed that the increase in the degree of weathering was accompanied by reductions in Na_2O, CaO and SiO_2, P_2O_5, and K_2O contents in various minerals. Mongelli et al. (1998) studied elemental mobility during the weathering of exposed lower crust: the kinzigitic paragneisses from the Calabria, southern Italy and concluded that light rare earth elements show enrichment over the heavy rare earth

Table 1.1 List of selected research studies carried out worldwide on major and trace element mobility

Location	**Study Type**	**Reference**
Mt. Etna volcano, Sicily.	Mobility and fluxes of major and trace metals	Aiuppa et al. (2000)
Amazon river	Major and trace elements distribution	Vital and Statteggar (2000)
Yamuna river	Sediment geochemistry/ mobility of elements during weathering and transport	Dalai et al. (2004)
Yamuna and chambal rivers	REE geochemistry	Rengarajan and Sarin (2004)
Gomati river	Major and trace element distribution	Singh et al. (2005)
Ganges alluvial plain	Sediment geochemistry	Tripathi et al., 2007
Deccan traps	Mobility of major and trace elements	Das and Krishnaswami (2007)
Gironde estuary, france	Mobility of trace metals	Schäfer et al. (2009)
Ganga river	Major, trace and REE geochemistry	Singh, 2009
Godavari river	Geochemical and mineralogical characteristics	Vuba et al (2013)

elements. Yingjun and Congqiang (1999) studied the trace element geochemistry during chemical weathering of granite in Longnan, Jiangxi and found that Na, Ca, Si, P, V, U and Sr are mobile; whereas Ti, Al, Fe and Zr are relatively conservative in nature. Aiuppa et al., (2000) studied mobility and fluxes of major and trace metals during basalt weathering and groundwater transport at Mt. Etna volcano of Sicily. The mobility trend of alkali and alkaline earth elements in Etnean groundwater is Na > Mg > K = Rb = Ca = Cs = Li > Sr >> Ba.

Vital and Statteggar (2000) studied the distribution of major and trace elements of the Amazon River sediments to understand the source area composition and changes in sediments due to sedimentation processes and weathering. Land and Ohlander (2000) studied the chemical weathering rates, erosion rates and mobility of major and trace elements in the boreal granitic till of Northern Sweden and concluded that Na followed by Si and S are the most mobile elements, whereas, Al and Fe were the least mobile elements. Patino et al. (2003) studied the trace element mobility during spheroidal weathering of basalts and andesites in Hawaii and Guatemala. This study revealed that the light rare earth elements (LREE) are highly mobile than the heavy rare earth elements (HREE). Botes and Standen (2005) investigated the trace element mobility from river sediments study and reported the very high mobility of Co,

Fe, Mn, Ni and Zn. Corteel et al., (2005) studied element and isotope mobility during water-rock interaction processes.

A number of studies were carried out on the headwaters of the rivers draining the Gangetic Plain (Derry et al., 1996; Blum et al., 1998; Krishnaswami,et al., 1999; Bickle et al., 2001, 2003; Galy and France-Lanord, 2001) and in the middle and lower reaches of these rivers (Sarin et al.,1989; Rai et al.,2010; Singh et al., 2010). Dalai et al. (2004) studied the sediment geochemistry of the Yamuna River and found that concentrations of Na, K and Fe of Yamuna River System sediments are significantly controlled by clay mineral abundances. Singh et al. (2005) studied the weathering of the Ganga Alluvial Plain (GAP) and inferred that the distribution of major and trace elements is controlled by the similar processes in these sediments and mineral sorting during fluvial transportation and deposition controls major and trace element distribution in the GAP weathering products. Das and Krishnaswami (2006) studied the abundance, relative mobility and flux of Ba in rivers of the Deccan Basalt, India and concluded that Ba is the least mobile element in all the alkaline earth elements and they also concluded mobility trend in decreasing order Na, Ca, Mg, Sr, K, Ba, Al, Fe and Ti. Tripathi et al. (2007) studied the geochemistry of sediments of Ganga Alluvial Plain and emphasized that sediments were delivered from moderately weathered sedimentary source regions and were subjected to a very low degree of chemical weathering after deposition. This study shows that the Ganga Alluvial Plain is a Quaternary extension of the Tertiary Himalaya. Singh (2009) studied the major, trace and REE geochemistry of Ganga River sediments and concluded that silicate weathering of Ganga River sediments was negligible at the source and has occurred only after entering into the plains due to change in climatic condition. Sediment chemistry seems to be modified by mineral sorting and post depositional feldspar weathering in plains. Rai et al. (2010) studied the chemical weathering in the Ganga River Basin, Northern India. This study demonstrated the importance of rivers draining the Ganga Plain and peninsular basins as a major source of Na and Sr. Singh (2010) studied the geochemistry of sediments of Ganga River, Bhagirathi River, Mandakini River, and Alaknanda River and proposed that these rivers have not undergone significant chemical weathering because of lower CIA values while physical weathering and erosion are dominant processes. HHCS (Higher Himalayan Crystalline Series) rocks acted as the predominant source rocks for Ganga River and its tributaries. Singh et al. (2010) studied the recycled sediments derived from Himalaya and concluded that the Sr isotopic ratios are higher in the GAP sediments than the Himalayan rocks. Singh (2011) studied the weathering and chemical variability in Ganga Plain sediments and claimed that maturity of sediments is increasing from the Ganga River to the Yamuna River to the Gomati River. This study also showed that recycling of sediments is the major factor for the increasing order of

maturity in the above rivers. Vuba et al (2013) studied the geochemical and mineralogical characteristics of clastic sediments from lower Godavari River and suggested that TiO_2 and ∑REE content shows a strong relationship which imply that REE geochemistry is controlled by titaniferous minerals.

The present study shows the better understanding of the chemical weathering of various minerals of the sediments, release of major and trace elements and mobility of major, trace and rare earth elements in Gomati River (Ganga Alluvial Plain- GAP).

1.7 Objectives

The present study encompasses the following objectives-

1. To look at the mobility of major and trace element during chemical weathering processes in Ganga Alluvial Plain (GAP).
2. To constrain the source of $^{87}Sr/^{86}Sr$ isotopic ratios in Ganga Alluvial Plain (GAP).

1.8 Methodology

Methodology adopted for this study includes following steps-

1. Sampling of recycled sediments from Himalaya within the Ganga Alluvial Plain (GAP) across the Gomati River Basin from four locations- Naimeserayan, Haidergarh, Sultanpur and Chandwak is done.
2. Geochemical analysis of mineral separates- biotite, muscovite, feldspar and sediments is being done by ICP-MS.
3. Sr isotopic analysis of mineral separates- biotite and muscovite is being done by TIMS.
4. Microanalysis of Biotite is done by SEM-EDX for elemental analysis of edge and basal surface of biotite grain.
5. Elemental modelling of bedload sediments and associated minerals of Gomati River Basin.

Chapter 2 Study Area

The Gomati River, an alluvial tributary of Ganga River, is a groundwaterfed stream and its whole drainage exists within the Ganga Alluvial Plain (GAP). It is located between $80^0$00'E to $83^0$10'E longitudes and $28^0$40'N to $24^0$40'N latitudes draining an area of 30,437 km^2 of the Ganga Alluvial Plain (figure 2.1). Gomati River originates from swampy area situated towards the south of Himalayan foothills and covers a distance of 900 km before meeting the Ganga River near Kaithi, Ghazipur district (Uttar Pradesh). It forms an elongated basin, trending in NW-SE direction. Gomati River redistributes the weathered products of the Ganga Plain as bedload sediments, suspended sediments and dissolved load. To study the recycling of sediments and its various components Gomati River Basin has been selected for study. This chapter discusses the characteristics like physiography, geology, climate etc. of the Ganga Alluvial Plain (GAP) as a whole and Gomati River Basin in particular.

2.1 Ganga Alluvial Plain

2.1.1 Physiography

In northern part of the Indian sub-continent, the Indo-Ganga-Brahmaputra Plain formed due to post-continental collisional erosion of Himalayas. Continent-continent collision or Indian Plate with its indented Eurasian Plate occurred no later than 57 Ma (Leech et al., 2005). The contact between the northern Ganga Plain and the Siwalik is marked by Himalayan Frontal Thrust (HFT). The sediments deposits in the foreland basin and the basin receives huge amount of sediments from the Himalayan as well as from the craton regions. This foreland basin separates the Himalayan Orogenic belt from the Indian Craton. The center part of the Indo-Ganga-Brahmaputra Plain is widely known as the Ganga Alluvial Plain (GAP). The Ganga Plain is the region of low elevation, low relief, high fertility and high population density. It extends from the Aravalli-Delhi ridge in the west to the Rajmahal Hills in the east, the Siwalik Hills in the north and the Bundelkhand-Vindhyan Plateau-Hajaribag Plateau in the south (Singh, 1996). The Ganga Plain is about 1000 km long and its width ranges between 450 km in the western part to 200 km in the eastern part. It covers an area of about 250,000 km^2 and located between longitudes 77 ºE to 88 ºE and latitudes 30ºN to 24ºN.

The Ganga Plain has been divided into four distinctive units from North to South (figure 2.1) (Pathak, 1982)

1. Bhabar Belt – a 10-30 km wide belt of gravelliferous sediments adjacent to Himalaya with steep slopes and ephemeral streams.

2. Terai Belt – a 10-50 km wide low lying area adjacent to Bhabar Belt with extensive development of swamps, ponds, small sandy rivers.

3. Central Alluvial Plain – represents the most important part of Ganga Plain, located between the Bhabar- Terai Belt and also the axial river. The drainage is mostly aligned in SE direction.

4. Marginal Alluvial Plain – the north sloping surface, located south of the axial river, and characterized by NE flowing gravelly to coarse sandy rivers. This area is made up of sediments from peninsular craton.

Singh (1996) divided the plain into three broad areas on the basis of landforms, characteristic deposits and tectonic settings (figure 2.1) which include;

1. Piedmont Zone (both Bhabar and Terai belt)
2. Central Ganga alluvial plain
3. Marginal alluvial plain.

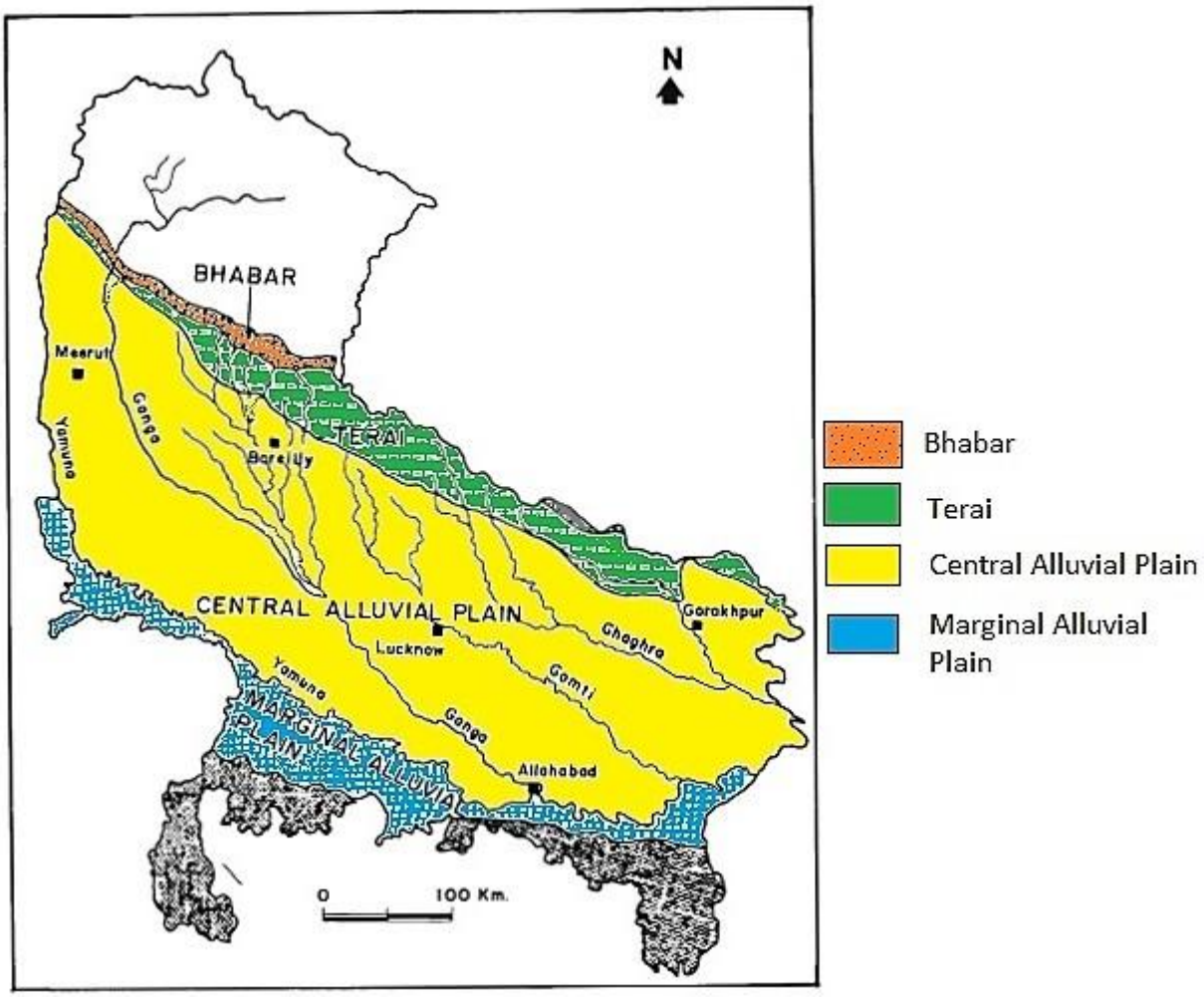

Figure 2.1 Four-fold subdivisions of Ganga plain in Uttar Pradesh (modified after Pathak, 1982).

2.1.2 Geology

The main geomorphic surfaces, interpreted as depositional surfaces of the Ganga Plain as described by Singh (1996) are the upland interfluve surface, the marginal plain upland surface, the megafan surface, the river valley terrace surface, the piedmont fan surface and the active flood plain surface. These sedimentary sequences are exposed in the cliff sections along the rivers of the Ganga Plain (Singh, 1996) and represent younging in age which has been explained as follows:

(i) **Upland Interfluve Surface:** It occurs as vast raised interfluves area in the northern Ganga Plain known as Bangar, Doab or Varanasi Older Alluvium. The Upland Interfluve surface has a general slope towards SE direction. Upland Interfluve Surface has incised active river channels and made up of muddy sediments. The age of Upland Interfluve Surface is 128–74 Ka BP (Singh, 1996).

(ii) **Marginal Plain Upland Surface:** It is present south of the Ganga River and extending upto the outcrops of the cratonic rocks. It slopes towards N-NE. Marginal Plain Upland Surface sediments are derived from the Peninsular Craton and are highly oxidized and reddish in colour. It also termed as Banda Older Alluvium or Bangar. The age of Marginal Plain Upland Surface is also 128–74 Ka BP (Singh, 1996).

(iii) **Megafan Surface:** It is located in the northern and central part of the Ganga Plain associated with the major Himalayan Rivers. These megafans are namely the Kosi, the Gandak, the Sarda (Ghaghra) and the Yamuna-Ganga (Ganga) megafans. Presently, these megafans are relict features and the active channels are mostly incised in the surface. These Surfaces shows muddy sediments. The age of Megafan Surface is 74–35 Ka BP (Singh, 1996).

(iv) **River Valley Terrace Surface**: In the Ganga Plain, the active rivers show incised and broad river valleys with terrace surfaces. The width of the River Valley Terrace Surface varies from about 0.5 to 60 Km, depending upon the size of the river valley. These also form part of Khadar and is known as older floodplain. The age of the River Valley Terrace Surface is 35–25 Ka BP (Singh, 1996).

(v) **Piedmont Fan Surface**: It is the 10-30 km broad belts of high slopes present near the Himalayan foothills. It is formed by coalescing piedmont fans. Numerous small, parallel to sub-parallel ephemeral streams are present on the Piedmont Surface. The age of the Piedmont Fan Surface is 25–10 Ka BP (Singh, 1996).

(vi) **Active Flood Plain Surface**: It comprises the active channel and the active floodplain. It represents the lower part of Khadar and lowland active floodplain. Active Flood Plain Surface is narrow in the rivers of the Ganga Plain due to entrenchment. It consists of sandy sediments of the channel and muddy sediments of the floodplain. The age of the Active Flood Plain Surface is 10 Ka BP (Singh, 1996).

Ganga River drains the Ganga Alluvial Plain (GAP) and originates from the Himalayan region, the northern Indian craton region and the Ganga plain region. Hydro-logically, Ganga River is influenced by two main phenomena- monsoon precipitation and melt of the snow in the Himalaya and therefore climate change will affect the availability of water in the Ganga basin (Moors, 2009). The main tributaries of Ganga River System are the Yamuna, the Ghaghra, the Kosi (originating from Himalayan region), the Son River (originates from the northern Indian craton region), and the Gomati River (originates within the Ganga plain region).

Lithologically, the Ganga Alluvial Plain is made up of inter-layered 1– 2 m thick fine sand and silty mud deposits showing huge intermittent calcrete horizons (Singh, 1996). Based on grain size, contact relationships, burrowing, mottling and calcretization in the plain, Singh (1996) identified two types of lithofacies associations: sandy interfluve deposits and muddy interfluve deposits. Sandy interfluve deposits are made up of 0.5–2.0 m thick lenticular sand bodies representing the meandering river deposits, and 1.0–2.0 m thick well sorted silty fine sand representing the sheet flood deposits with 10–50 cm thick discontinuous horizons of calcrete. Muddy interfluves deposits are made up of 0.2–1.0 m thick well sorted silt with extensive calcrete development, 1.0–2.0 m thick highly mottled fine sand deposits with 5–10 cm thick bedded calcrete and shell-bearing mud.

2.2 Gomati River Basin

2.2.1 Physiography

Gomati River is an alluvial river of Ganga Plain and is a major tributary of Ganga River with groundwaterfed characteristics. The Gomati River is about 900 km long and has a catchment area of 30,437 km^2 lying between latitudes 24°40’N and 28°40’N and longitudes 80°00’E-83°10’E forming the interfluve region of the Ganga and Ghaghara rivers (figure 2.2, 2.3). The river originates from Gomath Tal near the village of Madho Tanda located in Pilibhit district (Uttar Pradesh) about 50 km south of Himalayan foothills and lies in the piedmont zone. It flows through Ganga Alluvial Plain with ultimately meeting the Ganga River near Kaithi,

Ghazipur district (Uttar Pradesh). The Gomati drainage basin is gently sloping and trends in a NW-SE direction (Singh et al., 2010). The normal slope of the river is about 55 cm/km in its upper reaches, while in the lower reaches it is about 11 cm/km (Thakur, 2008). The tributaries of the Gomati River display dendritic to parallel network of entrenched alluvial tributaries. In downstream route, the river drains through the districts of Pilibhit, Shahjahanpur, Sitapur, Lucknow, Barabanki, Sultanpur, Jaunpur and Ghazipur. Figure 2.2 shows an active channel of Gomati River at Haidergarh.

Figure 2.2 Upstream view of the active channel of the Gomati River at Haidergarh.

The bedload sediments along Gomati River from four localities-Namisharayan (GR-01), Haidergarh (GR-02), Sultanpur (GR-03) and Chandwak (GR-04) within GAP have been collected and the muscovite, biotite and feldspar minerals of these samples have been separated and analyzed. Figure 2.3 displays the map of the Gomati River Basin showing sample locations (1-Naimeserayan; 2-Haidergarh; 3-Sultanpur and 4-Chandwak) along the Gomati River. The Gomati River has many tributaries draining through the GAP and actively incorporating into its sediment load. The Sai River is the main tributary of Gomati River draining nearly one third part of the Gomati River basin. Other tributaries are the Athhi Nala, the Behta Nadi, the Kalyani Nadi, the Kathna Nadi, Kundu Nala, the Loni Nadi, the Pili Nadi and the Sarayan

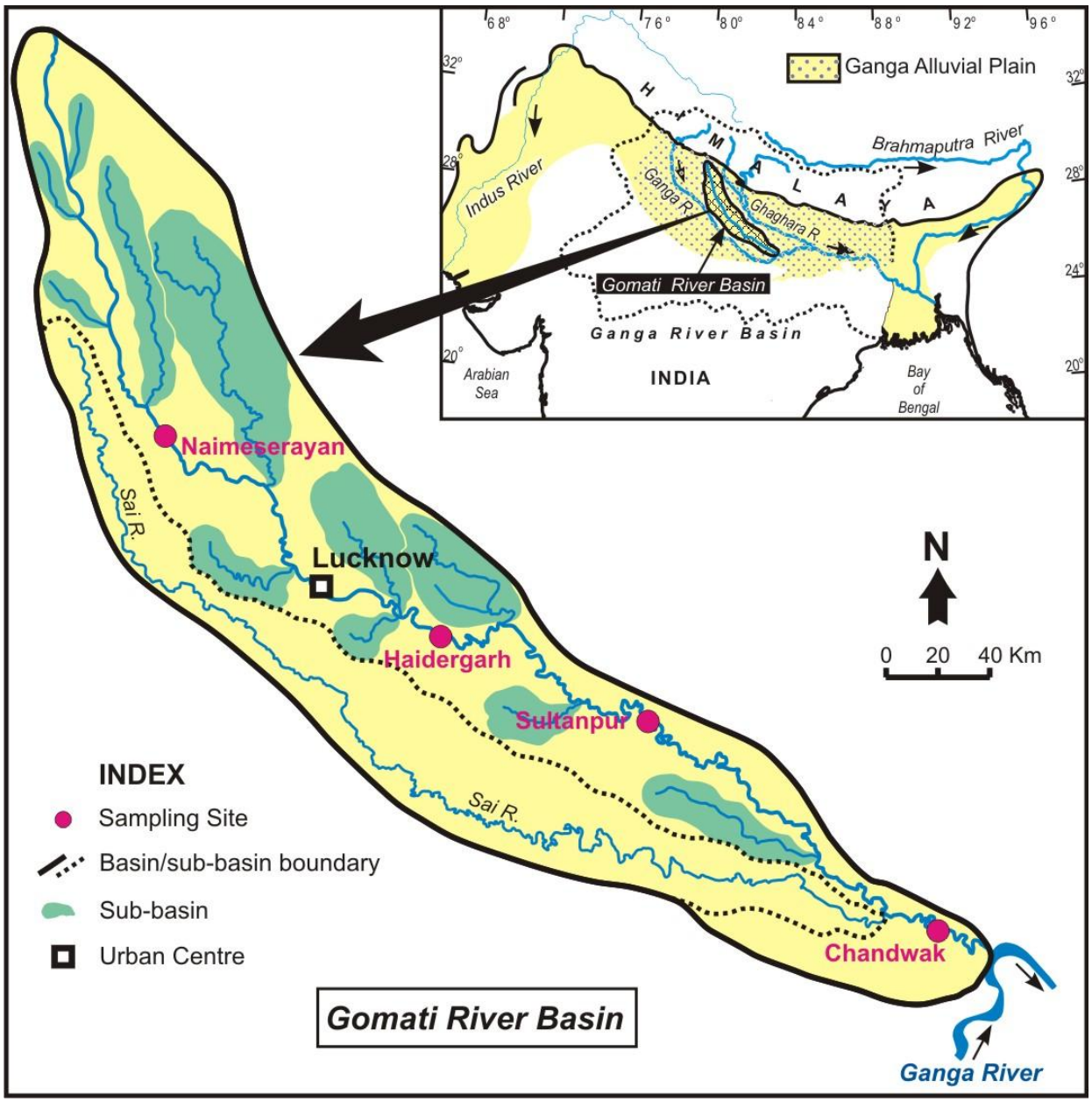

Figure 2.3. Map of the Gomati River Basin showing sample locations (1-Naimeserayan; 2-Haidergarh; 3-Sultanpur and 4-Chandwak) along the Gomati River for the sampling of bedload sediments used in the present study.

Nadi. The average annual water discharge of the Gomati to the Ganges is 7.39 x 109 m^3 (Rao 1979). The annual sediment load and annual sediment erosion rate of the Gomati River basin have been reported to be 6000 x 106 kg and 225 x 103 kg/km^2, respectively (Abbas and Subramaniam, 1984). Sedimentologically, the nature of the sediment transported by the Gomati River is almost same as those of its tributaries and is firmly controlled by the sediments available in the river basin for weathering processes. Geology of the Gomati River Basin affects the mobility of elements during weathering of the Ganga Plain.

2.2.2 Climate

The Gomati River basin experiences a humid sub-tropical climate with four distinct seasons; the monsoon season (June–September), the post-monsoon season (October–November), the winter season (December–February) and the summer season (March–May). Variation in temperature is extreme. Maximum temperature is 47° in summer months and minimum temperature is 2° in winter months. The daily mean maximum temperature is about 30ºC. Annual rainfall in the region varies from 87 to 125 cm. The major part of the rainfall is concentrated in the monsoon months, July–October, due to the SW Monsoon System and basin receives 84% of total rainfall. In monsoon season, rainwater interacts with the alluvium of the Ganga Plain and seeps into the groundwater to become a source of all tributaries of the Gomati River Basin. The post–monsoon season is characterized by moderate temperature and rainfall. Humidity is very high in the monsoon season. Figure 2.4a displays the monthly rainfall, maximum and minimum temperature variations in all the seasons at Lucknow. The hydrology of the Gomati River is controlled by the intensity of rainfall and the duration of the monsoon season. During the monsoon season, heavy rainfall causes 50-100 fold increase in the river's runoff. The river hydrograph is seasonally controlled and highly peaked with annual discharge of the river to be about 7390 × 106 m^3 (Rao 1975). Figure 2.4b displays the hydrograph of the Gomati River characterized by high peak in the monsoon season.

2.2.3 Geology

Geology of the Gomati River Basin influences the mobility of alkali and alkaline earth elements during the weathering of the Ganga Plain. Figure 2.5 shows the longitudinal profile of the Gomati River and downslope surface profile of the regional surface of the Ganga Plain. Longitudinal profile of river helps in interpreting the evolution of river undergoing various geologic processes. The profile starts at 186 m indicating the height of origin of Gomati River and ends at 62 m indicating the height at which it is merging with Ganga River above mean sea level. Elevation difference between the regional surface of the plain and longitudinal profile of the Gomati River shows that the river has incised from 5 to 20 m into the alluvial plain and exposed for weathering. The degree of river's incision increases towards downstream direction (Thakur, 2008).

Singh et al. (1999) have identified five lithofacies in the alluvial deposits exposed in the Gomati River valley margins of the Ganga Plain as shown in figure 2.5. These lithofacies are (i) mottled silt, (ii) variegated clayey silt, (iii) mottled silty sand, (iv) shelly clayey silt and (v)

bedded calcrete. The detailed description of each lithofacies which is exposed on the upland regional surface is as follows:

(i) Mottled Silt: It occurs as 0.5 to 1.5 m thick sheet like or lensoid units of well-sorted silt with little clay fraction and sometimes with calcrete nodules or ferruginous nodules. Mottling is common in the unit. It represents sheet flow deposits on the higher sloping surface of the alluvial plain. The average grainsize composition of this lithofacies is 5 % sand, 92 % silt and 3 % clay (Singh et al., 1999).

(ii) Variegated Clayey Silt: It consists of 1 to 4 m thick highly mottled clay rich silty sediments with intense degree of burrowing with ferruginous nodules. It may represent the deposit of the lower flat surface of the Alluvial Plain. The average grainsize composition of this lithofacies is 8 % sand, 81 % silt and 11 % clay (Singh et al., 1999).

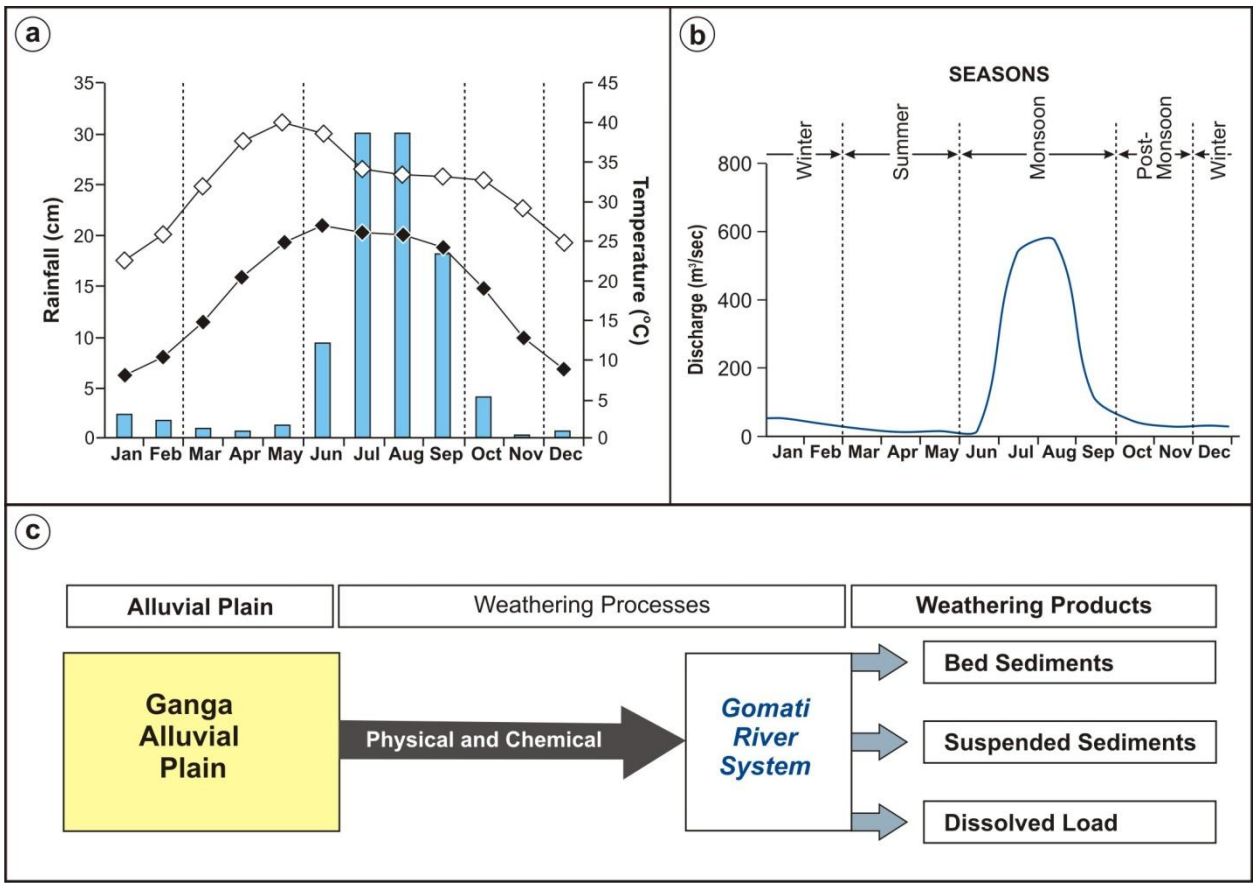

Figure 2.4 Gomati River Basin at Lucknow: (a) Climatograph showing monthly rainfall (in cm), maximum and minimum temperature variation (in °C) during four seasons the winter, the summer, the monsoon and post-monsoon; (b) Hydrograph of the Gomati River displaying seasonal variability in water discharges (Singh et al., 2013) and (c) weathering processes operating in the Ganga Alluvial Plain generate weathering products transported by the Gomati River as dissolved, bedload and suspended load largely during the monsoon and post-monsoon seasons. The Gomati River sediments are considered as weathering products of the Ganga Alluvial Plain having its ultimate sediment source in the Himalayan region.

(iii) Mottled Silty Sand: It represents 1-3 m thick units of silty fine sand showing high degrees of mottling. The unit shows upward fining of the grain size and consists of deposits of small channels. The average grainsize composition of this lithofacies is 50 % sand, 47 % silt and 3 % clay (Singh et al., 1999).

(iv) Shelly Clayey Silt: It comprises 1.0-4.0 m thick muddy successions of considerable lateral extent, rich in clay content and commonly containing molluscan shells. Mottling by roots is very common. The facies represents a deposit of larger lakes on the Alluvial Plain. The average grainsize composition of this lithofacies is 3 % sand, 87 % silt and 10 % clay (Singh et al., 1999).

(v) Bedded Calcrete: It represents 0.5-1.5 m thick bands of calcrete concretions, interlayered with silty and fine sandy sediments. It may show concretized ripple layers. It is diagenetically modified sandy-silt or silty-sand sediments, which can be laterally traced for 50-100 m. The average grainsize composition of bedded calcrete is 10 % sand, 83 % silt and 7 % clay (Singh et al., 1999).

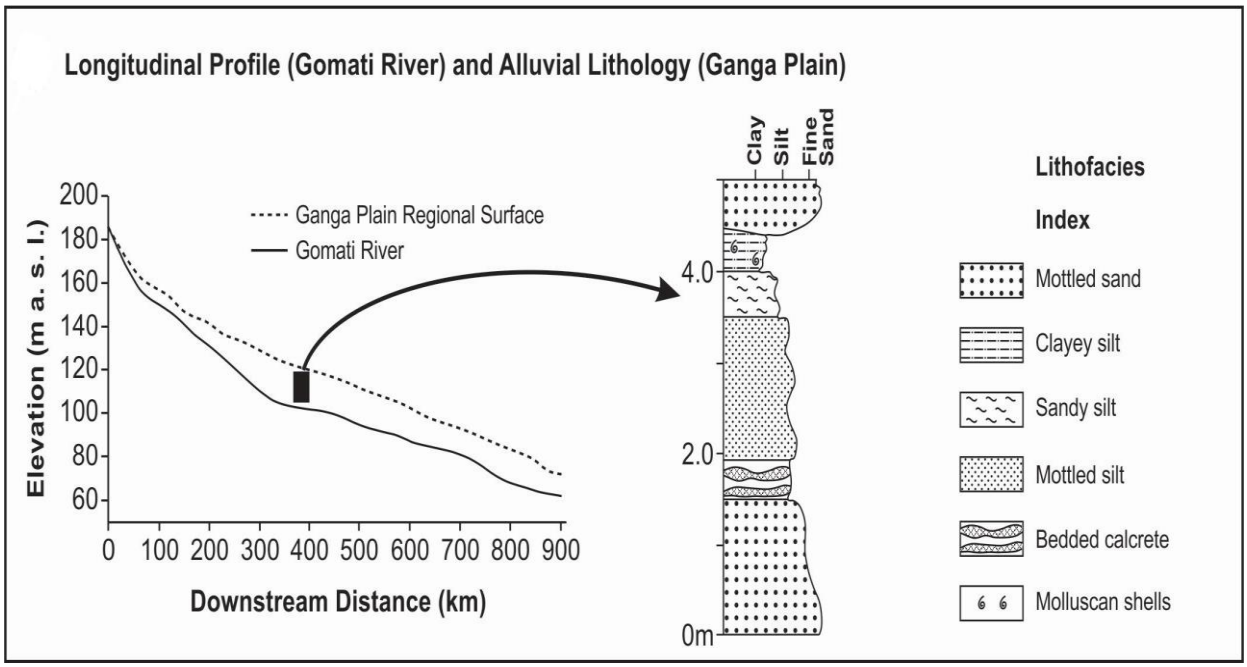

Figure 2.5 Longitudinal profile of Gomati River and Schematic vertical litholog showing various lithofacies of the alluvial deposits uncovered on the margin of the Gomati River valley at Lucknow (Singh et al., 1999)

2.2.4 River Water and Sediments

The Gomati River and its tributaries are alkaline in nature. The average abundance of ions in the Gomati River water (based on milligram per litre units) has been found to be as follows:

$HCO_3^- > Ca^{2+} > Na^+ > Mg^{2+} > (SiO_2) > SO_4^{2-} > Cl^- > K^+ > F^- > PO_4^{3-}$

Bicarbonate is the dominant ion, followed by calcium and sodium in the river water. The water chemistry of the Ganga remains almost same after its confluence with Gomati but sediment chemistry changes. It shows removal of Al, Ca, Mg, Fe, P, Cu, Mn and accumulation of Si, Na and Hg (Gupta and Subramanian, 1994). The Gomati River transports the weathering products of its alluvial basin to the Ganga River as its bed sediments, suspended sediments and dissolved load (figure 2.4c). The bulk chemistry of the Gomati River Sediments largely consists of oxides of three elements: Al, Si and Fe. Channel sediments of the river are mineralogically known as lithic graywacke (Kumar and Singh, 1978). The bedload sediments of Gomati River are composed of chiefly very fine sand (57%), fine sand (24%), silt and clay. The mineralogy of bed sediments reveals the dominance of quartz, followed by plagioclase, alkali feldspar, and mica. Average mineral composition of the river sand consists of quartz (55%), rock fragments (19%), muscovite (15%), K-feldspar (8%), biotite (2%) and plagioclase (1%) (figure 2.6a). The silt fraction of Gomati River sediments consists of quartz, plagioclase, alkali feldspar and mica. Clay fractions in the river sediments are mainly composed of illite (76%) along with montmorillonite (13%), kaolinite (7%) and metastable chlorite (4%) in minor amounts (figure 2.6b).

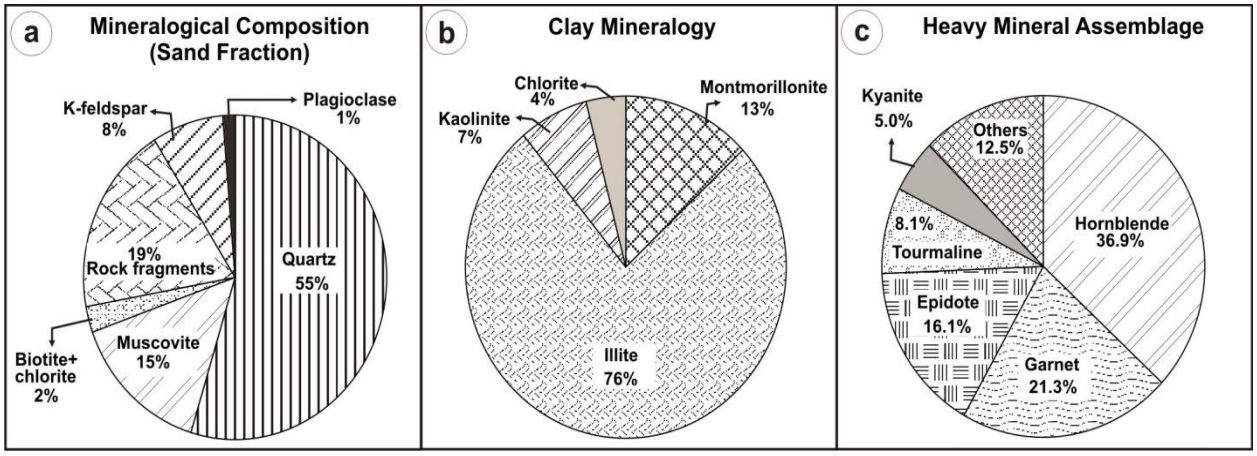

Figure 2.6 Pie diagrams display mineralogical properties of the Gomati River sediments: (a) sand fraction; (b) Clay fraction and (c) Heavy mineral assemblage dominated by hornblende, garnet and epidote. Note the mica rich sand fraction and illite dominated clay as weathering product of the Ganga Alluvial Plain (Kumar and Singh, 1978).

Illite is the main content in clay minerals. Quartz/feldspar and quartz/mica ratios give insight into the chemical and physical weathering processes operating in the basin. Both quartz and feldspar are products formed due to the mechanical breakdown of the rocks of the catchment area. Contrary to the behavior of quartz, feldspar is hugely susceptible to chemical weathering

and gives rise to clay minerals. Mean grain size of the bed load is very fine sand while suspended load varies from coarse silt to very fine silt (Kumar and Singh, 1978; Gupta and Subramanian, 1994). Heavy mineral assemblage in the river sediments are mainly composed of hornblende along with garnet, epidote and tourmaline (figure 2.6c).

Chapter 3 Analytical Techniques

This chapter provides detailed methodology of sampling and analytical techniques followed during present study. It also provides various steps undertaken along with the instrumentation used for the analysis undertaken during study.

3.1 Sampling

The field work has been carried out within the Central Ganga Alluvial Plain (GAP) within the Gomati River Basin (figure 2.3). The selection and preparation of samples forms a very important stage of any geochemical studies, therefore it has to be undertaken very carefully, starting from selection of the sample till the completion of the analysis. Four sampling sites were chosen for the sediments sampling. The 900 km long Gomati River was divided into four parts for the identification of sampling sites, which is based on the accessibility at these locations with the help of toposheets published by the Survey of India. These sampling locations were GR-01 at Naimeserayan; GR-02 at Haidergarh; GR-03 at Sultanpur and GR-04 at Chandwak. Sampling locations along with their details such as latitude, longitude and downstream distance from origin of Gomati River are presented in table 3.1 and shown in figure 3.1. The river sediment samples were collected by scooping the uppermost 5 cm of the channel bar deposits in areas where there is no water during the dry season (March, 2012). The sampling sites were selected carefully to minimize the effects of human activities. Figures 3.2 (a, b, c) display the deposited bedload sediments along with the mica-rich layers. Four sets of bedload sediments (GR-01 to GR-04) and four sets of mica-rich bedload sediments were collected from the Gomati River during the early summer season (March, 2012). All the collected bedload sediment samples were placed in polythene ziplock

Table 3.1 Sampling locations along with latitude, longitude and downstream distance from origin of Gomati River in the Ganga Alluvial Plain. Refer Fig. 3.1 for location along the Gomati River.

Sampling code	Sampling location	Latitude	Longitude	Downstream distance(km)
GR-01	Naimeserayan	27°21′47″N	80°24′40″E	245
GR-02	Haidergarh	26°39′46″N	81°13′14″E	476
GR-03	Sultanpur	26°16′15″N	82°05′30″E	660
GR-04	Chandwak	25°34′41″N	83°04′47″E	861

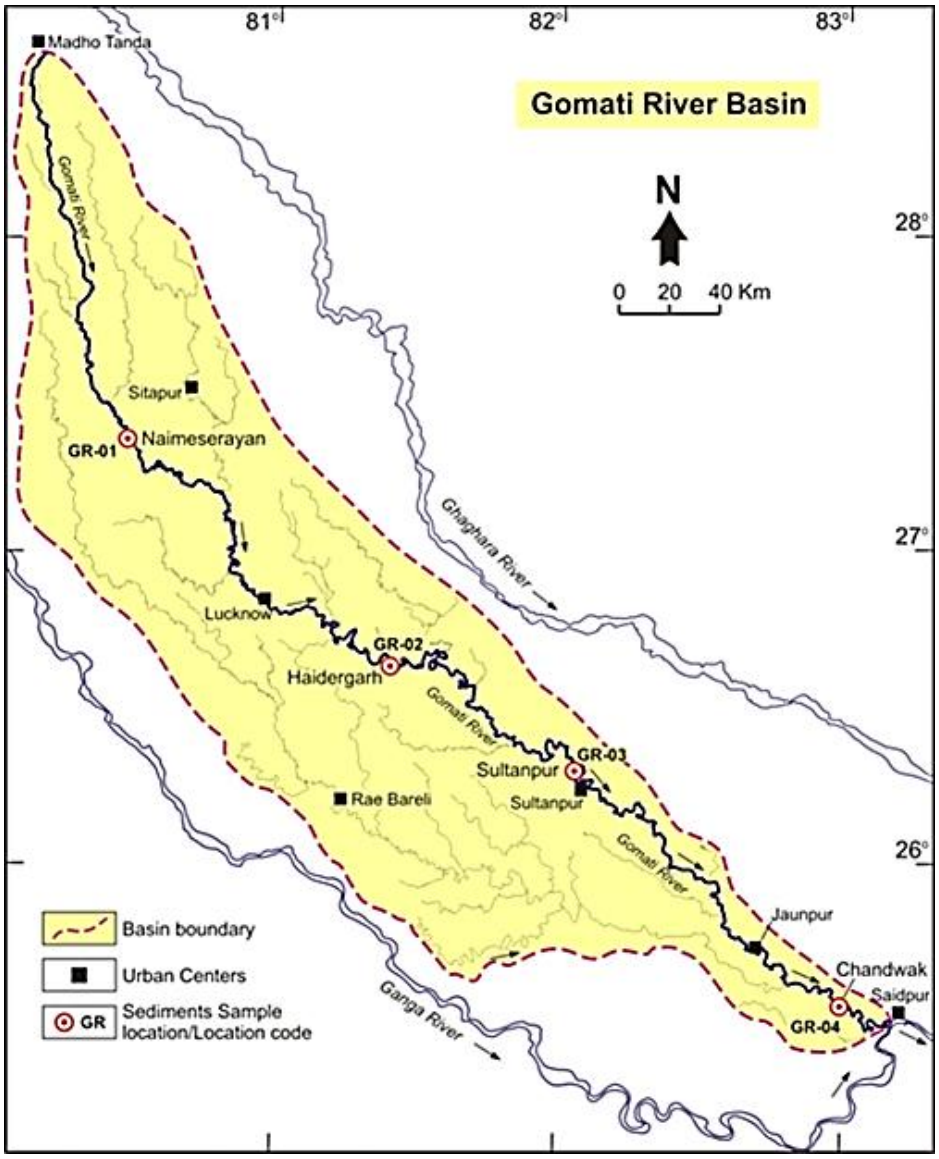

Figure 3.1 Location map of selected sampling sites -Naimeserayan (GR-01), Haidergarh (GR-02), Sultanpur (GR-03) and Chandwak (GR-04) along the Gomati River Basin.

bags and were packed carefully. The samples were transported to laboratory within two days and air dried prior to further sample processing and analysis.

3.2 Sample preparation and Mineral separation

The samples were air dried instead of drying them in oven. The bulk samples were sieved through 60 and 170 mesh sieves, fraction between 60-170 mesh sizes was taken for further analysis (figure 3.3a). The 60 to 170 mesh samples were washed with MQ water and air dried to remove the dust if there is any. The cleaned fractions were carried to mica vibrator where minerals were separated on the basis of roundness of minerals (figure 3.3b).

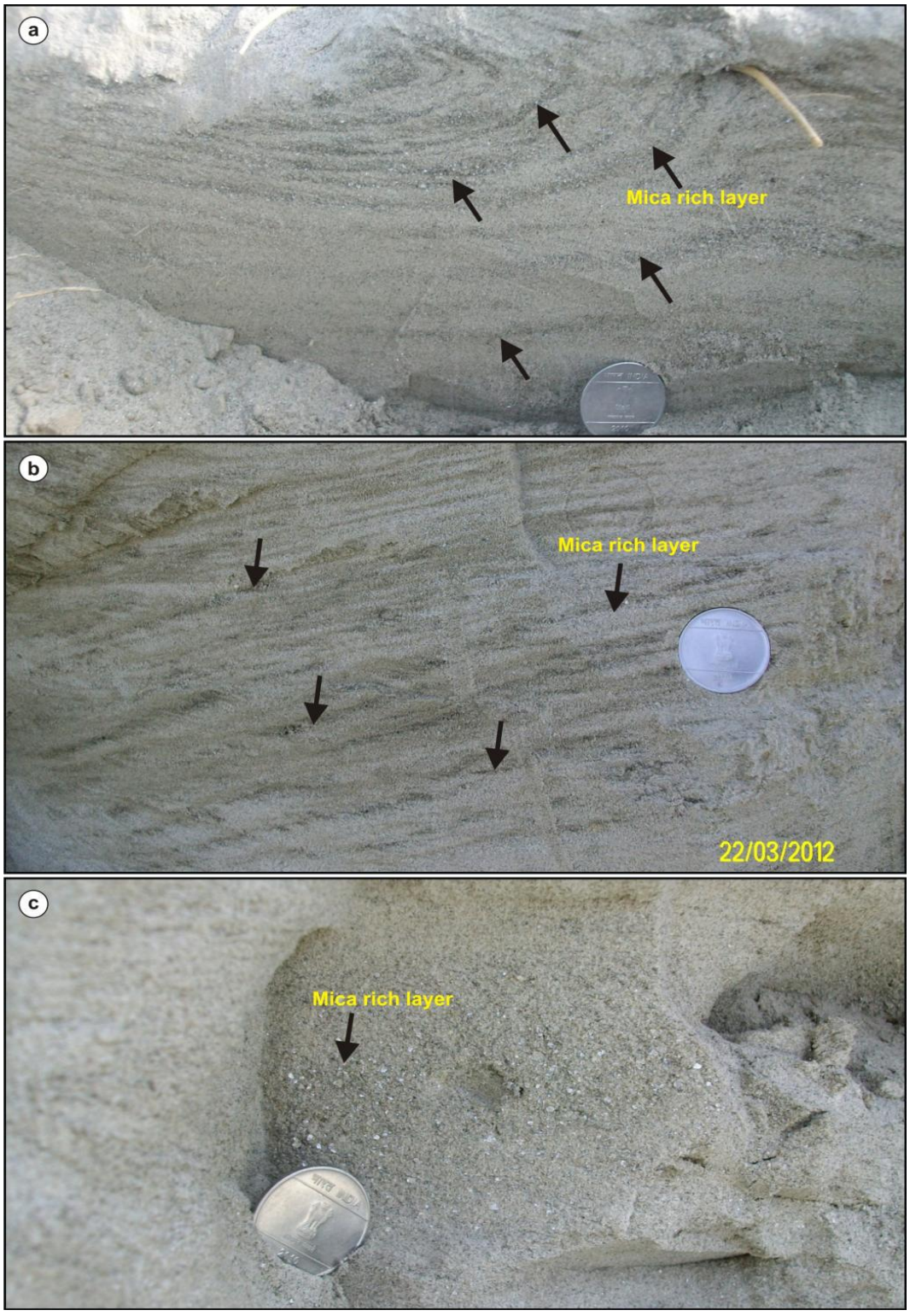

Figure 3.2 Field photographs of bedload sediments of the Gomati River at **(a)** Haidergarh (GR-02), **(b)** Sultanpur (GR-03) and **(c)** Chandwak (GR-04) sampling sites. Black arrow indicates exposed mica-rich layer within the bedload sediments. [Diameter of coin is 2.7 cm].

Most of the Quartz and Feldspars (rounded) and Mica (flat) were separated by passing trough mica vibrator. Quartz and Feldspar rich portion was kept for Feldspar separation. The mica - rich portion was further cleaned in isopropyl alcohol along with mild crushing in the agate

mortar to make the portion free from composite grains in the sample and air dried. Further, Biotite and Muscovite separation has been performed using the Frantz Isodynamic Magnetic Separator at Department of Earth Sciences, IIT- Roorkee (figure 3.3c). Details of separation of these minerals with the help of the Frantz Isodynamic Magnetic Separator and their functions are described below.

3.2.1 Frantz Isodynamic Magnetic Separator (Model LB-1)

Biotite and Muscovite separation of mineral has been performed using Isodynamic Magnetic Separator where mineral grains were allowed to pass through a magnetic field, which separated minerals on the basis of their magnetic susceptibilities. The Isodynamic separator consists of vibrating metal chute, electromagnet with two elongate pole pieces, sample holder and collector. The magnetic separator incorporates an electromagnet with two elongate pole pieces arranged. Arrangement of these two pole shows that space between poles is much wider on one side than narrow on the other side. A vibrating metal chute is parallel with pole pieces. Mineral grains were introduced into sample holder at upper end of chute and were glided towards lower end for sample collector. Those minerals having higher magnetic susceptibility moved towards the side of chute where pole gap was narrow and higher magnetic flux. Separation of mineral particles depend on voltage along with applied ampere to electromagnet, forward and side slope of slide and rate of feed to chute. At the lower end of the chute, particles were separated into two categories. One category consists of grains having higher magnetic susceptibility (biotite) and other consists of grains having lower magnetic susceptibility (muscovite). For mineral separation, magnetic field was set up at 1.2 ampere, 75-85 V voltage with a side slope of 18° and forward slope of 10°. By this process, biotite rich portion was separated from muscovite fractions. Further, muscovite rich portions were run at 12°-15° forward slope, 5° side slope, 2.2 ampere current and maximum voltage by which pure muscovite rich portions were separated. During magnetic separation, precaution was taken to clean the internal parts of the isodynamic separator using pressurised air followed by acetone. Further grains of pure biotite and muscovite have been handpicked using binocular microscope (NIKON). Feldspar has also been separated from Quartz with the help of binocular microscope (NIKON) at Department of Earth Sciences, IIT- Roorkee (figure 3.3d). Figure 3.3e, f, g shows separated mineral fractions- Biotite, Muscovite and Feldspar respectively. Table 3.2 shows the details of sample type and separated mineral fractions. Separated mineral fractions were dissolved for further analysis.

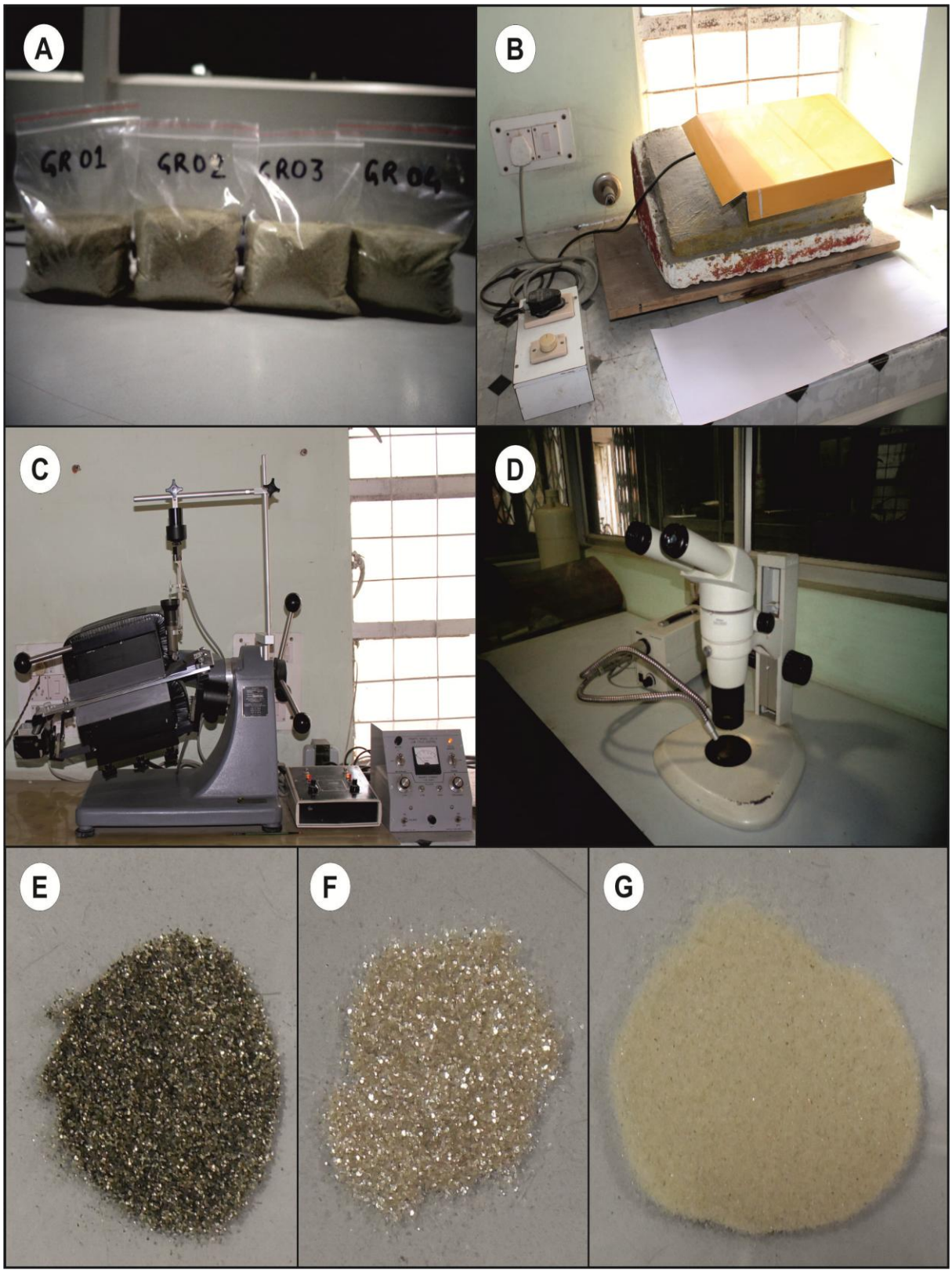

Figure 3.3 (a) Bedload sediment samples, (b) Instruments used during sample preparation - Mica vibrator, (c) Isodynamic separator- Frantz Isodynamic Magnetic Separator (Model LB-1), (d) Binocular Microscope, (e) Separated mineral fractions- Biotite, (f) Muscovite, (g) Feldspar

Table 3.2 Sampling locations along with the details of sample code and separated mineral fractions, GR is used for Gomati River.

Location (Code)	Sample type (Code)	Minerals fraction (Code)
Naimeserayan (GR-01)	Normal bedload (1nbl)	Feldspar (1nblF), Biotite (1nblB), Muscovite (1nblM)
	Mica-rich bedload (1mbl)	Feldspar (1mblF),Biotite (1mblB), Muscovite (1mblM)
Haidergarh (GR-02)	Normal bedload (2nbl)	Feldspar (2nblF), Biotite (2nblB), Muscovite (2nblM)
	Mica-rich bedload (2mbl)	Feldspar (2mblF),Biotite (2mblB), Muscovite (2mblM)
Sultanpur (GR-03)	Normal bedload (3nbl)	Feldspar (3nblF), Biotite (3nblB), Muscovite (3nblM)
	Mica-rich bedload (3mbl)	Feldspar (3mblF), Biotite (3mblB), Muscovite (3mblM)
Chandwak (GR-04)	Normal bedload (4nbl)	Feldspar (4nblF), Biotite (4nblB), Muscovite (4nblM)
	Mica-rich bedload (4mbl)	Feldspar (4mblF), Biotite (4mblB), Muscovite (4mblM)

3.3 Analytical methods and Instrumental Techniques

3.3.1 Sample dissolution for ICP-MS

The separated and collected minerals and sediments samples were prepared to powder for the geochemical analysis with the help of ICP-MS. The following protocols were followed during preparation of samples:

- Weigh about 20 mg of sample with the help of electronic balance on butter paper.
- Transfer the weighed sample into cleaned Teflon vial and moistened it with a few drops of MQ water. Labelling of each vial with detail information and handle carefully.
- Add 10 drops of concentrated HNO_3 followed by 3ml HF, close down the lid.
- Keep the vial on a hot plate for 48 hours at a temperature of 80°-90°C.
- Take down the cap and add few drops of MQ water. Evaporate the sample, add 10 drops concentrated HNO_3 and evaporate completely.

- Add 2ml of concentrated HCl, cap tightly and kept overnight at approximate temperature of 90° C.
- When it becomes jelly add 1 ml of 1:1 HNO_3 shake carefully and see if the samples have dissolved.
- If there is a residue and solution is not clear, sample have been evaporated completely and then added 1:3 concentrated HNO_3 and concentrated HCl.
- Then dry them slowly at low heat.
- When they are almost dry, repeat the last step.
- Dissolve the contents of vial with 10 drops of HNO_3.
- Solution was makeup up to 100 ml volume with Milli Q water.
- Keep solution in cleaned polythene sample bottles for analysis with proper labelling.

After dissolution samples have been taken for ICP-MS analysis. Major and trace elements along with REEs of minerals and sediments were measured by Inductively Coupled Plasma Mass Spectrometer (ICP-MS: Perkin Elmer, ELAN DRC-e) at Institute Instrumentation Centre, IIT- Roorkee (figure 3.4). Duplicate analysis was done for all the samples to provide quality control of the data.

3.3.2 Inductively Coupled Plasma Mass Spectrometry (ICP-MS)

ICP-MS is a type of mass spectrometry which has a very low detection limit and can detect metals and non-metals in parts per trillion (ppt) ranges on non-interfered low-background isotopes. It can easily handle both simple and complex sample matrixes (Garbarino et al., 2006). It measures most of the elements in the periodic table. The instrument used for the analysis is Inductively Coupled Plasma Mass Spectrometer ELAN DRC–e Perkin Elmer Sciex Instrument, controlled by an IBM-PC-XT micro-computer and associated software in the laboratory at the Institute Instrumentation Centre, IIT Roorkee. This instrument ionizes samples into plasma and after that a quadrupole mass spectrometer separate and quantify those ions. An ICP-MS chiefly comprises of four main units-

i. Sample introduction and aerosol generation,
ii. Ionization by an argon plasma source,
iii. Mass discrimination and
iv. Detection system.

Figure 3.4 Photograph showing Inductively Coupled Plasma Mass Spectrometer (ICP-MS: Perkin Elmer, ELAN DRC-e) at the Institute Instrumentation Centre, IIT- Roorkee.

Sample solution is introduced by a nebulizer into argon plasma as aerosol droplets. The aerosol then passes into a spray chamber where larger droplets are removed via a drain. This method is essential to produce droplets small enough to be vaporized in the plasma torch. Plasma torch generates the plasma that serves as the ion source of the ICP mass spectrometer. The atmospheric pressure at ICP ion source and the high vacuum mass spectrometer are linked by the interface. The vacuum system supplies high vacuum for ion optics, quadrupole and detector. The lense focuses ions into a beam for transmission into the quadrupole. The quadrupole mass spectrometer works by permitting only one mass to go through the detector at a time and sorts on the mass to charge ratio (m/z) of the ions. The quadrupole does this by setting up the right combination of voltage and radio frequencies to manage the ions with the selected m/z between the four rods of the quadrupole. The mass spectrometer can move to count m/z required to measure the elements of interest in the sample which is analyzed. The detector counts individual ions passing through the quadrupole.

3.3.3 Sample dissolution for the Sr isotopic analysis

For Sr isotopic analysis the digestion process consists of HF-HNO_3-HCl treatment only. The sample dissolution has been according to the protocol which is being followed at National Facility of Geochronology/ Isotope Geology at Institute Instrumentation Centre, IIT-Roorkee:

- A batch of four samples has been undertaken due to availability of four separation column. Vial number and the sample number have been listed on a page of the lab register.
- Weigh about 100 mg of sample on a butter paper. Transfers it into the vial cross check the weight.
- Wet the samples with a few drops of MQ water to avoid loss of samples due to charging.
- Add 10 drops of concentrated HNO_3 followed by 3 ml HF, close down the lid.
- Keep the vial on a hot plate for 48 hours at a temperature of 80°-90°C.
- Take down the cap and add few drops of MQ water. Evaporate the sample, add 10 drops concentrated HNO_3 and evaporate completely.
- Add approximately 2ml of concentrated HCl, cap tightly and kept overnight at approximate temperature of 90° C.
- When it becomes jelly add 1 ml of 1:1 HNO_3 shake carefully and see if the samples have dissolved.
- There should be a clear solution if not evaporate completely and then add 1:3 concentrated HNO_3 and concentrated HCl.
- Dry them slowly at low heat.
- When they are almost dry, repeat the last step.
- Add 1ml of 2N HCl in each vial shake slightly and put on low heat. They should dissolve completely.
- If they do not dissolve, dry them completely, add 2ml of 6 N HCl and put on low heat, when they dissolve add few drops of MQ water to bring them 2N.
- If still not dissolved add a few drops of $HClO_4$ to each vials and dry now add 2 N HCl. They would dissolve.

This is the procedure for the dissolution of sample for Sr isotopic analysis. After the dissolution process was over the samples were transferred to a centrifuge tube for centrifugation.

Before loading the dissolved samples on the column, it must be free of any trace of precipitate. Even though the sample after dissolving in 2N HCl appears clear, traces of precipitate may still present. Precipitate can be removed by centrifuging the sample prior to loading. The centrifuge tubes carrying the dissolved samples were kept in the centrifuge for ~10 minutes which lead to settling down of the heavier materials in the bottom. After that the

homogenous solution sample was ready for loading for Sr separation to the primary column. Details information is described about Ion exchange chromatography in the following section:

3.3.4 Ion exchange chromatography

Ion exchange chromatography refers to any exchange method involving the distribution of components between a fixed (stationary) and a moving (mobile) phase. The mobile phase is also called the eluent. The stationary phase is a porous solid. Separation of individual components is possible because of differing affinities of the various components towards the stationary and mobile phases, causing different components to move at different rates along the column. The process, in which an eluent makes a compound move along a column, is called elution (Blichert, 1993).

In another words, chromatography occurs due to differences in the movement of the sample constituents resulting from difference in the partioning between two phases. The one phase is an ion exchange resin and the other is either a non- complexioing or a complexing solution leading to the separation of either non-complexed or complexed ions. The resin is generally packed in a suitable glass tube in the column held vertically, and the sample solution is poured on the top of the column. An ion chromatography column for Sr is shown in figure 3.5a. The clean solution of sample (volume 1 ml) from centrifuge tube was loaded into the column on the resin bed. The resin used is Bio-Rad AG 50*8, 200–400 mesh H^+ form cation exchange resin. As the sample moved along the column, all the ions in the samples were adsorbed on the surface of resin. Elution was done with 2N HCl. Sr is a cation and it was attached to the sulphonate group of the resin. By adding more and more HCl to the column, the H^+ ions keep on attaching themselves to the resin. Soon the resin becomes loaded with H^+ ions and the Rb starts detaching from the resin. Later on, Sr followed the same process. Sr has positive charge of two, which is the reason Sr forms stronger bond to the resin than Rb. After elution of Sr, regeneration was done. This was done with the help of 6N HCl which removes all other ions from the column. The protocol for elution for separation at Institute Instrumentation Centre, IIT- Roorkee is illustrated in the table 3.3. A, B, C, D in table 3.3 shows the column name for four samples. First of all sample was loaded on the column and after washing it 9ml 2N HCl was loaded and rejected from the column. Further 5ml 2N HCl was loaded. After this Rb fraction can be collected. Further 8ml 2N HCl was loaded and rejected from the column. After this 8ml 2N HCl was loaded and Sr fraction was collected. After the collection of Sr fraction column was loaded with 12ml 6N HCl for collection of REE fraction. Further column was washed with 20ml 6N HCl for regeneration.

Table.3.3 Protocol for elution process for separation of Sr at Institute Instrumentation Centre, IIT-Roorkee.

Steps				
Sample No:	**A**	**B**	**C**	**D**
Load 8ml 2N HCl				
Load 1ml of 2N HCl (Sample)				
Wash 1ml 2N HCl				
Load and reject 9ml 2N HCl				
Load and collect 5ml 2N HCl(Rb fraction)				
Load and reject 8 ml 2N HCl				
Load and collect 8 ml 2N HCl(Sr fraction)				
Load and collect 12 ml 6N HCl for REE fraction				
Wash with 20 ml 6N HCl for regeneration				
Wash with 20 ml 6N HCl for regeneration				
Wash with 5 ml 2 N HCl				
Wash with 10 ml MQ				

3.3.5 Sample loading for Thermal Ionization Mass Spectrometer (TIMS)

Sample processing for Thermal Ionization Mass Spectrometer involves following steps:

i. **External heating instrument for filaments**

The most extensively used filaments are rhenium, tantalum, and tungsten. For loading of Sr, a single filament assembly was used on which tungsten filaments were welded. The filaments were degassed before loading to remove all the gases present so that these do not interfere with ionization process at the time of analysis. The degassing was done in the Degassing Unit at Institute Instrumentation Centre, IIT-Roorkee. This is a normal procedure followed every time before sample loading. These degassed filaments were then put in the socket of heating instrument. All these filaments were to be handed carefully with the help of forceps with no hand touching to prevent any contamination. 1 µl of TaF_5 was loaded on filament in the centre with the help of micropipette. TaF_5 was used for the base and provided adhesive surface for the sample, and also removed the organic impurities from the sample (Birck, 1986).

The current was increased gradually up to 0.8 ampere to heat the filament and then maintained so that the TaF_5 base becomes viscous and forms a uniform layer over the filament. However, this layer sometimes did not spread over the whole of the filament uniformly as in the case of tantalum filament, and gets bent during the process of its making. As the TaF_5 becomes viscous, the current was slowly reduced to zero. With the help of the same microlitre tip, $TaF_5$was put on all the filaments, which were to be used for the sample loading.

After this process, 2µ litre of MQ water was put into the vial containing sample, which was in the nitrate form [for Sr, it is Sr $(NO_3)_2$]. In nitrate form, sample was easily dissolved in water. Then, 1 µ litre was taken in the pipette from this amount of sample and the sample was loaded on the filament again at the centre of the filament. The current was increased up to 0.8 ampere and maintained for some time till it becomes dry. After that the current was increased till the fumes started coming. Further this current was maintained for some more time till the fumes stopped emerging. The temperature was again increased very slowly till the filament glow bright red. This current was maintained for 15 to 20 seconds and then the current was gradually reduced up to zero. Now the sample was ready to go into turret. All the samples had to follow the same process except that the tip of the pipette had to be changed for each sample. Care should be taken while loading the sample.

The following precautions were taken during sample loading:

a) Tips should be changed for each and every sample after loading and care should be taken so that the same tip is not repeated for the other sample.

b) Current should be increased very slowly otherwise it could lead to loss of sample or burning of filament.

c) After loading the sample, the current should be maintained for some time till the fumes stopped coming. This was done so that the fumes of phosphoric acid could not enter the source chamber during ionization process as removal of fumes from the chamber is very difficult.

ii. Placing of loaded filament on turret

In TRITON T1 turret is a circular wheel with 21 notches, which are all numbered around the wheel, in which filaments can be fixed. In this turret, both single and double filaments can be loaded.

iii. Sample analysis in TIMS

All the samples were analysed in the TRITON T1 Mass Spectrometer (figure 3.5b), installed at the Institute Instrumentation Centre, IIT- Roorkee. For Sr, isotopic ratios $^{88}Sr/^{86}Sr$, $^{87}Sr/^{86}Sr$ and $^{84}Sr/^{86}Sr$ of the mixture were measured.

iv. Data acquisition procedure

When the source vacuum attained a pressure of $5*10^{-8}$mbr in the turret, data acquisition procedure was started. Firstly, Triton software on the desktop was opened and 'Tune' window was selected. In the Cup Configuration Tab, appropriate cup configuration file was selected and 'Set Collector' button was clicked till all the cups were configured in position. A green signal came that indicated the cup configuration was ready for further procedure. Care was taken at this stage since the cup configuration is the most vulnerable part of the instrument. Appropriate sample position was then selected in the 'Sample Wheel' Tab. When the position is ready, a green signal came. 'Filament Control' Tab was then selected to control the current passing through the filament with the following settings:

For Strontium

Up to 2000 mA at a speed of 1000mA/minute. The next 2000-3000 mA at a speed of 500 mA/minute, and. For the rest 3000-3900 mA at a speed of 100 mA/minute.

The signal for ^{88}Sr started coming out at around 3800 mA. As the current reached 3500 mA, ^{88}Sr and H_3 in the 'Scan Control' Tab was selected and the 'set' button was clicked. Then the analyzer was opened. Sometimes signal come faster. In such case, heating was stopped as soon as the optimal signal came (~1.5-2.5V). If the signal came late, the filament was heated upto a little more until a stable beam achieved. The ^{85}Rb peak has been used to monitor the presence of ^{87}Rb so that ^{87}Sr signal is only ^{87}Sr.

The strontium isotopic estimations of the biotite and muscovite minerals were carried out by TIMS at the National facility of Geochronology/Isotope Geology at the IITRoorkee. Isotopic composition of Sr was measured in static multi collector mode with internal and external uncertainties better than 10 ppm. The accuracy of measurement has been revealed by evaluating the NIST SRM 987 several times. The average value for $^{87}Sr/^{86}Sr$ of SRM 987 during the time of analysis was 0.710248 ± 10 ($n = 20$, 1σ).

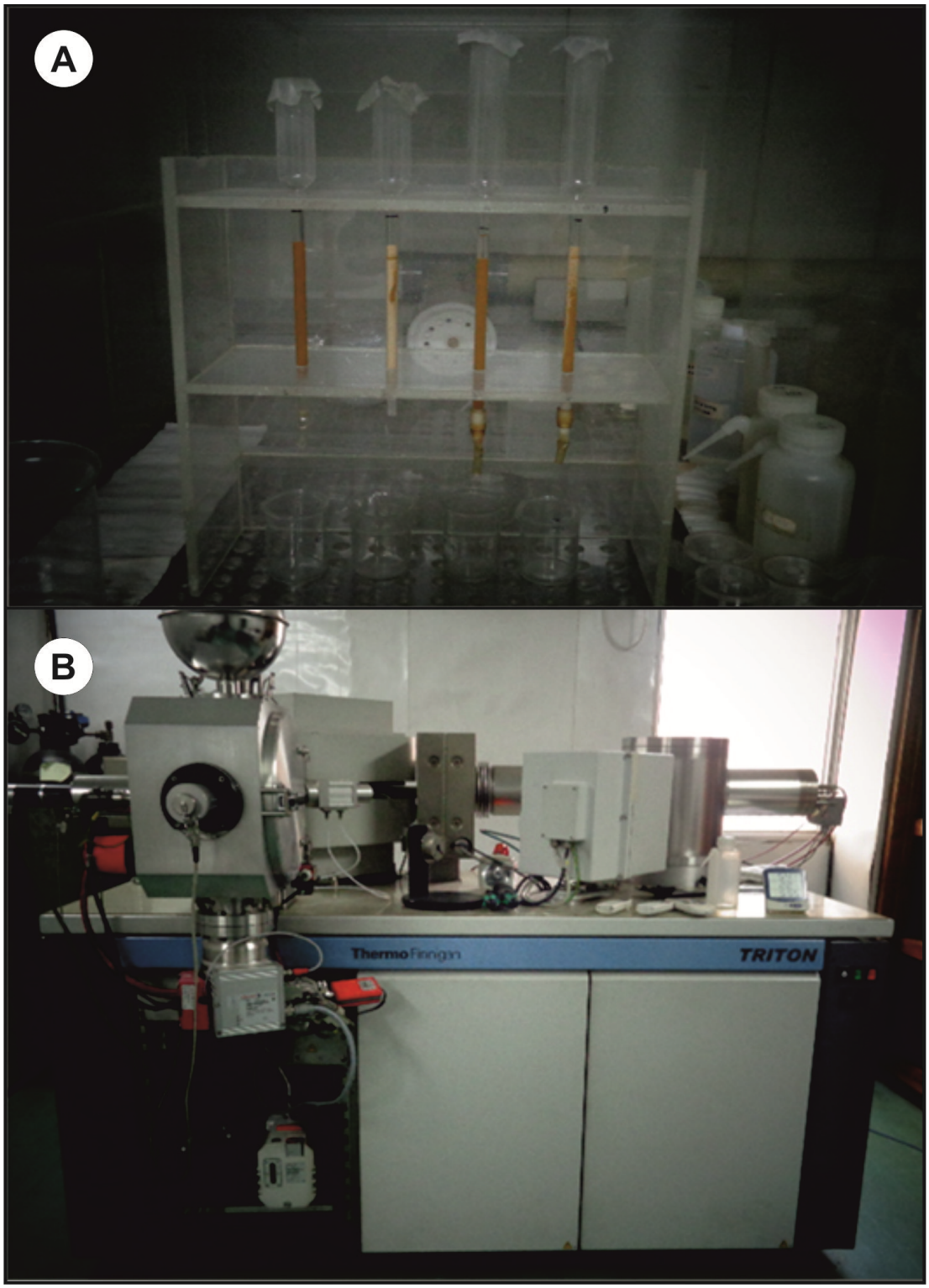

Figure 3.5 Instruments used at National facility of Geochronology/Isotope Geology at the Institute Instrumentation Centre, IIT- Roorkee (A) Ion Exchange Column, (B) Thermal Ionisation Mass Spectrometer (TIMS)-TRITON T1 Model

3.3.6 Thermal Ionisation Mass Spectrometer (TIMS) TRITON T1

TIMS is a highly sensitive isotope mass spectrometry which has the ability to make accurate measurements of isotopic ratios of elements that can be ionize thermally by flowing current

along a thin metal ribbon or ribbons under vacuum. This ion beam then goes through a magnetic field and the original ion beam is scattered into separate beams on the premise of their mass to charge ratio. These isolated beams are guided to the collectors, where the ion beam is changed over into voltage comparison of voltage corresponding to individual ion beams yield exact isotope ratio. This technique is used for the isotope ratio measurements of the elements such as Rb- Sr, Sm-Nd and U-Th-Pb and also for the measurement of REE by isotopic dilution analysis (Dickin, 1995). Most of the mass spectrometer currently used in Isotope Geology is based on the model designed by Neir (1940).The modern Nier-type mass spectrometer consists of three essential parts.

- A source of positively charged mono-energetic beam of ions
- A magnetic analyzer
- An ion collector

In the source region, neutral sample molecules are ionized and then forwarded to the mass analyzer. Analyzer is the prime part of mass spectrometer. The mass analyzer separates ions according to their mass to charge ratio. After the segregation of ions, they are detected and the signal is passed on to a data system for analysis. All mass spectrometer comprises of a vacuum system so that the low pressure or high vacuum needed for operation can be maintained. High vacuum minimizes ion molecule reactions, scattering and neutralization of the ions.

3.3.7 Microanalysis of mica using Scanning Electron Microscope (SEM)

The analysis of mica grains has been done with the help of Scanning Electron Microscope with attached Energy Dispersive X-Ray (EDX) Spectrometer as shown in figure 3.6. The Scanning Electron Microscope uses electrons to form an image of high resolution and magnification and the EDX uses the energy of the X-rays to determine the elemental composition of the specimen. The main function of the EDX is the quantitative analysis of the very small volume of the materials. Under electron bombardment, the constituent atoms emit X-rays. The EDX consists of a solid state detector, typically a Si (Li) detector and an electronic device (analyzer) which performs pulse height analysis. The detector generates pulses whose amplitude is proportional to energies of the incident X-ray photons. The analyzer sorts the pulses according to their height in the channels and counts the number of pulses collected in each channel. X-ray emissions are measured by a Si (Li) detector and are electronically processed to obtain rapid qualitative and semi-quantitative analysis of a sample. X-ray emissions are also used to perform X-ray scanning images which provide information

on the quantification of major and minor elements over a selected area (Goldstein et al., 2003). The collection and process of complete X-ray spectrum is simultaneously used for the identification of elements. The electron gun and column, sample chamber and X-Ray Spectrometer are maintained under a secondary vacuum by means of an oil diffusion pump backed by a mechanical rotary pump. Such a vacuum is required to enhance the filament life, and minimize scatter of the electron beam and adsorption of the low energy X-ray.

Large grains (<200 μm diameter) of mica (biotite) were handpicked with the help of microscope for the analysis. These mica grains were mounted with the help of sputter coater using carbon. Coated biotite samples were placed in EDX spectrometer attached with Scanning Electron Microscope for their analysis. These coated samples were analyzed at unweathered surface and weathered or disturbed surface of samples for their micro chemical analysis.

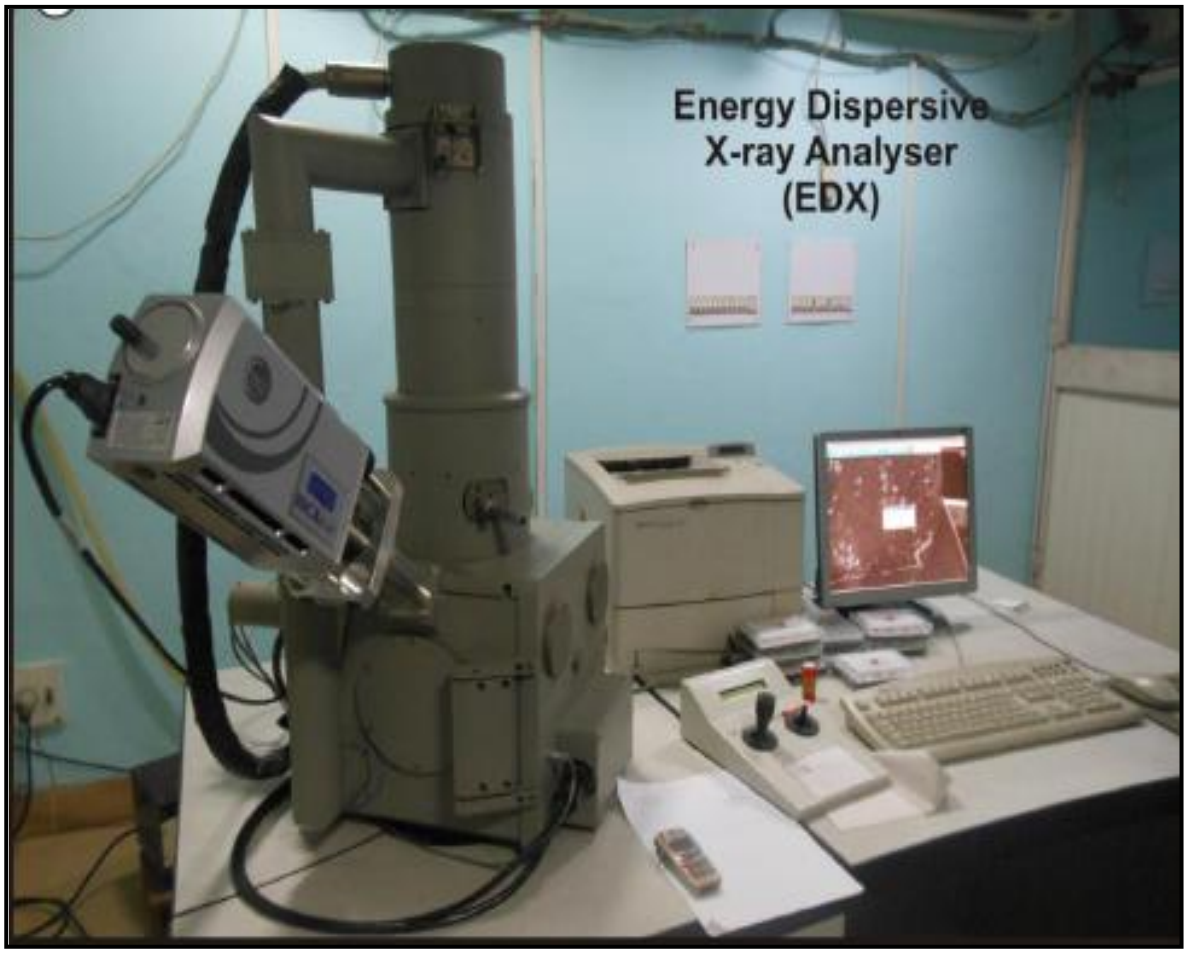

Figure 3.6 Scanning Electron Microscope with attached Energy Dispersive X-Ray (EDX) Spectrometer for analysis of mica (biotite) grains

3.4 Apparatus used in the laboratory

a) Teflon and Savillex beakers

Teflon is the universally used material for solution and sample storage apparatus. Teflon is a fluorocarbon that can be heated up to about 260 °C temperature without thermally degradation or melting and has excellent chemical resistance to acids and alkaline solvents. Teflon is among the cleanest available materials for ultrapure trace elements. A transparent variety of white Teflon is polytetrafluoroethylene used for savillex beakers. Centrifuge tubes, Pipette and Micro tips were used for samples and acid to be carried and used for mixing and adding.

b) Cleaning protocol for the vials

First remove the ink marks outside the vials by rubbing the stains with tissue papers soaked in acetylene and then the vials are soaked in RO water in the beaker without touching them barehanded. These vials are put in beaker containing RO water with mixing of soap solution distilled water for 12 hours for intense cleaning. The vials are heated on the hot plate dipped in 1:1 HNO_3 for 48 hours. The vials are then soaked in 1:1 HCl and put over the hot plate for 48 hours after which the HCl is replaced by RO water and again put on the hot plate for the next 48 hours. Finally before using the vials, they are rinsed in MQ (distilled) water three times for removing all contaminants and kept in the oven for drying and then stored in a contamination free place for use.

After laboratory work and data generation, the geochemical study of bedload sediments, mica- minerals and feldspar and identification of sources of $^{87}Sr/^{86}Sr$ isotopic ratios in Ganga Alluvial Plain (GAP) are presented in the following chapters.

Chapter 4 Results

This chapter incorporates dataset generated from the geochemical analysis of normal (nbl) and mica-rich bedload (mbl) sediments and minerals- Biotite (B), Muscovite (M) and Feldspar (F) as well as Sr isotopic analyses of mica minerals- Biotite and Muscovite from the Gomati River Basin.

4.1 Major elements

Major element composition in river sediments is utilized to study the inter-element relationships and geochemical processes operating on a river basin (Rollinson, 1993). Major elements of minerals and sediments were measured by Inductively Coupled Plasma Mass Spectrometer (ICP-MS: Perkin Elmer, ELAN DRC-e) at Institute Instrumentation Centre, IIT-Roorkee. For the digestion of samples HF-HNO_3-HCl treatment was used. In this treatment when HF is used, it makes volatile compound Silicon tetrafluoride-SiF_4 with Si and gets evaporated. Therefore, Si was not detectable in this procedure. Table 4.1, 4.2, 4.3 list major oxides (Al_2O_3, CaO, $FeO_{(T)}$, K_2O, MgO, MnO, Na_2O, P_2O_5 and TiO_2) (in wt %) in Biotite, Muscovite and Feldspar minerals of normal bedload and mica-rich bedload sediments respectively. In Biotite major elements Al_2O_3 ranges from 29.04 - 33.55 wt%, CaO from 0.43 - 1.14 wt%, $FeO_{(T)}$ from 10.56 - 13.02 wt%, K_2O from 0.60 - 0.99 wt%, MgO from 13.90 - 17.14 wt%, MnO from 0.59-0.88 wt%, Na_2O from 0.13 - 0.69 wt%, P_2O_5 from 1.13 - 1.26 wt%, TiO_2 from 1.10 - 1.45 wt%. In Muscovite major elements Al_2O_3 ranges from 30.98 - 38.46 wt%, CaO from 0.36 - 0.44 wt%, $FeO_{(T)}$ from 2.05 - 3.19 wt%, K_2O from 1.57 - 2.70 wt%, MgO from 2.55 - 3.84 wt%, MnO from 0.03-0.09 wt%, Na_2O from 0.45 - 1.03 wt%, P_2O_5 from 1.20 - 1.62 wt%, TiO_2 from 0.43 - 0.73 wt%. In Feldspar major elements Al_2O_3 ranges from 7.32 - 12.01 wt%, CaO from 2.36 - 5.72 wt%, $FeO_{(T)}$ from 0.11 - 2.72 wt%, K_2O from 0.19 - 0.37 wt%, MgO from 0.08 - 0.99 wt%, MnO from 0.00-0.03 wt%, Na_2O from 1.97 - 2.78 wt%, P_2O_5 from 0.01 - 0.02 wt%, TiO_2 from 4.1 - 12.11 wt%.

In mica-rich bedload sediments, Al_2O_3 ranges from 6.59 - 7.89 wt%, CaO from 10.71 - 19.44 wt%, $FeO_{(T)}$ from 1.23 - 2.07 wt%, K_2O from 2.20 - 2.78 wt%, MgO from 0.56 - 1.09 wt%, MnO from 0.02-0.03 wt%, Na_2O from 1.05 - 1.17 wt%, P_2O_5 from 0.02 - 0.02 wt%, TiO_2 from 0.46 - 0.90 wt%. In normal bedload sediments, Al_2O_3 ranges from 7.72 - 10.02 wt%, CaO from 10.05 - 25.82 wt%, $FeO_{(T)}$ from 1.23 - 2.82 wt%, K_2O from 2.20 - 3.12 wt%, MgO from 0.57 – 1.39 wt%, MnO from 0.02 - 0.04 wt%, Na_2O from 0.97 - 1.13 wt%, P_2O_5 from 0.02 - 0.03 wt%, TiO_2 from 0.33 - 0.98 wt%.

Table 4.1 Chemical composition of major elements in Biotite mineral of normal and mica-rich bedload sediments of Gomati River (wt %)

Sample	Al_2O_3	CaO	$FeO_{(T)}$	K_2O	MgO	MnO	Na_2O	P_2O_5	TiO_2
01 mbl B	32.23	0.83	11.50	0.74	15.01	0.74	0.30	1.13	1.10
02 mbl B	30.15	0.70	10.56	0.76	14.05	0.59	0.44	1.17	1.17
03 mbl B	29.04	1.14	10.95	0.60	13.90	0.88	0.39	1.15	1.15
04 mbl B	30.83	1.13	10.97	0.71	15.07	0.74	0.69	1.21	1.24
01 nbl B	31.88	1.10	12.07	0.71	14.94	0.79	0.14	1.26	1.38
02 nbl B	32.99	0.51	12.70	0.94	16.45	0.62	0.18	1.23	1.41
03 nbl B	32.55	0.55	13.02	0.96	15.83	0.66	0.13	1.24	1.45
04 nbl B	33.55	0.43	13.66	0.99	17.14	0.71	0.69	1.25	1.40

Table 4.2 Chemical composition of major elements in Muscovite mineral of normal and mica-rich bedload sediments of Gomati River (wt %)

Sample	Al_2O_3	CaO	$FeO_{(T)}$	K_2O	MgO	MnO	Na_2O	P_2O_5	TiO_2
01 mbl M	36.38	0.36	2.45	1.75	2.94	0.07	0.97	1.21	0.50
02 mbl M	38.46	0.42	2.32	1.63	2.83	0.05	0.88	1.20	0.43
03 mbl M	33.91	0.40	2.33	1.57	2.77	0.05	1.03	1.26	0.48
04 mbl M	34.62	0.36	2.05	1.66	2.55	0.03	0.45	1.26	0.49
01 nbl M	35.55	0.40	2.89	1.91	3.16	0.09	0.85	1.42	0.57
02 nbl M	36.33	0.44	3.19	2.70	3.84	0.07	0.83	1.62	0.73
03 nbl M	35.53	0.44	2.97	2.49	3.62	0.06	0.83	1.53	0.72
04 nbl M	30.98	0.43	2.30	1.88	3.37	0.04	0.84	1.48	0.56

Table 4.3 Chemical composition of major elements in Feldspar mineral of normal and mica-rich bedload sediments of Gomati River (wt %)

Sample	Al_2O_3	CaO	$FeO_{(T)}$	K_2O	MgO	MnO	Na_2O	P_2O_5	TiO_2
01 mbl F	12.01	2.78	2.72	0.37	0.99	0.03	2.78	0.02	4.10
02 mbl F	9.71	3.83	0.20	0.28	0.17	0.00	2.63	0.01	7.80
03 mbl F	7.47	5.72	0.17	0.21	0.17	0.00	1.97	0.02	12.11
04 mbl F	8.18	3.28	0.15	0.27	0.11	0.00	2.18	0.01	6.81
01 nbl F	9.42	2.36	0.11	0.32	0.08	0.00	2.45	0.02	4.54
02 nbl F	9.09	3.19	0.17	0.26	0.11	0.00	2.46	0.01	6.46
03 nbl F	7.32	2.88	0.14	0.19	0.16	0.00	2.09	0.02	5.71
04 nbl F	8.43	2.56	0.13	0.29	0.08	0.00	2.20	0.01	5.16

Figure 4.1 display bar diagram showing the distribution of Al_2O_3, K_2O and $FeO_{(T)}$ concentrations (in wt %) in the Biotite, Muscovite and Feldspar mineral of mica-rich and normal bedload sediments. The average concentration of Al_2O_3 in the biotite, muscovite and feldspar minerals of normal bedload sediments is 32.74 %, 34.6 % and 8.57 %, respectively. In the mica rich bedload sediments, the average Al_2O_3 content in the biotite, muscovite and feldspar minerals is 30.56 %, 35.84 % and 9.34 % respectively. The average K_2O content in the biotite, muscovite and feldspar minerals of normal bedload sediments is 0.9 %, 2.24 % and 0.27

%, respectively. In the mica rich bedload sediments, the average K_2O concentration in the biotite, muscovite and feldspar minerals is 0.7 %, 1.65 % and 0.28 % respectively. The average $FeO_{(T)}$ concentration in the biotite, muscovite and feldspar minerals of normal bedload sediments is 12.8 %, 2.84 % and 0.14 %, respectively. In the mica rich bedload sediments, the average $FeO_{(T)}$ concentration in the biotite, muscovite and feldspar minerals is 10.9 %, 2.28 % and 0.81 % respectively. Figure 4.2 displays bar diagram showing the distribution of MgO, Na_2O and CaO concentrations (in wt %) in the Biotite, Muscovite and Feldspar mineral of mica-rich and normal bedload sediments. The average concentration of MgO in the biotite, muscovite and feldspar minerals of normal bedload sediments is 16.09 %, 3.5 % and 0.11 %, respectively. In the mica rich bedload sediments, the average MgO content in the biotite, muscovite and feldspar minerals is 14.51 %, 2.77 % and 0.36 % respectively. The average concentration of Na_2O in the biotite, muscovite and feldspar minerals of normal bedload sediments is 0.28 %, 0.84 % and 2.3 %, respectively. In the mica rich bedload sediments, the average Na_2O content in the biotite, muscovite and feldspar minerals is 0.45 %, 0.83 % and 2.39 % respectively. The average concentration of CaO in the biotite, muscovite and feldspar minerals of normal bedload sediments is 0.65 %, 0.43 % and 2.75 %, respectively. In the mica rich bedload sediments, the average CaO content in the biotite, muscovite and feldspar minerals is 0.95 %, 0.39 % and 3.9 % respectively. Al_2O_3 and K_2O have higher percentage in muscovite. CaO and Na_2O have higher percentage in feldspar. MgO and $FeO_{(T)}$ have higher percentage in biotite.

Table 4.4 Chemical composition of major elements in normal and mica-rich bedload sediments of Gomati River (wt %)

Sample	Al_2O_3	CaO	$FeO_{(T)}$	K_2O	MgO	MnO	Na_2O	P_2O_5	TiO_2
01 mbl	6.98	10.71	1.23	2.40	0.56	0.02	1.17	0.02	0.90
02 mbl	7.89	19.44	2.07	2.78	1.09	0.03	1.06	0.02	0.48
03 mbl	6.59	13.24	1.24	2.20	0.62	0.02	1.13	0.02	0.46
04 mbl	7.30	18.44	1.68	2.23	0.81	0.02	1.05	0.02	0.70
01 nbl	7.72	10.05	1.23	2.20	0.57	0.02	1.13	0.02	0.43
02 nbl	10.02	25.82	2.82	3.12	1.39	0.03	0.97	0.02	0.98
03 nbl	8.76	24.09	2.12	2.29	0.89	0.04	1.11	0.03	0.33
04 nbl	7.89	19.08	1.67	2.48	0.80	0.02	1.11	0.02	0.72

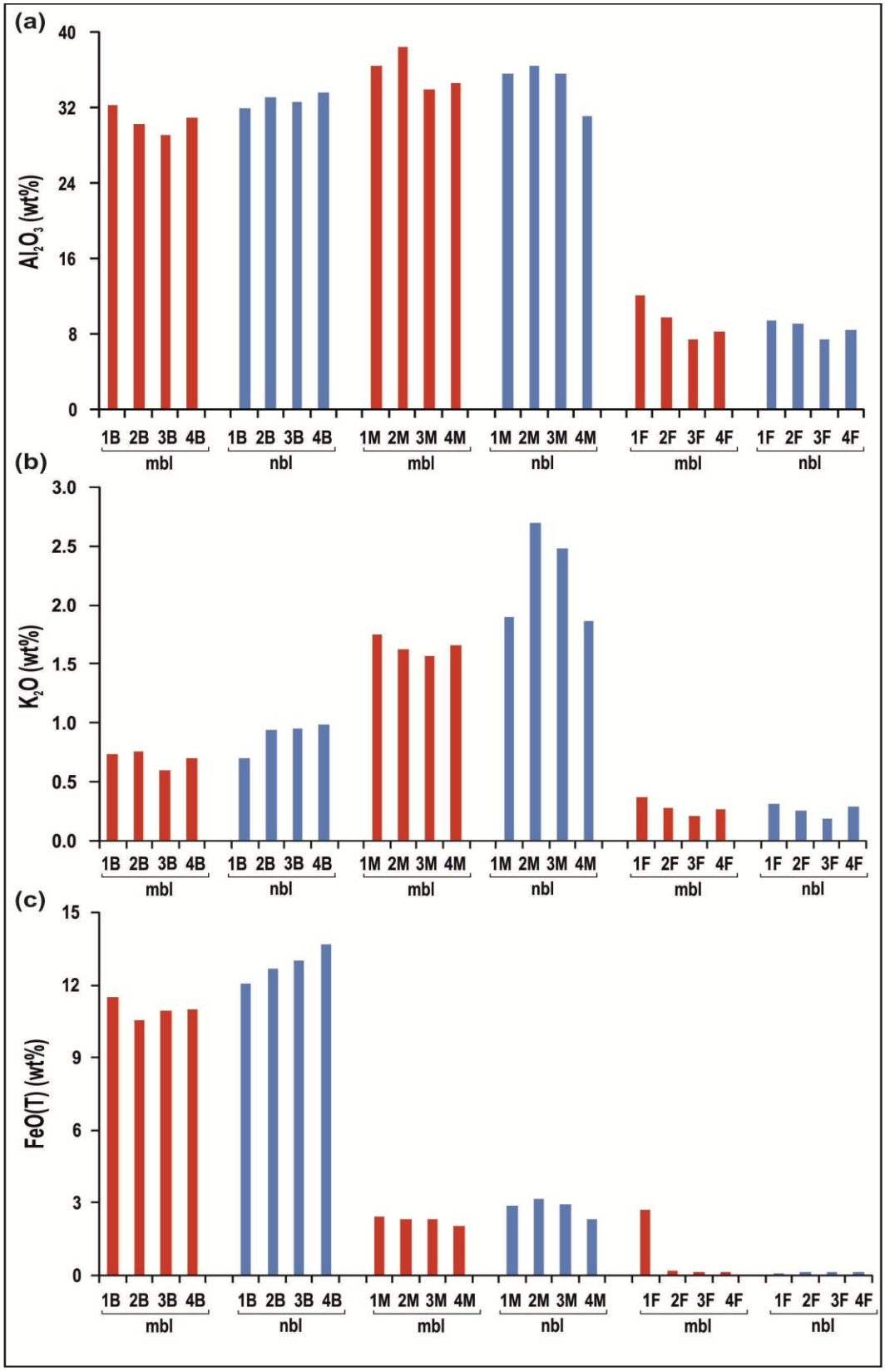

Figure 4.1 Bar diagram showing the distribution pattern of (a) Al_2O_3, (b) K_2O and (c) $FeO_{(T)}$ in Biotite, Muscovite and Feldspar mineral of mica-rich and normal bedload sediments. 1, 2, 3, 4 are the sample locations and B, M, F are Biotite, Muscovite and Feldspar. mbl and nbl represents mica-rich bedload and normal bedload.

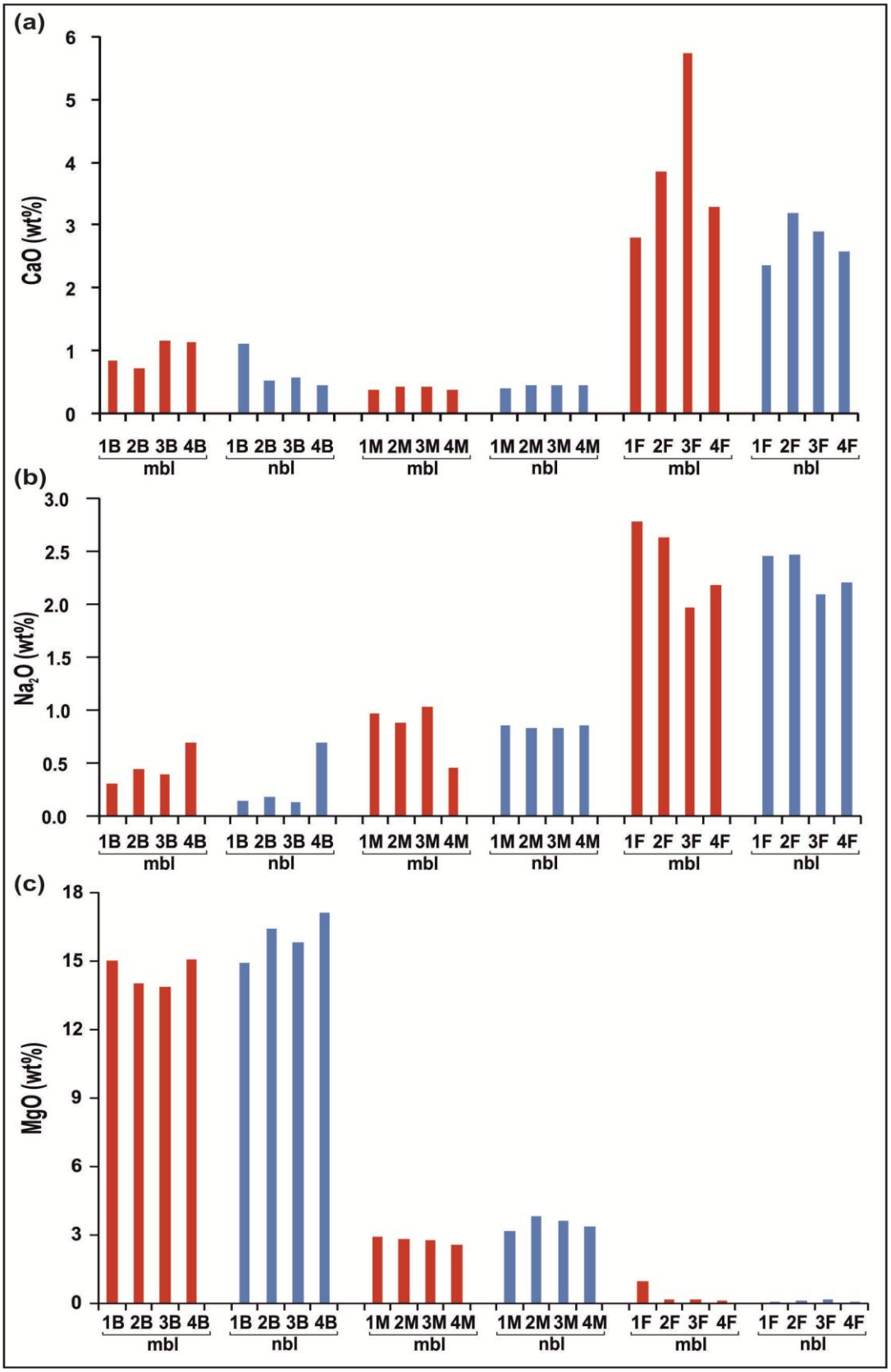

Figure 4.2 Bar diagram showing the distribution pattern of (a) CaO, (b) Na_2O and (c) MgO in Biotite, Muscovite and Feldspar mineral of mica-rich (mbl) and normal bedload (nbl) sediments.

4.2 Trace elements

Trace elements (As, Ba, Be, Bi, Co, Cr, Cs, Cu, Ga, Hg, Li, Ni, Pb, Rb, Se, Sr, U, V and Zn) concentrations (in ppm) in Biotite and Muscovite mineral of normal bedload sediments of Gomati River are presented in Table 4.5. Table 4.6 presents the trace elements (As, Ba, Be, Bi, Co, Cr, Cs, Cu, Ga, Hg, Li, Ni, Pb, Rb, Se, Sr, U, V and Zn) concentrations (in ppm) in Biotite and Muscovite mineral of mica-rich bedload sediments of Gomati River. Trace elements (As, Ba, Be, Bi, Co, Cr, Cs, Cu, Ga, Hg, Li, Ni, Pb, Rb, Se, Sr, U, V and Zn) concentrations (in ppm) in Feldspar mineral of bedload sediments of Gomati River are presented in Table 4.7. Trace elements (As, Ba, Be, Bi, Co, Cr, Cs, Cu, Ga, Hg, Li, Ni, Pb, Rb, Se, Sr, U, V and Zn) concentrations (in ppm) in normal and mica-rich bedload sediments of Gomati River are presented in Table 4.8.

Table 4.5 Distribution of trace elements in Biotite and Muscovite mineral of normal bedload sediments of Gomati River (ppm)

Sample Code	01 nbl B	02 nbl B	03 nbl B	04 nbl B	01 nbl M	02 nbl M	03 nbl M	04 nbl M
As	436.1	433.4	387.5	487.0	301.0	704.9	99.5	318.4
Ba	521.8	485.3	443.0	473.3	1190.6	1363.5	1406.5	1402.5
Be	5.1	8.6	3.8	8.5	9.5	14.4	13.9	12.9
Bi	4.8	4.6	3.2	4.6	0.8	3.7	0.8	2.4
Co	179.8	203.3	223.2	289.3	27.8	23.9	26.7	20.1
Cr	469.9	487.8	523.5	528.1	340.1	422.8	434.8	373.7
Cs	84.4	123.4	139.5	134.7	35.2	47.5	37.5	26.8
Cu	765.1	863.6	785.6	782.2	285.4	361.1	495.8	294.9
Ga	135.4	158.9	141.8	154.6	316.6	444.1	423.4	361.3
Hg	40.9	47.0	16.2	46.8	43.2	114.9	80.5	41.1
Li	340.1	438.2	443.3	423.7	292.6	336.8	319.7	231.7
Ni	2258.8	2205.7	2072.3	2168.5	841.8	1099.5	1143.2	808.2
Pb	127.5	130.0	186.8	184.9	120.5	101.6	137.5	88.7
Rb	1390.2	1881.2	1980.6	1952.4	1343.5	1840.1	1641.3	1241.1
Se	37.9	35.1	27.2	43.7	30.5	41.7	42.5	38.2
Sr	87.0	89.2	105.8	133.2	122.1	167.6	151.7	150.6
U	39.9	9.6	9.9	3.2	0.0	21.8	6.5	3.3
V	1228.4	1155.0	1311.7	1303.1	831.6	950.2	868.6	816.7
Zn	306.4	403.9	364.4	405.1	110.1	134.4	145.4	122.5

In normal bedload Biotite As ranges from 387.5 to 487.0 ppm, Ba from 443.0 to 521.8 ppm, Be from 3.8 to 8.6 ppm, Bi from 3.2 to 4.8 ppm, Co from 179.8 to 289.3 ppm, Cr from 469.9 to 528.1ppm, Cs from 84.4 to 139.5 ppm, Cu from 765.1 to 863.6 ppm, Ga from 135.4 to 158.9 ppm, Hg from 16.2 to 47.0 ppm, Li from 340.1 to 443.3 ppm, Ni from 2072.3 to 2258.8 ppm, Pb from 127.5 to 186.8 ppm, Rb from 1390.2 to 1980.6 ppm, Se from 27.2 to 43.7 ppm,

Sr from 87.0 to 133.2 ppm, U from 3.2 to 39.9 ppm, V from 1155.0 to 1311.7 ppm and Zn from 306.4 to 405.1 ppm. In normal bedload Muscovite As ranges from 99.5 to 704.9 ppm, Ba from 1190.6 to 1406.5 ppm, Be from 9.5 to 14.4 ppm, Bi from 0.8 to 3.7 ppm, Co from 20.1 to 27.8 ppm, Cr from 340.1 to 434.8 ppm, Cs from 26.8 to 47.5ppm, Cu from 285.4 to 495.8 ppm, Ga from 316.6 to 444.1 ppm, Hg from 41.1 to 114.9 ppm, Li from 231.7 to 336.8 ppm, Ni from 808.2 to 1143.2 ppm, Pb from 88.7 to 137.5 ppm, Rb from 1241.1 to 1840.1 ppm, Se from 30.5 to 42.5ppm, Sr from 122.1 to 167.6 ppm, U from 0.0 to 21.8 ppm, V from 816.7 to 950.2 ppm and Zn from 110.1 to 145.4 ppm.

In mica-rich bedload Biotite As ranges from 208.9 to 235.3 ppm, Ba from 377.0 to 562.2 ppm, Be from 2.6 to 9.1 ppm, Bi from 3.3 to 6.6 ppm, Co from 155.7 to 195.2 ppm, Cr from 397.4 to 547.2 ppm, Cs from 66.6 to 103.9 ppm, Cu from 638.3 to 692.9 ppm, Ga from 113.3 to 149.3 ppm, Hg from 25.2 to 66.8 ppm, Li from 282.7 to 383.4 ppm, Ni from 1730.8 to 1960.4 ppm, Pb from 84.4 to 167.4 ppm, Rb from 1039.4 to 1509.2 ppm, Se from 36.3 to 45.4 ppm, Sr from 95.9 to 130.9 ppm, U from 13.6 to 68.5 ppm, V from 1046.8 to 1307.0 ppm and Zn from 245.1 to 325.4 ppm. In mica-rich bedload Muscovite As ranges from 154.5 to 292.8 ppm, Ba from 1066.8 to 1290.5 ppm, Be from 5.2 to 10.5 ppm, Bi from 1.6 to 4.1 ppm, Co from 14.3 to 19.5 ppm, Cr from 270.9 to 341.7 ppm, Cs from 21.0 to 32.4 ppm, Cu from 220.7 to 272.8 ppm, Ga from 261.2 to 289.4 ppm, Hg from 41.7 to 125.0 ppm, Li from 206.6 to 259.3 ppm, Ni from 604.7 to 783.2 ppm, Pb from 78.8 to 138.4 ppm, Rb from 921.1 to 1235.0 ppm, Se from 29.4 to 46.7 ppm, Sr from 102.9 to 155.1 ppm, U from 3.4 to 10.2 ppm, V from 570.1 to 907.9 ppm and Zn from 82.1 to 96.8 ppm.

In mica-rich bedload Feldspar As ranges from 39.48 to 59.12 ppm, Ba from 322.0 to 450.7 ppm, Be from 2.66 to 4.62 ppm, Bi from 0.04 to 0.17 ppm, Co from 0.47 to 10.79 ppm, Cr from 1.04 to 22.44 ppm, Cs from 2.29 to 9.29 ppm, Cu from 1.66 to 9.39 ppm, Ga from 16.34 to 27.61 ppm, Hg from 1.05 to 2.42 ppm, Li from 7.11 to 29.38 ppm, Ni from 1.97 to 26.74 ppm, Pb from 23.04 to 34.61 ppm, Rb from 82.91 to 199.7 ppm, Se from -1.42 to 0.64 ppm, Sr from 109.5 to 147.4 ppm, U from 0.54 to 0.94 ppm, V from 2.90 to 24.29 ppm and Zn from 9.69 to 61.67 ppm. In normal bedload Feldspar As ranges from 29.22 to 68.00 ppm, Ba from 263.2 to 419.0 ppm, Be from 3.22 to 4.02 ppm, Bi from 0.01 to 0.06 ppm, Co from 0.36 to 0.60 ppm, Cr from 0.20 to 1.96 ppm, Cs from 2.22 to 3.51 ppm, Cu from 1.37 to 2.47 ppm, Ga from 14.08 to 20.77 ppm, Hg from 0.47 to 1.26 ppm, Li from 7.47 to 8.25 ppm, Ni from 1.76 to 3.02 ppm, Pb from 22.54 to 37.50 ppm, Rb from 74.95 to 121.8 ppm, Se from -1.79 to -1.31 ppm, Sr from 99.18 to 131.56 ppm, U from 0.47 to 0.79 ppm, V from 2.55 to 3.26 ppm and Zn from 7.44 to 31.40 ppm.

Table 4.6 Distribution of trace elements in Biotite and Muscovite mineral of mica-rich bedload sediments of Gomati River (ppm)

Sample Code	01 mbl B	02 mbl B	03 mbl B	04 mbl B	01 mbl M	02 mbl M	03 mbl M	04 mbl M
As	210.5	208.9	214.5	235.3	154.5	292.8	238.9	245.1
Ba	562.2	471.5	377.0	379.2	1134.4	1066.8	1118.0	1290.5
Be	9.1	3.9	2.6	6.6	5.2	10.4	7.8	10.5
Bi	4.1	6.5	3.3	6.6	1.6	4.1	4.1	1.6
Co	155.7	164.3	186.8	195.2	16.2	18.7	19.5	14.3
Cr	439.4	397.4	448.0	547.2	307.5	270.9	282.4	341.7
Cs	103.9	89.3	66.6	82.1	31.8	26.9	32.4	21.0
Cu	692.9	661.8	638.3	688.7	258.8	220.7	272.8	251.5
Ga	149.3	122.9	113.3	124.4	289.3	274.7	261.2	289.4
Hg	66.4	50.1	66.8	25.2	125.0	41.7	66.8	92.1
Li	383.4	351.6	282.7	294.4	259.3	234.1	248.2	206.6
Ni	1768.3	1861.1	1730.8	1960.4	783.2	604.7	761.9	688.4
Pb	108.7	157.7	84.4	167.4	78.8	88.5	138.4	108.3
Rb	1509.2	1298.9	1039.4	1218.7	1235.0	1084.3	1077.5	921.1
Se	43.8	41.4	45.4	36.3	41.3	46.7	29.4	38.9
Sr	121.2	95.9	102.1	130.9	102.9	137.4	137.0	155.1
U	20.3	13.6	44.2	68.5	3.4	10.2	10.2	6.8
V	1046.8	1307.0	1108.1	1116.7	743.5	907.9	644.4	570.1
Zn	325.4	322.0	245.1	250.4	91.5	82.1	96.8	86.0

In mica-rich bedload sediments As ranges from 51.86 to 76.53 ppm, Ba from 302.9 to 394.6 ppm, Be from 2.09 to 3.84 ppm, Bi from 0.06 to 0.11 ppm, Co from 3.66 to 6.76 ppm, Cr from 15.89 to 27.64 ppm, Cs from 3.84 to 6.6 ppm, Cu from 3.75 to 7.53 ppm, Ga from 18.75 to 24.43 ppm, Hg from 0.8 to 1.52 ppm, Li from 15.03 to 24.9 ppm, Ni from 13.18 to 21.37 ppm, Pb from 14.16 to 15.55 ppm, Rb from 93.34 to 135.14 ppm, Se from -0.4 to 0.33 ppm, Sr from 73.45 to 77.44 ppm, U from 1.46 to 2.18 ppm, V from 22.67 to 35.02 ppm and Zn from 26.59 to 49.18 ppm. In normal bedload sediments As ranges from 62.09 to 88.24 ppm, Ba from 391.69 to 481.08 ppm, Be from 2.17 to 4.19 ppm, Bi from 0.04 to 0.11 ppm, Co from 3.66 to 9.41 ppm, Cr from 23.8 to 41.26 ppm, Cs from 4.18 to 8.91 ppm, Cu from 2.99 to 8.35 ppm, Ga from 24.46 to 33.21 ppm, Hg from 1.17 to 1.86 ppm, Li from 19.83 to 34.39 ppm, Ni from 14.68 to 29.45 ppm, Pb from 14.7 to 16.52 ppm, Rb from 116.5 to 185.5 ppm, Se from 0.45 to 2.40 ppm, Sr from 71.8 to 81.15 ppm, U from 1.6 to 4.82 ppm, V from 27.65 to 49.07 ppm and Zn from 29.21 to 67.06 ppm.

In the mica rich bedload sediments, the average As content in the biotite, muscovite and feldspar minerals is 217.3 ppm, 232.8 ppm and 52.7 ppm respectively. The average concentration of As in the biotite, muscovite and feldspar minerals of normal bedload sediments is 435.9 ppm, 355.9 ppm and 50.3 ppm respectively. In the mica - rich bedload sediments,

Table 4.7 Distribution of trace elements in Feldspar mineral of bedload sediments of Gomati River (ppm)

Sample code	01 mbl F	02 mbl F	03 mbl F	04 mbl F	01 nbl F	02 nbl F	03 nbl F	04 nbl F
As	56.06	59.12	39.48	56.36	40.42	29.22	63.71	68.00
Ba	450.78	367.71	322.03	397.75	419.09	350.50	263.20	390.27
Be	4.62	4.16	2.66	3.35	4.02	4.01	3.22	3.23
Bi	0.14	0.17	0.06	0.04	0.05	0.03	0.06	0.01
Co	10.79	0.66	0.55	0.47	0.36	0.60	0.51	0.41
Cr	22.44	2.97	2.31	1.04	1.96	1.34	0.57	0.20
Cs	9.29	2.70	2.29	3.05	2.58	2.62	2.22	3.51
Cu	9.39	2.57	1.66	1.82	1.61	2.47	1.37	2.38
Ga	27.61	19.71	16.34	18.65	20.77	18.27	14.08	18.84
Hg	2.42	1.68	1.05	1.30	1.26	1.02	0.47	1.08
Li	29.38	9.93	7.69	7.11	8.04	8.25	7.47	8.25
Ni	26.74	2.41	2.96	1.97	1.76	3.02	1.81	1.81
Pb	34.61	29.41	23.04	25.26	37.50	26.47	22.54	25.58
Rb	199.76	107.27	82.91	101.18	121.84	100.03	74.95	112.35
Se	0.64	-0.77	-1.42	-1.09	-1.31	-1.50	-1.79	-1.60
Sr	147.42	141.31	114.26	109.58	131.56	125.06	99.18	110.78
U	0.75	0.67	0.94	0.54	0.49	0.67	0.79	0.47
V	24.29	4.31	3.38	2.90	2.73	3.26	2.55	2.61
Zn	61.67	12.63	9.69	10.66	11.90	31.40	7.44	11.36

Table 4.8 Distribution of trace elements in mica-rich and normal bedload sediments of Gomati River (ppm)

Sample code	01 mbl	02 mbl	03 mbl	04 mbl	01 nbl	02 nbl	03 nbl	04 nbl
As	51.86	61.72	67.67	76.53	62.09	62.11	70.45	88.24
Ba	337.26	394.68	302.99	357.41	393.20	481.08	421.60	391.69
Be	2.56	2.09	3.84	2.22	2.17	2.46	2.47	4.19
Bi	0.08	0.11	0.06	0.06	0.04	0.08	0.06	0.11
Co	3.66	6.76	3.94	5.69	3.66	9.41	7.20	5.78
Cr	15.89	27.64	17.48	22.43	23.80	41.26	28.81	26.67
Cs	4.22	6.60	3.84	5.14	4.18	8.91	5.14	5.31
Cu	3.75	7.53	3.98	5.52	2.99	8.35	5.82	5.31
Ga	19.96	24.43	18.75	22.36	24.46	33.21	28.39	25.51
Hg	1.12	1.52	0.80	1.01	1.23	1.86	1.17	1.33
Li	17.67	24.99	15.03	19.96	19.83	34.39	22.54	21.60
Ni	13.18	21.37	13.46	18.32	14.68	29.45	22.63	19.10
Pb	15.55	15.52	14.37	14.16	16.52	16.05	16.05	14.70
Rb	104.80	135.14	93.34	114.99	116.54	185.56	133.14	126.16
Se	-0.40	0.33	0.29	0.19	0.89	0.45	2.40	1.42
Sr	73.45	75.93	77.44	74.61	79.32	71.80	81.15	78.73
U	1.46	1.68	1.70	2.18	2.05	1.80	4.82	1.60
V	22.67	35.02	23.89	30.40	27.65	49.07	40.09	32.32
Zn	28.35	49.18	26.59	40.33	29.21	67.06	44.39	39.77

the average Ba content in the biotite, muscovite and feldspar minerals is 447.4 ppm, 1152.4 ppm and 384.5 ppm respectively. The average concentration of Ba in the biotite, muscovite and feldspar minerals of normal bedload sediments is 480.8 ppm, 1340.7 ppm and 355.7 ppm respectively. In the mica rich bedload sediments, the average Li content in the biotite, muscovite and feldspar minerals is 328.05 ppm, 237.05 ppm and 13.53 ppm respectively. The average concentration of Li in the biotite, muscovite and feldspar minerals of normal bedload sediments is 411.3 ppm, 295.1 ppm and 8 ppm respectively. In the mica rich bedload sediments, the average Co content in the biotite, muscovite and feldspar minerals is 175.5 ppm, 17.19 ppm and 3.12 ppm respectively. The average concentration of Co in the biotite, muscovite and feldspar minerals of normal bedload sediments is 223.8 ppm, 24.6 ppm and 0.47 ppm respectively. In the mica rich bedload sediments, the average Cr content in the biotite, muscovite and feldspar minerals is 458.02 ppm, 300.6 ppm and 7.19 ppm respectively. The average concentration of Cr in the biotite, muscovite and feldspar minerals of normal bedload sediments is 502.3 ppm, 392.8 ppm and 1.02 ppm respectively. In the mica rich bedload sediments, the average Cu content in the biotite, muscovite and feldspar minerals is 670.4 ppm, 250.9 ppm and 3.86 ppm respectively. The average concentration of Cu in the biotite, muscovite and feldspar minerals of normal bedload sediments is 799.1 ppm, 359.2 ppm and 1.96 ppm respectively. In the mica rich bedload sediments, the average Ni content in the biotite, muscovite and feldspar minerals is 1830.1 ppm, 709.5 ppm and 8.52 ppm respectively. The average concentration of Ni in the biotite, muscovite and feldspar minerals of normal bedload sediments is 2176.3 ppm, 973.2 ppm and 2.10 ppm respectively. In the mica rich bedload sediments, the average Rb content in the biotite, muscovite and feldspar minerals is 1266.5 ppm, 1079.4 ppm and 122.7 ppm respectively. The average concentration of Rb in the biotite, muscovite and feldspar minerals of normal bedload sediments is 1801.07 ppm, 1516.4 ppm and 102.2 ppm respectively. In the mica rich bedload sediments, the average V content in the biotite, muscovite and feldspar minerals is 1144.6 ppm, 716.4 ppm and 8.72 ppm respectively. The average concentration of V in the biotite, muscovite and feldspar minerals of normal bedload sediments is 1249.5 ppm, 866.7 ppm and 2.79 ppm respectively. In the mica rich bedload sediments, the average Sr content in the biotite, muscovite and feldspar minerals is 112.5 ppm, 133.1 ppm and 128.1 ppm respectively. The average concentration of Sr in the biotite, muscovite and feldspar minerals of normal bedload sediments is 103.8 ppm, 148 ppm and 116.6 ppm respectively. Figure 4.3 displays the bar diagram showing the distribution of trace elements As, Ba and Li; Co, Cr and Cu; Ni, Rb and V; Sr and Zn (in ppm) in the Biotite, Muscovite and Feldspar mineral of mica-rich and normal bedload sediments.

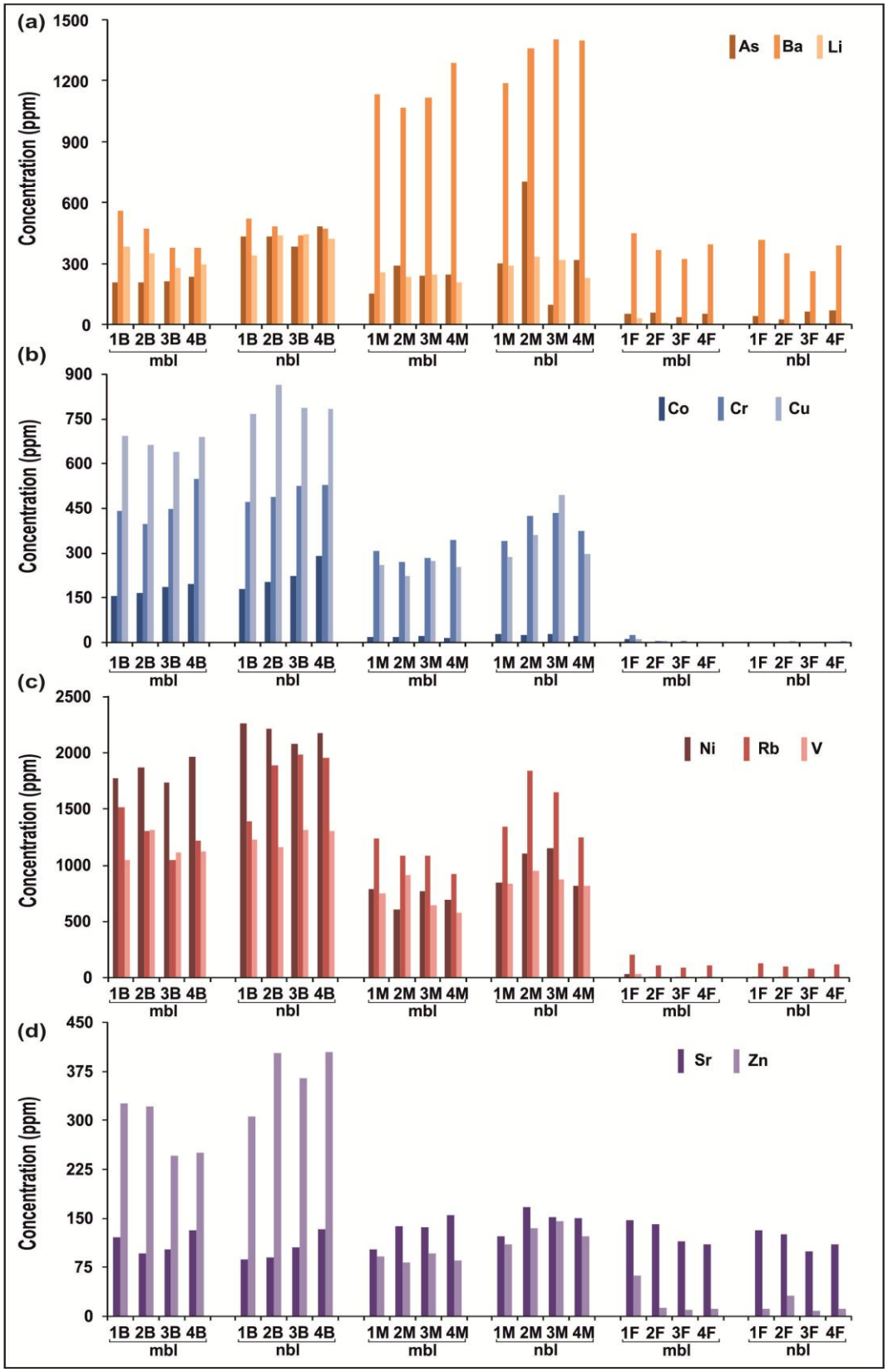

Figure 4.3 Trace elements in the minerals of Gomati River sediments: distribution (in ppm) of (a) As, Ba and Li; (b) Co, Cr and Cu; (c) Ni, Rb and V; (d) Sr and Zn in Biotite, Muscovite and Feldspar minerals

In the mica rich bedload sediments, the average Zn content in the biotite, muscovite and feldspar minerals is 285.7 ppm, 89.1 ppm and 23.6 ppm respectively. The average concentration of Zn in the biotite, muscovite and feldspar minerals of normal bedload sediments is 369.9 ppm, 128.1 ppm and 15.52 ppm respectively.

4.3 Rare Earth Elements

The REE concentrations in the bedload sediments and associated silicate minerals (biotite, muscovite and feldspar) of the Gomati River along with some important fractionation ratios are presented in table 4.9 and 4.10. REE concentrations are widely variable in normal bedload and mica-rich bedload (33.4 – 471 ppm; 40.1 - 1444.6 ppm respectively). These tables also shows ΣREE (sums of La to Lu), light REE (LREE: sums of La, Ce, Pr, Nd, Sm and Eu), heavy REE (HREE: sums of Gd, Dy, Ho, Er, Yb and Lu). The ratios of $(La/Sm)_N$ and $(Gd/Yb)_N$ were used to measure the degree of LREE and HREE, respectively. The ratio of $(La/Yb)_{UCC}$ quantifies the inclination of the UCC normalized REE pattern; when the ratio of $(La/Yb)_{UCC}$ is greater than or equal to 1, the patterns of LREE incline to right side, meaning that the sediment sample is rich in LREE and low in HREE. The concentration of ΣREE in the normal bedload and mica-rich bedload sediments ranged from 88.9 to 323.1 ppm with a mean value of 108.8 ppm. Biotite contains higher average ∑REE concentrations as compared to other minerals and whole sediment. Furthermore LREEs (La to Eu) are more enriched than HREEs (Gd to Lu). LREE/HREE shows ratio ranging from 1.1 – 14; 5.6 – 16 in mica-rich bedload and normal bedload respectively. La, Ce and Nd are the dominant elements in all the samples. All REE values are normalised with the REE values of Chondrite and Upper Continental Crust (UCC) in order to eliminate complication in variation of the absolute concentrations of REE due to natural abundance (Taylor & McLennan, 1988).

4.3.1 Biotite

In biotite (01nblB - Naimeserayan) of normal bedload sediments in upstream direction, ΣREE content is 471 ppm. In downstream direction, biotite registered 70% depletion in ΣREE concentration at sample locations (02 - Haidergarh, 03 - - Sultanpur and 04 - Chandwak). This depletion in ΣREE content of biotite indicates a significant removal of REE during chemical weathering of the Gomati River Basin. Biotite of mica-rich bedload sediments (01mblB - Naimeserayan) was even lower ΣREE content of 375 ppm than those of normal bedload sediments (01nblB - Naimeserayan). In downstream direction, ΣREE show a significant enrichment in the biotite of mica-rich bedload sediments at 02mblB - Haidergarh (455 ppm),

Table 4.9 REE concentrations (ppm) in biotite, muscovite and feldspar minerals and sediments of mica-rich bedload together with some important fractionation ratios.

	Naimeserayan				Haidergarh				Sultanpur				Chandwak			
REE	**1mblB**	**1mblM**	**1mblF**	**1mbl**	**2mblB**	**2mblM**	**2mblF**	**2mbl**	**3mblB**	**3mblM**	**3mblF**	**3mbl**	**4mblB**	**4mblM**	**4mblF**	**4mbl**
La	83.4	98.9	8.3	20.0	100.6	13.7	9.3	20.2	142.1	25.3	12.9	29.0	329.4	16.1	115.6	28.8
Ce	158.8	110.7	16.3	38.0	198.9	26.9	17.6	38.7	284.0	49.8	25.7	54.9	638.9	32.1	163.0	55.9
Pr	17.8	93.9	1.8	4.2	21.9	3.0	1.9	4.2	31.2	5.4	2.8	6.0	71.5	3.5	13.2	6.1
Nd	64.3	95.2	6.8	15.2	79.2	10.5	7.1	15.5	112.2	19.5	10.8	21.7	256.4	12.9	39.0	22.2
Sm	12.1	89.8	1.3	2.7	14.5	1.9	1.3	3.0	21.1	3.5	2.2	3.8	46.1	2.4	4.9	4.1
Eu	2.3	88.2	0.9	0.8	2.2	0.9	0.8	0.8	3.5	1.1	0.8	0.9	6.2	0.9	1.5	0.9
Gd	12.7	87.9	1.5	3.0	14.9	2.0	1.3	3.2	21.8	3.6	2.4	4.0	45.4	2.4	5.0	4.4
Dy	9.6	92.3	1.3	2.1	9.9	1.3	0.8	2.3	16.4	2.1	2.1	2.7	24.5	1.4	1.8	3.1
Ho	2.1	84.6	0.3	0.5	2.0	0.3	0.2	0.5	3.5	0.4	0.4	0.5	4.5	0.3	0.4	0.6
Er	6.4	86.3	0.9	1.3	5.9	0.9	0.5	1.4	10.6	1.2	1.3	1.5	12.5	0.8	1.1	1.8
Yb	4.9	87.7	0.6	1.0	4.3	0.7	0.3	1.1	7.9	0.9	1.1	1.0	8.0	0.5	0.7	1.2
Lu	0.8	83.5	0.1	0.2	0.7	0.2	0.1	0.2	1.2	0.2	0.2	0.1	1.2	0.1	0.1	0.2
LREE	338.7	576.6	35.4	80.9	417.2	56.9	38.1	82.4	593.9	104.6	55.2	116.4	1348.5	67.8	337.2	118.1
HREE	36.3	522.3	4.7	8.0	37.8	5.2	3.1	8.6	61.4	8.5	7.5	9.8	96.1	5.5	9.1	11.3
∑REE	375.1	1098.9	40.1	88.9	454.9	62.1	41.3	90.9	655.3	113.1	62.7	126.2	1444.6	73.2	346.2	129.4
LREE/HREE	9.3	1.1	7.5	10.1	11.1	10.9	12.3	9.6	9.7	12.4	7.4	11.8	14.0	12.4	37.1	10.4
$(La/Sm)_N$	1.0	0.2	0.9	1.1	1.0	1.1	1.1	1.0	1.0	1.1	0.9	1.2	1.1	1.0	3.6	1.1
$(Gd/Yb)_N$	1.3	0.5	1.2	1.5	1.7	1.5	2.2	1.5	1.4	2.1	1.1	2.0	2.8	2.2	3.5	1.8
$(La/Yb)_N$	1.1	0.1	0.8	1.3	1.5	1.4	1.9	1.2	1.2	1.9	0.8	1.9	2.7	1.9	10.4	1.5

Subscript N indicates the normalized abundance with UCC (Rudnick & Gao, 2003)

Table 4.10 REE concentrations (ppm) in biotite, muscovite and feldspar minerals and sediments of normal bedload together with some important fractionation ratios.

	Naimeserayan				Haidergarh				Sultanpur				Chandwak			
REE	**1nblB**	**1nblM**	**1nblF**	**1nbl**	**2nblB**	**2nblM**	**2nblF**	**2nbl**	**3nblB**	**3nblM**	**3nblF**	**3nbl**	**4nblB**	**4nblM**	**4nblF**	**4nbl**
La	104.74	49.32	17.37	21.85	28.99	13.50	7.45	20.10	25.06	19.89	16.31	73.58	26.50	15.63	7.98	27.07
Ce	200.35	96.69	27.53	42.74	57.83	26.78	14.16	39.40	53.82	39.65	30.34	145.02	56.89	29.70	14.88	52.69
Pr	22.35	10.72	2.59	4.60	6.49	2.86	1.52	4.30	5.99	4.26	3.12	15.76	6.30	3.39	1.57	5.73
Nd	81.89	38.95	8.52	16.94	24.73	10.45	5.52	16.05	23.89	15.38	10.98	56.05	25.08	12.78	5.68	20.71
Sm	15.40	7.17	1.41	3.19	5.19	1.97	1.03	3.03	5.30	2.69	1.89	9.85	5.51	2.45	1.05	3.72
Eu	2.83	1.53	0.95	0.75	1.22	0.83	0.70	0.83	1.42	1.05	0.67	1.84	1.40	1.06	0.72	0.90
Gd	16.41	6.98	1.51	3.25	5.88	2.08	1.17	3.29	6.30	2.85	1.93	9.68	6.33	2.62	1.06	3.73
Dy	11.72	4.24	1.00	2.15	5.18	1.43	0.78	2.26	5.74	1.95	1.19	5.38	5.69	1.87	0.71	2.28
Ho	2.35	0.87	0.19	0.41	1.13	0.30	0.17	0.46	1.31	0.39	0.23	1.00	1.24	0.40	0.15	0.44
Er	7.07	2.50	0.54	1.17	3.41	0.91	0.49	1.30	3.96	1.16	0.60	2.84	3.74	1.15	0.42	1.30
Yb	5.14	1.89	0.35	0.75	2.60	0.75	0.34	0.91	2.91	0.84	0.37	1.84	2.82	0.89	0.26	0.88
Lu	0.77	0.30	0.05	0.11	0.39	0.13	0.05	0.13	0.45	0.14	0.05	0.26	0.42	0.14	0.04	0.13
LREE	427.56	204.38	58.37	90.07	124.45	56.39	30.38	83.71	115.48	82.92	63.31	302.10	121.68	65.01	31.88	110.82
HREE	43.46	16.78	3.64	7.84	18.59	5.60	3.00	8.35	20.67	7.33	4.37	21.00	20.24	7.07	2.64	8.76
∑REE	471.02	221.16	62.01	97.91	143.04	61.99	33.38	92.06	136.15	90.25	67.68	323.10	141.92	72.08	34.52	119.58
LREE/HREE	9.84	12.18	16.04	11.49	6.69	10.07	10.13	10.03	5.59	11.31	14.49	14.39	6.01	9.20	12.08	12.65
$(La/Sm)_N$	1.03	1.04	1.87	1.04	0.85	1.04	1.09	1.01	0.72	1.12	1.31	1.13	0.73	0.97	1.15	1.10
$(Gd/Yb)_N$	1.60	1.85	2.15	2.15	1.13	1.39	1.72	1.80	1.08	1.70	2.57	2.63	1.12	1.48	2.04	2.11
$(La/Yb)_N$	1.31	1.69	3.18	1.87	0.72	1.17	1.42	1.42	0.56	1.53	2.81	2.58	0.61	1.14	1.97	1.98

Subscript N indicates the normalized abundance with UCC (Rudnick & Gao, 2003)

03mblB - Sultanpur (655 ppm) and 04mblB - Chandwak (1445 ppm). The ratio of LREE/HREE in mica-rich and normal bedload shows wide variation from 9.3 to 14 and from 5.6 to 9.8 respectively. The values for other characteristics parameters of $(La/Sm)_N$, $(Gd/Yb)_N$ and $(La/Yb)_N$ in mica-rich bedload range from 1 to 1.1, from 1.3 to 2.8, from 1.1 to 2.7 respectively. The values for $(La/Sm)_N$, $(Gd/Yb)_N$ and $(La/Yb)_N$ in normal bedload range from 0.7 to 1, from 1.1 to 1.6, from 0.6 to 1.3 respectively.

In figure 4.4(a) REEs in biotite are enriched relative to upper continental crust. All biotite samples shows similar UCC normalized pattern. Biotite shows fractionated, parallel to sub-parallel REE patterns; REE patterns are enriched in LREE and slightly depleted in HREE with Eu depletion. REE concentration is increasing in downstream direction in biotite of mica-rich bedload and decreasing in normal bedload. It seems mica-rich sample receives unweathered biotite locally. In figure 4.4(b) REEs in biotite are also enriched relative to upper continental crust. Three locations (Haidergarh, Sultanpur, Chandwak) show overlapping abundances of REE patterns, whereas Naimeserayan (01 nbl B) shows high values in REE compared to the other three locations. Eu anomaly is also present in this area. Biotite of mica-rich bedload has distinctly higher abundances of REE than biotite of normal bedload. All Biotite samples show nearly similar UCC normalized REE pattern. Middle REE and HREEs are enriched in biotite of normal bedload relative to upper continental crust. Chondrite normalized REE (Sun & McDonough, 1989) patterns of biotite show similar behaviour in all the samples with LREE enrichment and HREE depletion (Figure 4.5 a,b). Negative Eu anomaly is more pronounced in biotite in both mica-rich and normal bedload. Chondrite-normalised REE pattern of biotite is strongly dependent on mineral weathering signature in the Gomati River Basin. The REE pattern in biotite of most upstream sample (01nblB - Naimeserayan) show the constant decrease with overlapped REE pattern of all biotite of downstream samples (02nblB - Haidergarh, 03nblB – Sultanpur and 04nblB - Chandwak). This consistent decrease is dependent on the Gomati River water composition and linked with low weathering resistance of biotite itself. The REE pattern showed significant removal of REE from biotite occurred in downstream direction of the Gomati River. On the other hand, chondrite-normalised REE patterns of biotite in mica-rich bedload sediments display constant downstream enrichment in all samples (01mblB - Naimeserayan to 04mblB - Chandwak).

4.3.2 Muscovite

The normal and mica-rich bedload show decrease in REE in downstream direction except for Haidergarh area (62 ppm) which shows lower REE than Chandwak. Total REE is higher in mica - rich sediments (1098.9 ppm) than normal sediments (221.2 ppm). The ratio of

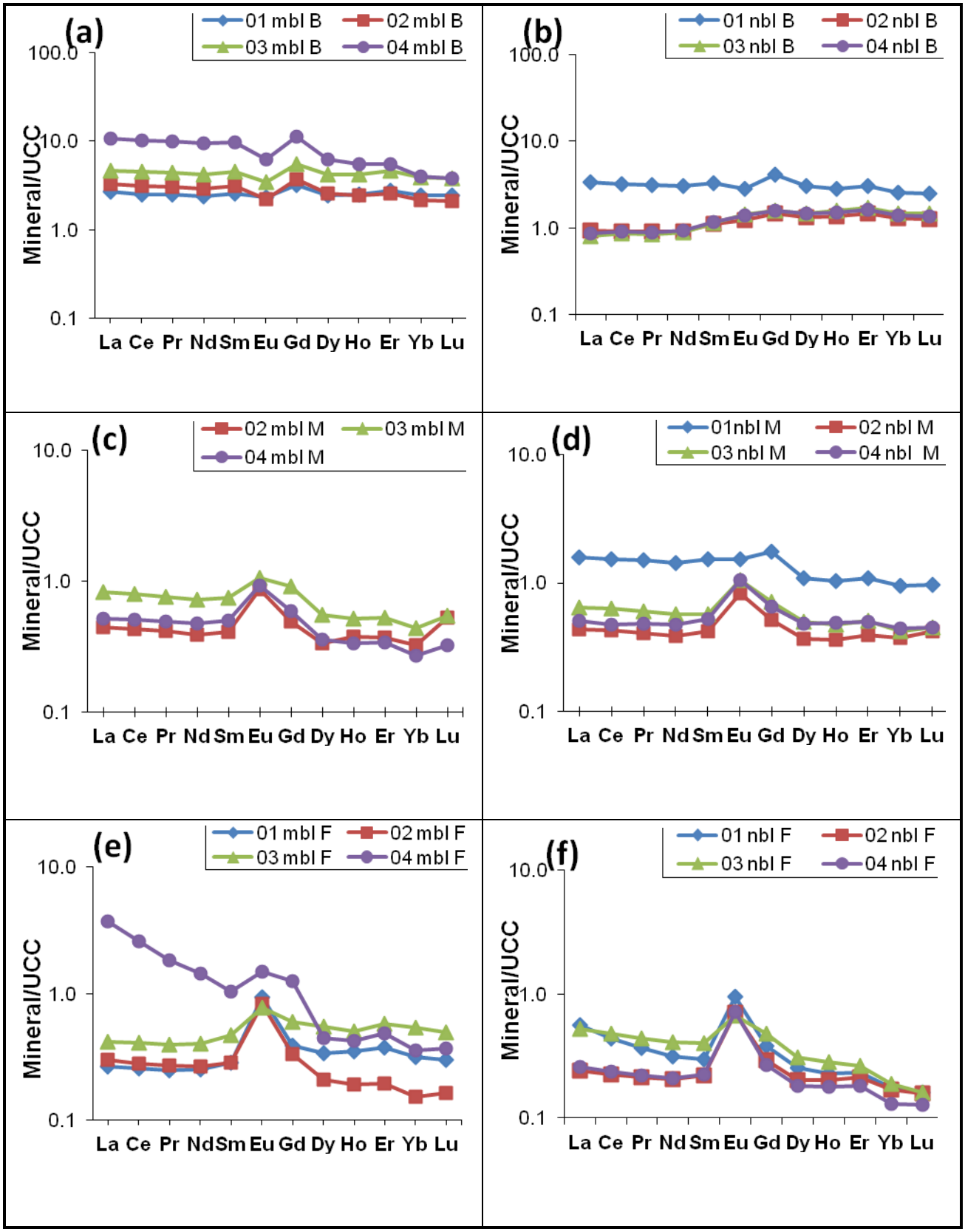

Figure 4.4 UCC normalized REE patterns of (a,b) Biotite, (c,d) Muscovite and (e,f) Feldspar in mica-rich bedload and normal bedload sediments

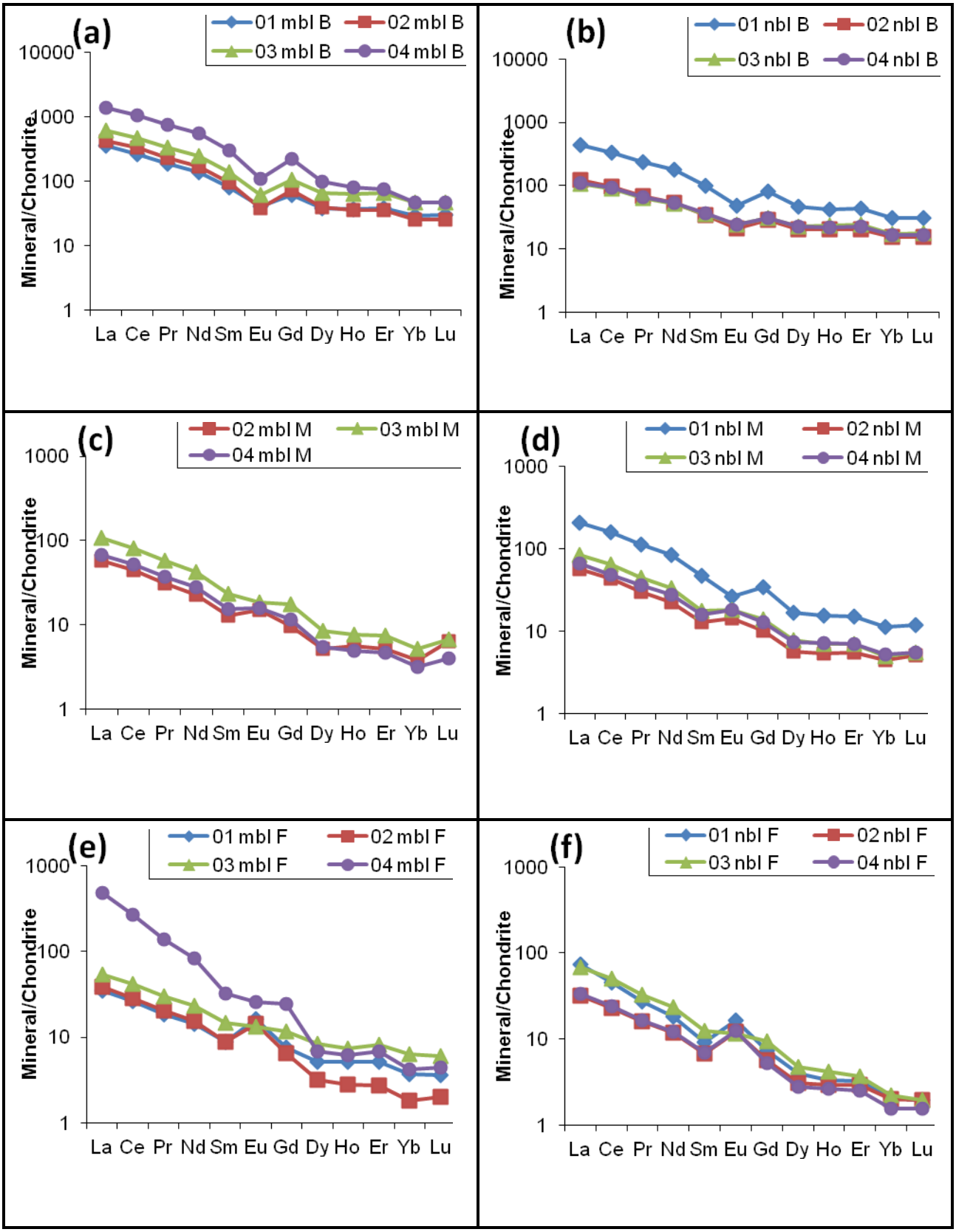

Figure 4.5 Distribution pattern of REE normalized to Chondrite of (a,b) Biotite, (c,d) Muscovite and (e,f) Feldspar in mica-rich bedload and normal bedload sediments

LREE/HREE in mica-rich and normal bedload shows wide variation from 1.1 to 12.4 and from 9.2 to 12.2 respectively. The values for other characteristics parameters of $(La/Sm)_N$, $(Gd/Yb)_N$ and $(La/Yb)_N$ in mica-rich bedload range from 0.2 to 1.1, from 0.5 to 2.2, from 0.1 to 1.9 respectively. The values for $(La/Sm)_N$, $(Gd/Yb)_N$ and $(La/Yb)_N$ in normal bedload range from 1 to 1.1, from 1.4 to 1.8, from 1.1 to 1.7 respectively.

An almost uniform REE pattern is observed in muscovite with positive Eu anomaly (Figure 4.4 c,d). Mixing and homogenizing effects of sedimentary processes produce uniform REE pattern and reflect the abundance in the UCC (Sholkovitz, 1995). All samples show depletion relative to UCC except sample 01nbl M which shows enrichment relative to UCC. Chondrite-normalised REE pattern of muscovite shows overlapping LREE enrichment with nearly flat HREE as shown in figure 4.5 c, d. The muscovite of upstream part of the river basin (01nblM - Naimeserayan) show slight enrichment as compared to others. At the same time, all REE pattern in muscovite show depletion of the one order of magnitude compared to that of biotite in the Gomati River Sediments. Slightly positive Eu anomaly is observed in muscovite.

4.3.3 Feldspar

The mica-rich bedload shows increase in REE in downstream direction from Naimeserayan (40.1 ppm) to Chandwak (346.2 ppm). The ratio of LREE/HREE in mica-rich and normal bedload shows wide variation from 7.4 to 37.1 and from 10.1 to 16 respectively. The values for other characteristics parameters of $(La/Sm)_N$, $(Gd/Yb)_N$ and $(La/Yb)_N$ in mica-rich bedload range from 0.9 to 3.6, from 1.1 to 3.5, from 0.8 to 10.4 respectively. The values for $(La/Sm)_N$, $(Gd/Yb)_N$ and $(La/Yb)_N$ in normal bedload range from 1.1 to 1.9, from 1.7 to 2.6, from 1.4 to 3.2 respectively.

REEs in feldspar are slightly depleted relative to upper continental crust (Figure 4.4 e,f). Two types of samples of feldspar shows nearly similar REE patterns with positive Eu anomaly however sample from Chandwak -04 mbl F shows LREE enrichment and HREE depletion. Positive Eu anomaly shows that Feldspar minerals are enriched in Eu due to the substitution of Eu^{2+} for Sr^{2+} and Ca^{2+}. (Taylor and Mclennan, 1985). Chondrite normalized REE patterns of feldspar show nearly similar behaviour in all the samples with LREE enrichment and HREE depletion (Figure 4.5 e, f). In feldspar, chondrite normalised REE pattern are characterized with weak positive Eu-anomaly. Feldspar (04mblF - Chandwak) in the mica rich bedload sediments from distal part of the Gomati River Basin show significant LREE enrichment as compared with feldspar of other bedload sediments.

4.3.4 Sediment

Average ∑REE is increasing downstream from Naimeserayan (88.9 ppm) to Chandwak (129.4 ppm) in mica-rich bedload. At Chandwak sediments from Sai River are also added, hence its values are very different. The ratio of LREE/HREE in mica-rich and normal bedload shows variation from 9.6 to 11.8 and from 10 to 14.4 respectively. These values are higher than observed in the Chinese river sediments (Range: 3.66 to 7.67 (Zhu et al., 1997). The LREE/HREE ratio showed that the content of LREE is significantly higher than that of HREE. The content of LREE accounted for 90.6-93.5% of the ΣREE content. The values for other characteristics parameters of $(La/Sm)_N$, $(Gd/Yb)_N$ and $(La/Yb)_N$ in mica-rich bedload range from 1 to 1.2, from 1.5 to 2, from 1.2 to 1.9 respectively. The degree of LREE fractionation $(La/Sm)_N$ was slightly lower than that of HREE fractionation $(Gd/Yb)_N$.

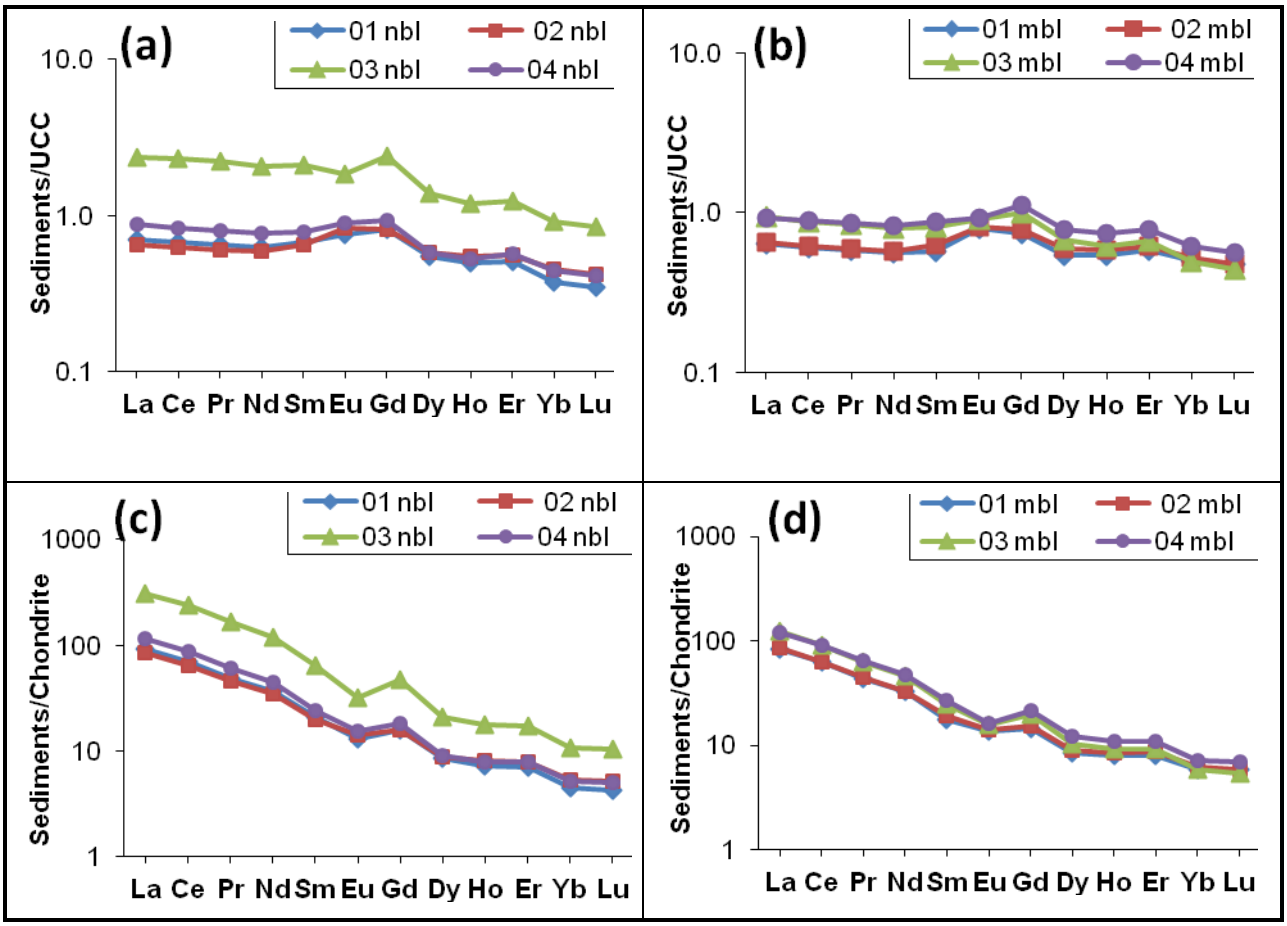

Figure 4.6 UCC and Chondrite normalized REE patterns of (a, c) normal bedload and (b, d) mica-rich bedload of Gomati river sediments.

Gomati river sediments of normal and mica rich bedload are normalized to UCC and chondrite. All bedload samples (except 03nbl - Sultanpur) show similar and overlapping UCC-normalised pattern with each other and produce near neighbour concentration (Eu-Gd) anomalies (Figure 4.6 a,b). The normal bedload sediments of Sultanpur (03nbl) displays the REE enrichment when compare with the bedload sample of other locations. Sediments normalized to UCC shows alike REE patterns and are close to 1 indicating close similarity to average Upper Continental Crust (UCC). MREEs are enriched relative to LREE and HREE. The UCC-normalized patterns of all bedload sediments samples (normal and mica-rich) are more linear and display convex shapes, showing slight enrichment of Eu and Gd. Chondrite normalized patterns of REE have been used for provenance studies (McLennan et al., 1989). Chondrite-normalised REE patterns of all bedload samples (normal and mica-rich) of the Gomati River are displayed in figure 4.6 c,d. The patterns for all bedload samples (except 03nbl - Sultanpur) are similar and overlapping with each other. The characteristic observation in the all pattern is a strong LREE enrichment and HREE depletion with a weak positive Gd anomaly and a negative Eu anomaly. The positive Gd-anomaly has been observed in all bedload sediments along with all biotite samples indicating the common chemical weathering process related to the both type of sediments.

4.4 Sr isotopic ratios

The result obtained from Sr ratio analysis of Biotite and Muscovite mineral are listed in table 4.11. All reported values of the $^{87}Sr/^{86}Sr$ ratio of the Gomati River are notably higher than the global average river water value (0.7119). The $^{87}Sr/^{86}Sr$ ratio of Biotite ranges between 0.72391 (02 mbl B) and 0.73278 (03 nbl B). The Sr isotopic ratio of Muscovite range from 0.74733 (03 mbl M) to 0.78256 (03 nbl M).

Figure 4.7 shows the variation of $^{87}Sr/^{86}Sr$ ratio among Biotite, Muscovite and suspended sediments of Naimeserayan and Haidergarh area. The Sr isotopic ratio is increasing from Biotite to Muscovite to sediments in Gomati River Basin. This difference in $^{87}Sr/^{86}Sr$ values of minerals and sediments may be due to the variation in weathering susceptibility of minerals as Biotite weathers very easily whereas weathering of Muscovite is two orders of magnitude slower than Biotite. Therefore, Biotite loses more Sr into river water due to water-rock interaction and Sr mobility than Muscovite.

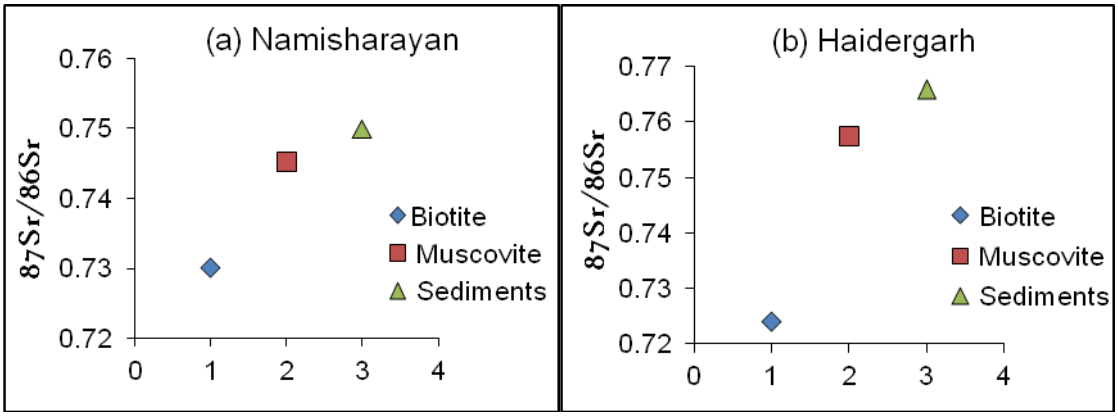

Figure 4.7 $^{87}Sr/^{86}Sr$ ratio of Biotite, Muscovite and sediments of (a) Naimeserayan and (b) Haidergarh area (normal bedload)

Table 4.11 Sr isotopic ratios of muscovite and biotite minerals in Gomati river bed load sediments

Location	**Sample Code**	**Minerals**	**$^{87}Sr/^{86}Sr$**	**1/Sr**
Mica-rich bedload (mbl)				
Naimeserayan	01 mbl M	Muscovite	0.745207± 5	0.010
	01 mbl B	Biotite	0.730051 ± 9	0.008
Haidergarh	02 mbl M	Muscovite	0.757487 ± 6	0.007
	02 mbl B	Biotite	0.723917 ± 17	0.010
Sultanpur	03 mbl M	Muscovite	0.74733 ± 26	0.007
	03 mbl B	Biotite	0.725249 ± 8	0.010
Chandwak	04 mbl M	Muscovite	0.763845 ± 18	0.006
	04 mbl B	Biotite	0.728749 ± 11	0.008
Normal bedload (nbl)				
Naimeserayan	01 nbl M	Muscovite	0.758778 ± 88	0.008
Haidergarh	02 nbl M	Muscovite	0.776183 ± 13	0.006
	02 nbl B	Biotite	0.727705 ± 21	0.011
Sultanpur	03 nbl M	Muscovite	0.782564 ± 13	0.007
	03 nbl B	Biotite	0.732788 ± 76	0.009
Chandwak	04 nbl B	Biotite	0.728287 ± 9	0.008

Trends in Figure 4.8 shows that lower of $^{87}Sr/^{86}Sr$ have lower Sr content (Biotite, 0.7239-0.7327) and higher $^{87}Sr/^{86}Sr$ has higher Sr content (Muscovite, 0.7452-0.7825). Biotite has lower $^{87}Sr/^{86}Sr$ and lower Sr content in sediments of Gomati River Basin. This may be due to two reasons- one is decrease in Sr concentration and second is variation in intensity of weathering of carbonates and silicates. This is credited to relative increase in carbonate weathering (which lowers $^{87}Sr/^{86}Sr$ of rivers) and dilution of Sr concentration due to increase in water discharge (Tripathi et al., 2010).

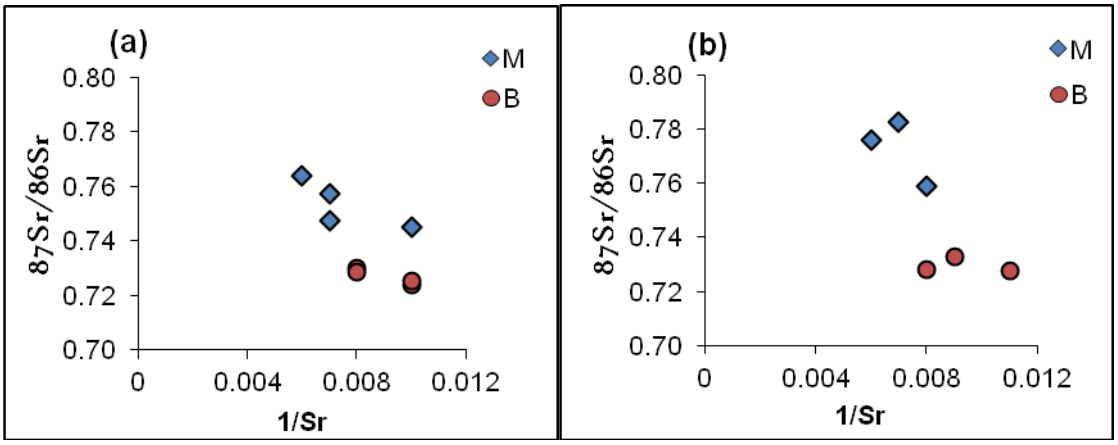

Figure 4.8 Mixing Plot of $^{87}Sr/^{86}Sr$ vs. 1/Sr for Muscovite and Biotite minerals of (a) mica-rich bedload (mbl) and (b) normal bedload (nbl)

Table 4.12 Geochemical composition of clastic sedimentary rocks from the Chakrata Formation, Lesser Himalaya Pelites (Rashid, 2002) and biotite and tourmaline leucogranites and HHCS metasediments from Zanskar (Ayres and Harris, 1997) (major -wt%, trace -ppm).

	Lesser Himalaya Rocks		Higher Himalaya Rocks		
	Pelites	**Quartzites**	**Biotite leucogranite**	**Tourmaline leucogranite**	**Metasediments**
Al_2O_3	16.34	2.22	14.74	14.77	15.93
CaO	0.30	0.15	0.70	0.6	1.41
Fe_2O_3	5.43	0.74	1.00	0.87	6.58
K_2O	4.19	0.56	4.43	4.09	3.47
MgO	1.56	0.38	0.17	0.16	2.8
MnO	0.05	0.02	0.02	0.04	0.1
Na_2O	1.10	0.10	3.91	4.42	1.92
P_2O_5	0.09	0.01	0.17	0.17	0.3
TiO_2	0.73	0.08	0.09	0.06	0.7
La	64.99	12.03	10.8	5.8	37.4
Ce	90.20	17.45	23.2	12	76.6
Sm	10.03	1.45	3	1.3	7
Eu	1.67	0.38	0.63	0.27	1.35
Dy	6.26	1.20	-	-	-
Yb	5.28	0.87	1.29	0.95	5.9
Lu	0.79	0.13	0.18	0.14	0.9

For comparative study major and REE, data of Lesser Himalayan rocks - Chakrata Formation (Rashid, 2002), Higher Himalayan rocks from Zanskar (Ayres and Harris, 1997) and alluvial sediments of Behta Nala section in Gomati River Basin (Kuvar, 2012) is used. For Sr isotope study data of the Ramnagar cliff section (Baskey, 2009), Sr isotopic data of water of Gomati River Basin (Paliwal, 2007) and data of Behta Nadi cliff section (Geethumol, 2008) and is used. These data are presented in tables 4.12, 4.13, 4.14, 4.15 and 4.16 respectively.

Table 4.13 Major oxides distribution (wt%) in alluvial sediments of the Behta Nala section in the Gomati River Basin of Ganga Plain (Kuvar, 2012)

Sample	A01	A02	A03	A04	A05	A06	A07	A08	A09	A10	A11	A12	A13	A14	A15	A16
Al_2O_3	12.99	5.86	7.42	8.31	9.06	10.3	7.85	7.55	11.7	11.18	9.57	12.84	7.59	11.84	12.37	7.65
CaO	6.85	25.11	8.11	7.66	6.83	8.46	6.96	9.42	10.3	8.58	5.27	6.76	24.4	12.41	7.97	24.2
Fe_20_3	6.02	3.27	2.94	3.86	4.45	4.61	3.82	3.79	6.73	5.36	5.6	6.56	4.88	6.29	5.95	5.09
K_2O	3.7	2.04	2.28	2.76	3.03	3.08	2.77	2.64	3.55	2.55	2.63	3.25	2.43	3.29	3.3	2.5
MgO	4.59	3.17	3.43	3.31	3.55	4.25	2.88	2.86	5.23	3.04	3.05	3.61	3.28	4.22	4.03	3.3
MnO	0.08	0.07	0.06	0.06	0.06	0.07	0.05	0.06	0.06	0.07	0.07	0.09	0.16	0.09	0.08	0.11
Na_2O	1.14	1.09	1.63	1.44	1.42	1.33	1.41	1.31	1.22	2.55	1.71	1.49	0.7	1.02	1.18	1.01
P_2O_5	0.12	0.06	0.12	0.15	0.13	0.15	0.15	0.13	0.11	0.15	0.11	0.17	0.04	0.11	0.15	0.04
TiO_2	0.66	0.4	0.4	0.47	0.51	0.56	0.46	0.45	0.65	0.7	0.59	0.73	0.47	0.65	0.65	0.49

Table 4.14 Sr isotope data of the Ramnagar cliff section (Baskey, 2009)

Events	Sample no.	Depth (m)	$^{87}Sr/^{86}Sr$
Event 5 (4.2m)	S12	0	0.732957
Event 4 (3.9m)	S11	4	1.394329
	S10	7.3	0.738905
Event 3 (7.5m)	S9	8.6	0.733038
	S8	9.5	0.765556
	S7	11.5	0.765109
	S6	15.2	0.751044
Event 2 (2.3m)	S5	16.1	0.761807
	S4	17.3	0.762344
	S2	18.5	0.759996
	S1	20	0.747045

Table 4.15 Sr isotopic data of water of Gomati River Basin (Paliwal, 2007)

Sample no.	Location	$^{87}Sr/^{86}Sr$	1/Sr
GW- 4	Haidergarh	0.727728±22	0.002
GW- 9	Sultanpur	0.729630±26	0.003
GW- 14	Chandwak	0.727616±15	0.003
GW- 25	Namisharayan	0.730650±14	0.003

Table 4.16 Sr isotope data of the cliff section, right margin of the Behta Nadi (Geethumol, 2008)

Units	Sample Id	$^{87}Sr/^{86}Sr$
A	S 1	0.743758± 14
	S 2	0.761481± 62
B	S 3	0.741307± 99
	S 4	0.765473± 41
	S 5	0.763931± 82
C	S 6	0.753120± 37
D	S 7	0.743758± 38
	S 8	-
E	S 9	0.733305± 59
	S 10	0.740060± 80
F	S 11	0.724380± 62
	S 12	0.732295± 87
G	S 13	0.737412± 89
	S 14	--
H	S 15	--
	S 16	0.743224± 11
	S 17	--

4.5 Microanalysis of Mica Minerals

Mica minerals are phyllosilicate minerals and consist of octahedral (o-layer) sheet sandwich between two identical tetrahedral (t-layer) sheets producing the characteristic of t-o-t layer. The octahedral units are linked to others by sharing octahedral edges. In biotite, all the

three octahedral sites are occupied by elements (trioctahedral mica); whereas in muscovite, only two octahedral sites are occupied by elements (dioctahedral mica). Since the t-o-t structure is negatively charged, an interlayer cation (K) neutralises the electrical structure. In the Gomati River sediments, both mica minerals (muscovite and biotite) are present in the bedload deposits of the Gomati River as the weathering products of the Gomati River Basin. Scanning Electron Microscopic analysis along with Energy dispersive X-ray microanalyses were performed for

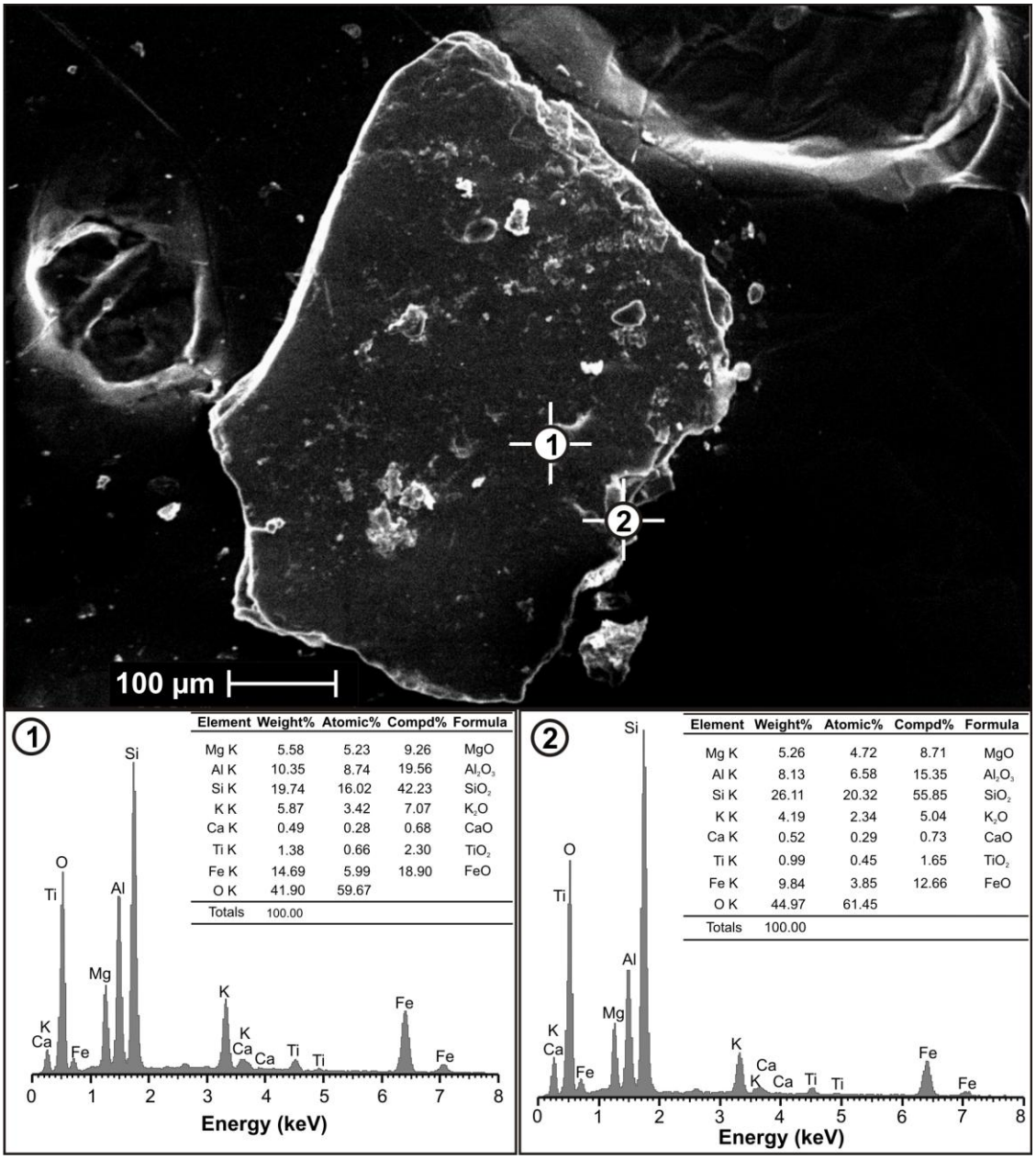

Figure 4.9 Scanning Electron Micrograph showing **(1)** unweathered basal portion and **(2)** weathered marginal portion of biotite flake. Energy Dispersive spectrum of these portion showing peaks of elements along with data table showing percentage of weight atom and formula. Biotite flake selected from the bedload sediments sample collected at Naimeserayan (GR-01).

semi-quantitative elemental analysis of edge and basal surface of biotite minerals. Elemental quantitative analyses yielded the weight, atomic and compound percentages with formula of the elements with elemental peaks. Figure 4.9 shows the microphotograph of biotite grain isolated from the bedload sediments samples collected at Naimeserayan (GR-01). The margins of the biotite grain display the distinctive tonal changes due to weathering effects. The scattering of elemental peaks with the percentage table of atomic, weight and compound at the unweathered basal and weathered edge of biotite grain are also displayed in figure 4.9. The atomic percentage of Al at basal surface is 8.74 and decreased to 6.58 at the marginal edge. The atomic

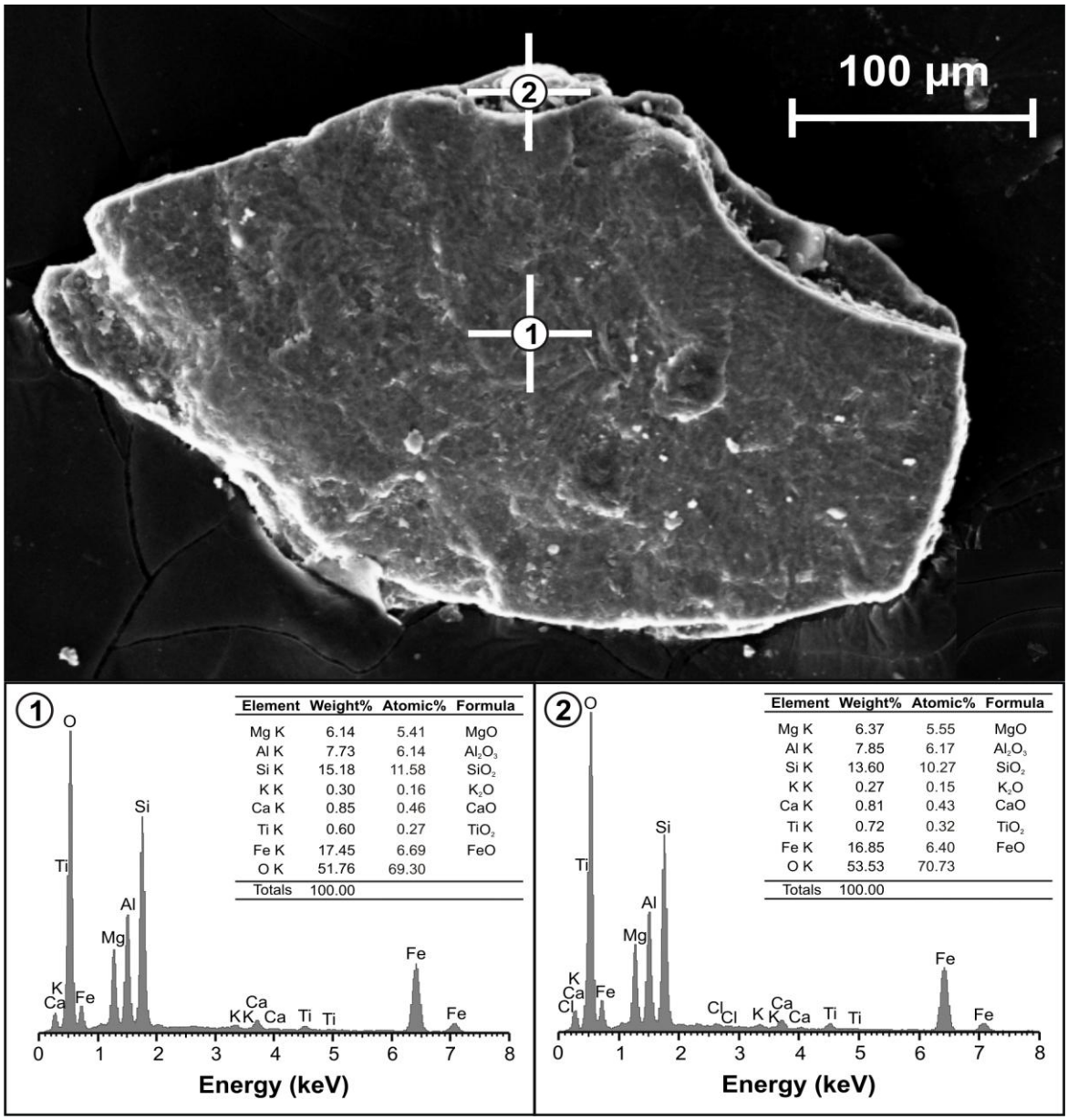

Figure 4.10 Scanning Electron Micrograph showing **(1)** unweathered basal portion and **(2)** weathered marginal portion of biotite flake. Energy Dispersive spectrum of these portion showing peaks of elements along with data table showing percentage of weight atom and formula. Biotite flake selected from the bedload sediments sample collected at Chandwak (GR-04).

percentage of Si, K, Ti, and Fe is 16.02, 3.42, 0.66 and 5.99 at the basal surface; whereas 20.32, 2.34, 0.45 and 3.85 at the marginal edge of biotite grain, respectively.

Figure 4.10 shows the microphotograph of another biotite grain isolated from the bedload sediments samples collected at Chandwak (GR-04). The atomic percentage of Fe at basal surface is 6.69 and reduced to 6.40 at the marginal edge of biotite grain. The atomic percentage at the basal surface and at the marginal edge indicated that the reduction of Si, K, Ti and Fe and the deposition of Al along the marginal edge of biotite grain. The present SEM - EDX observations show the distinct tonal and chemical changes in the edge and basal sections of biotite grains during the weathering processes of the Gomati River Basin.

Chapter 5 Discussions

This chapter deals with discussions on the results generated from work carried out. It includes the comparative study of distribution of major and trace-elements of minerals- Biotite, Muscovite, Feldspar and bedload sediments and major and trace elements correlations, analysis of Sr isotope in mica minerals as well as for sediments and water system.

5.1 Major-Elements Distribution

The major elements are those elements which are having concentrations greater than one part per hundred (or > 1 wt %). Major elements are used in two primary ways- one is for rock classification and second is for the construction of variation diagrams. The variation diagrams are used to show interrelationships between elements in the data set and geochemical processes may be deduced from these relationships (Rollinson, 1993).

5.1.1 Minerals

The layer of mica minerals incorporated a wide variety of elements in their crystal structures. Significant concentrations of elements occurring in the mica minerals are Si, Al, Fe, Ti, Mn, Cr, V, Mg, K, Na, Rb, and Ca etc. A comparative study of major elements distribution for the minerals- Biotite, Muscovite, and Feldspar of the Gomati River bedload sediments is done. For better plotting of patterns data is normalize with Upper Continental Crust (UCC). In present study data is normalized to UCC (Rudnick & Gao, 2003). Normalization is essential for removing Oddo-Harkins effect otherwise data will show zigzag pattern. Figure 5.1 and 5.2 shows UCC normalized distribution patterns for major element oxide of Biotite (B), Muscovite (M) and Feldspar (F) minerals in mica-rich and normal bedload sediments respectively. The entire data show similar pattern among them. Figure 5.3 displays the comparison of UCC normalized distribution patterns for major element oxide of Biotite (B), Muscovite (M) and Feldspar (F) minerals in mica-rich and normal bedload sediments. Biotite show enrichment in Al_2O_3, P_2O_5, FeO, MgO, MnO,TiO_2 and depletion in Na_2O, K_2O, CaO relative to UCC. Muscovite show enrichment in Al_2O_3, P_2O_5, and depletion in Na_2O, K_2O, FeO, MnO, CaO. Except for CaO, and TiO_2, all other major elements are depleted in Feldspar relative to UCC. Biotite has higher percent of Al_2O_3, P_2O_5, FeO, MgO, MnO, than Muscovite and Feldspar.

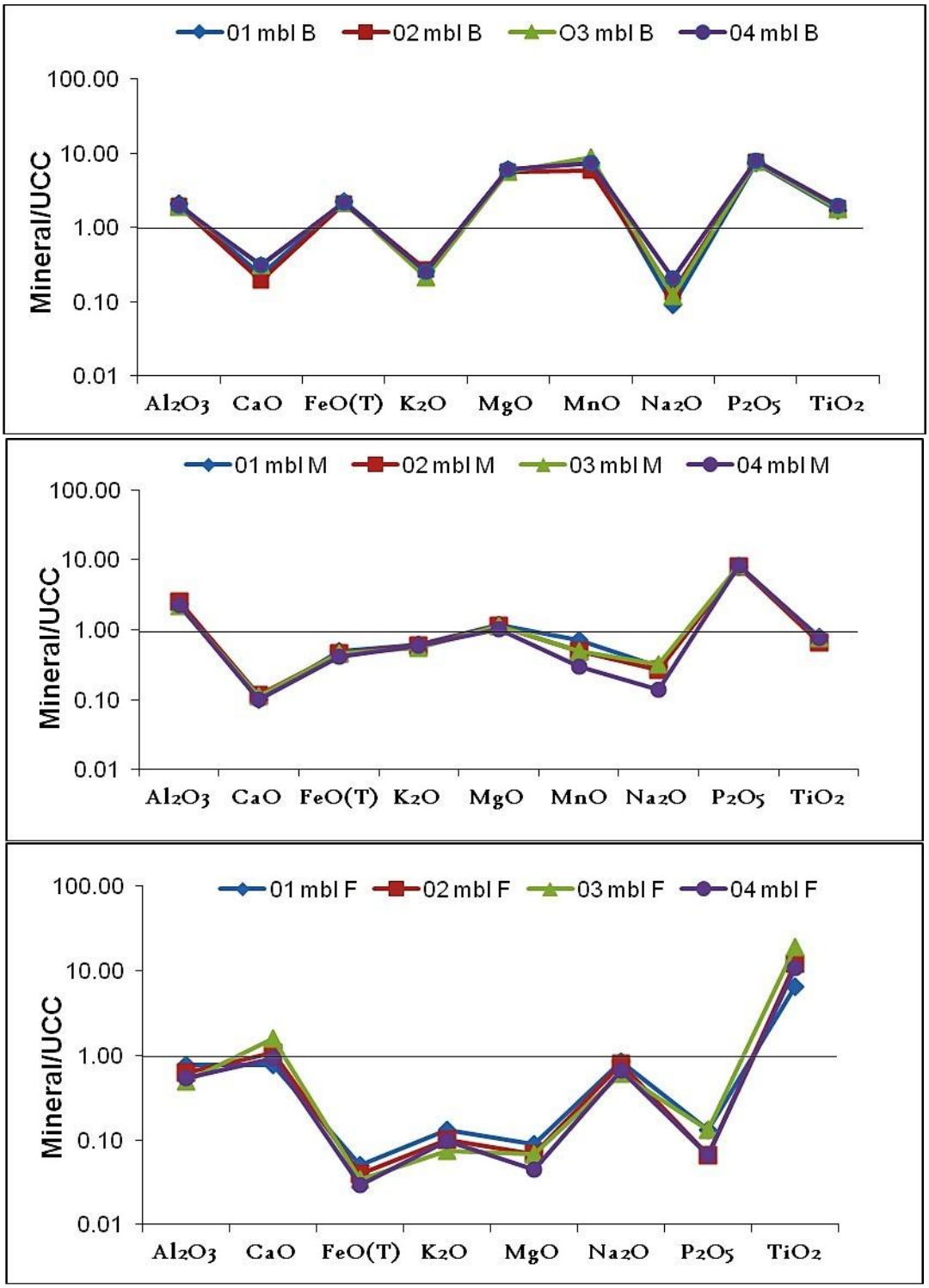

Figure 5.1 UCC normalized distribution patterns for major element oxides of Biotite (B), Muscovite (M) and Feldspar (F) minerals in mica-rich bedload sediments

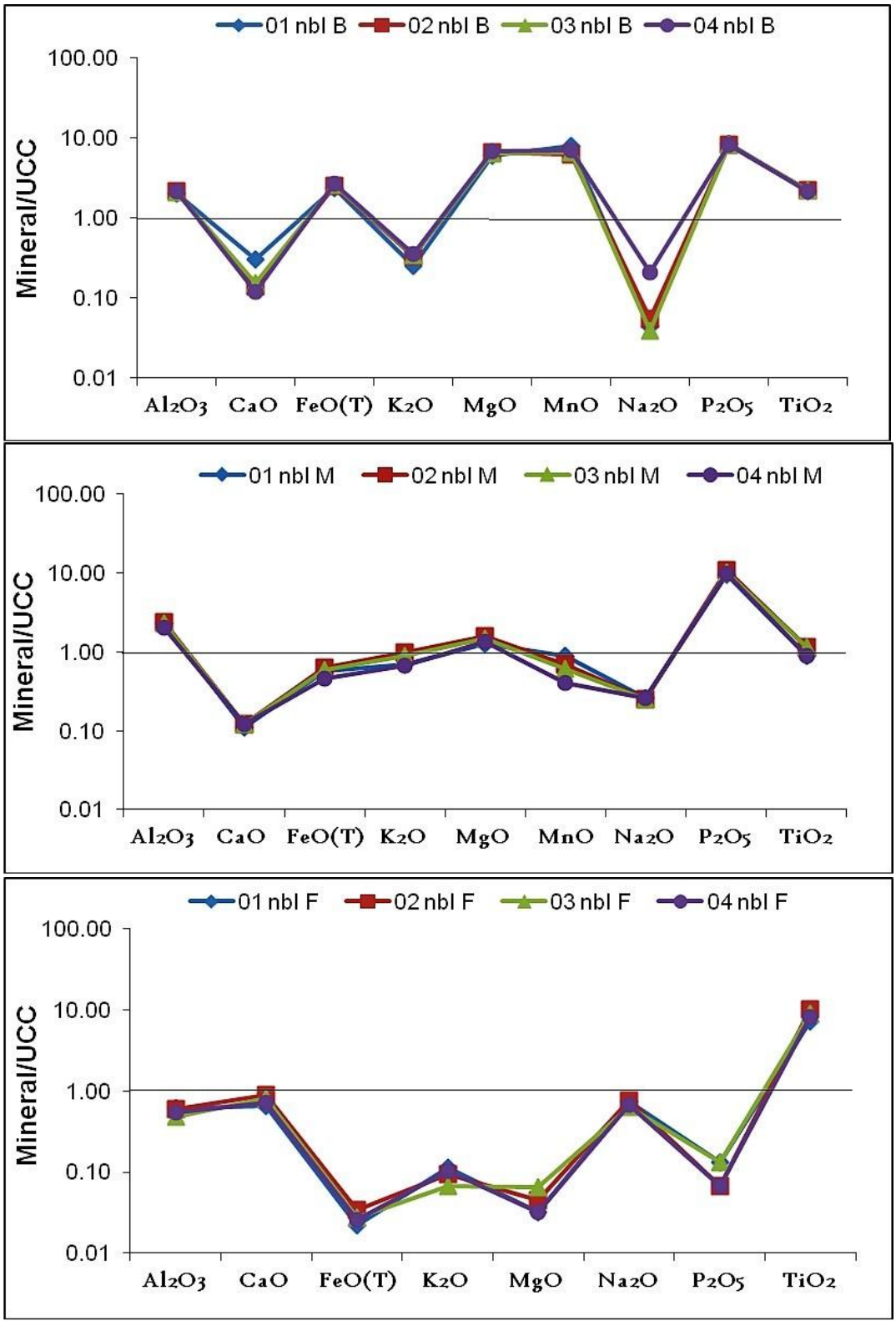

Figure 5.2 UCC normalized distribution patterns for major element oxide of Biotite (B), Muscovite (M) and Feldspar (F) minerals in normal bedload sediments

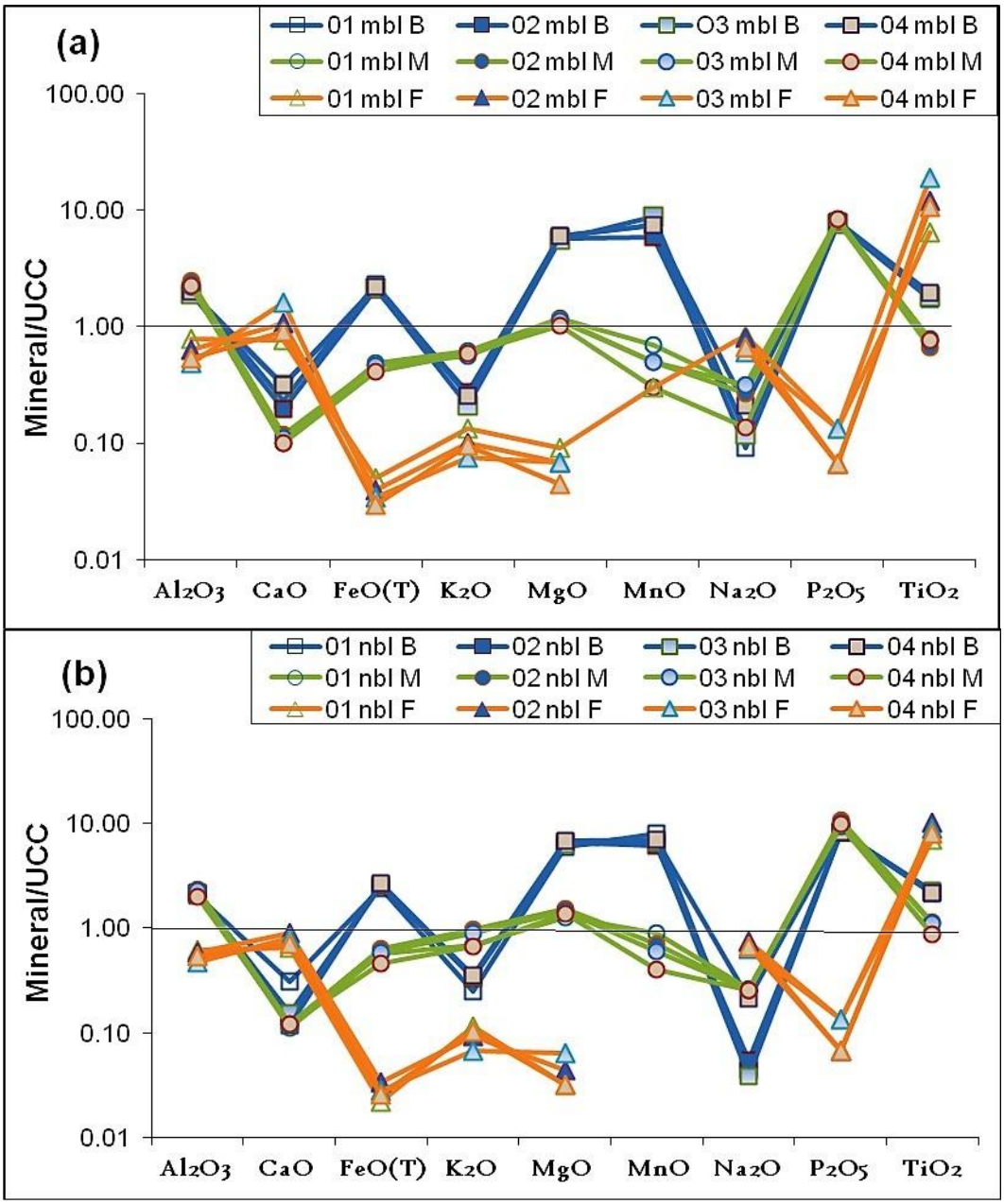

Figure 5.3 UCC normalized distribution patterns for major element oxides of Biotite (B), Muscovite (M) and Feldspar (F) minerals in (a) mica-rich and (b) normal bedload sediments.

Muscovite shows higher percent of K_2O and equal percent of Al_2O_3, P_2O_5 to Biotite. Feldspar has higher percent of CaO, Na_2O and TiO_2 than Muscovite and Biotite. The interactions between minerals and water play an important role in geochemical processes i.e., soil formation, elemental mobility, nutrient availability etc. Due to chemical weathering of minerals in natural system, various elements are released into solution.

5.1.2 River Sediments

Bulk chemical variations in the major elements of bedload sediments from the Gomati River are displayed in Figure 5.4. Sediments are enriched in CaO and TiO_2 and depleted in Al_2O_3, $FeO_{(T)}$,MgO ,MnO, Na_2O, P_2O_5 relative to UCC. The high concentration of K_2O with compare to Na_2O may indicate the presence of potassic feldspar.

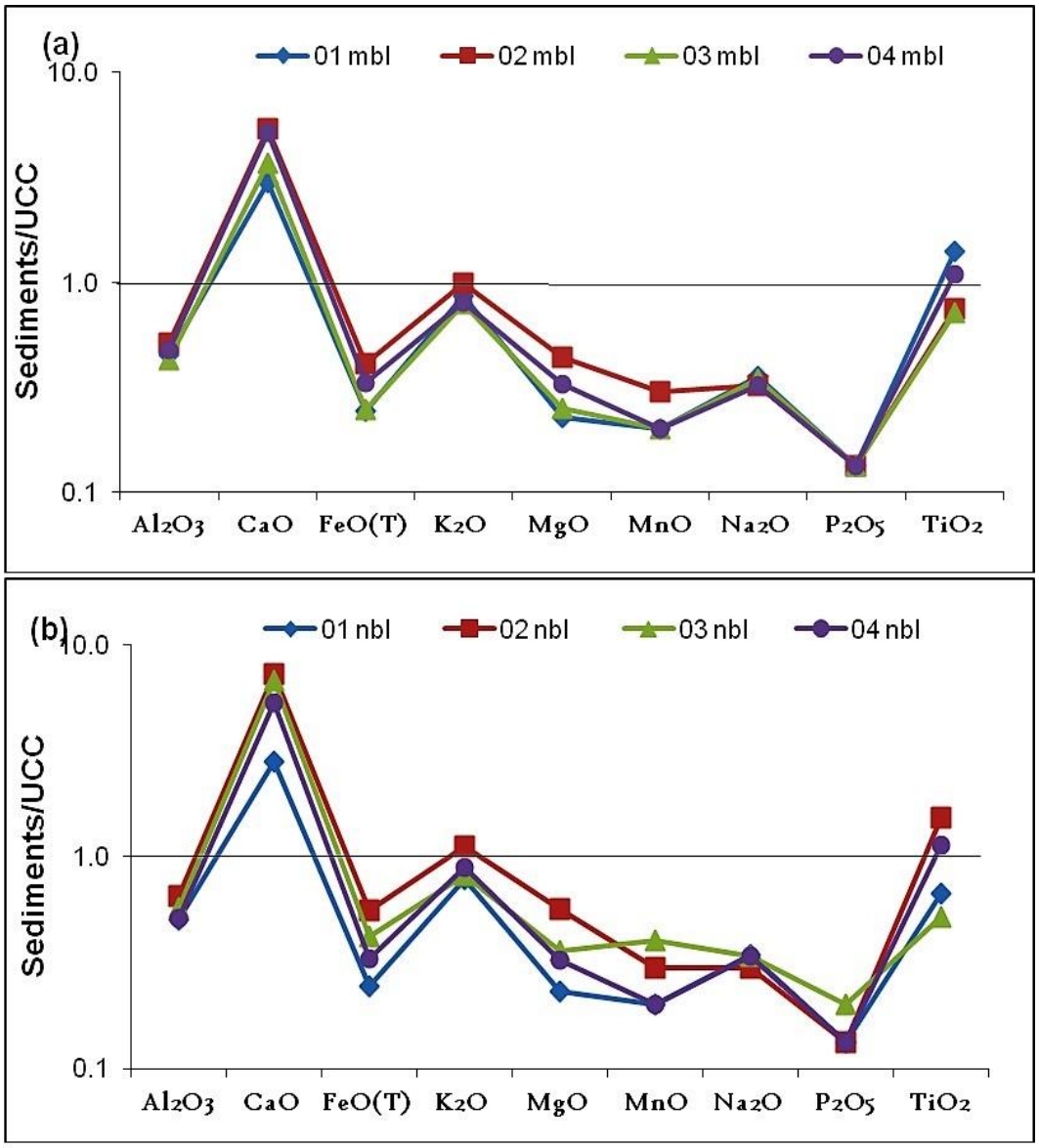

Figure 5.4 UCC normalized distribution patterns for major element oxide of **(a)** mica-rich (mbl) and **(b)** normal bedload (nbl) sediments in Gomati River.

5.2 Trace-Elements Distribution

Trace elements are chemical elements having concentrations less than 1000 ppm or 0.1 % of a rock composition (Rollinson, 1993)

5.2.1 Minerals

In Gomati River Basin trace element concentrations are higher in biotite than muscovite and feldspar. Trioctahedral micas (Biotite) incorporate a large number of elements by a variety of isomorphic substitution. Trace elements are depleted in Feldspar as Feldspar is highly susceptible to chemical weathering and gives rise to clay minerals. The distribution of trace elements in various mineral of the Gomati River Sediments is considered in the present study. Figure 5.5 and 5.6 displays UCC normalized distribution patterns for trace elements of Biotite (B), Muscovite (M) and Feldspar (F) minerals in mica-rich and normal bedload sediments respectively. Most of the trace elements show higher concentrations in the biotite mineral and lower concentrations in feldspar mineral of the Gomati River Sediments. Enrichment or depletion of trace elements in sediment is controlled by biotite and muscovite mineral, example- except Ba, Be and Sr all trace elements are 3 to 4 order magnitude higher than feldspar. The UCC normalized distribution patterns for trace element concentrations of Biotite, Muscovite and Feldspar in sample locations show nearly similar pattern. Biotite show enrichment in As, Co, Cs, Cr, Cu, Ga, Li, Ni, Pb, Rb, V and Zn. Muscovite show enrichment in As, Ba, Co, Cs, Cr, Cu, Ga, Li, Ni, Pb, Rb, V and Zn. Feldspar show enrichment in As and other trace elements are depleted. Figure 5.7 displays the comparison of UCC normalized distribution patterns for trace elements of Biotite (B), Muscovite (M) and Feldspar (F) minerals in mica-rich and normal bedload sediments. Trace element concentrations are higher in minerals of normal bedload sediments compared to mica-rich bedload sediments. Garcon et al., (2014) reported trace-elements concentrations in common silicate minerals present in the sediments of the Ganga River. It is important to note that the of Ti, V, Cr, Co, Ni and Rb in the biotite minerals have higher concentrations than other common silicate minerals present in the Ganga River Sediments (Garcon et al., 2014).

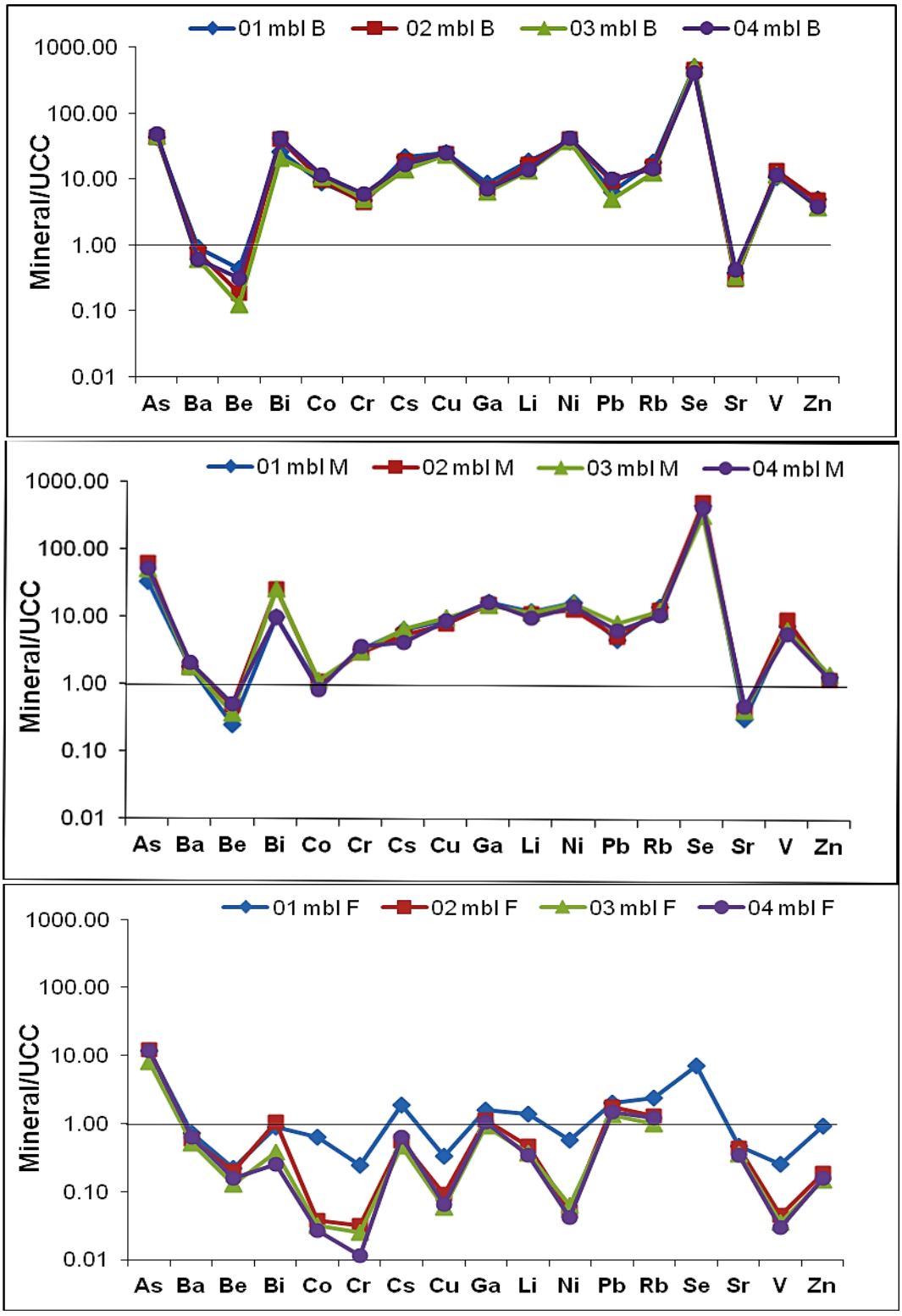

Figure 5.5 UCC normalized distribution patterns for trace elements of Biotite (B), Muscovite (M) and Feldspar (F) minerals in mica-rich bedload sediments

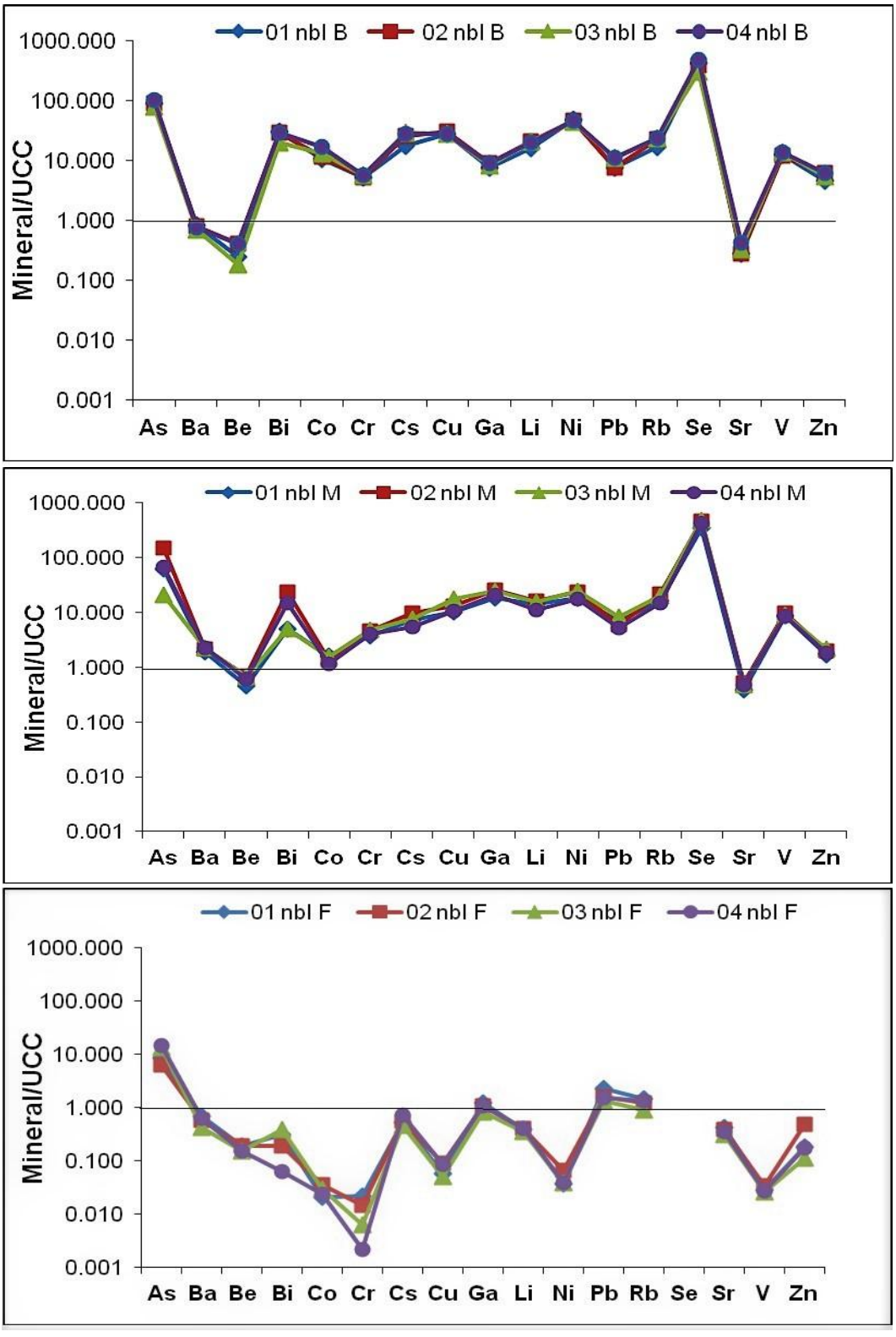

Figure 5.6 UCC normalized distribution patterns for trace elements of Biotite (B), Muscovite (M) and Feldspar (F) minerals in normal bedload sediments

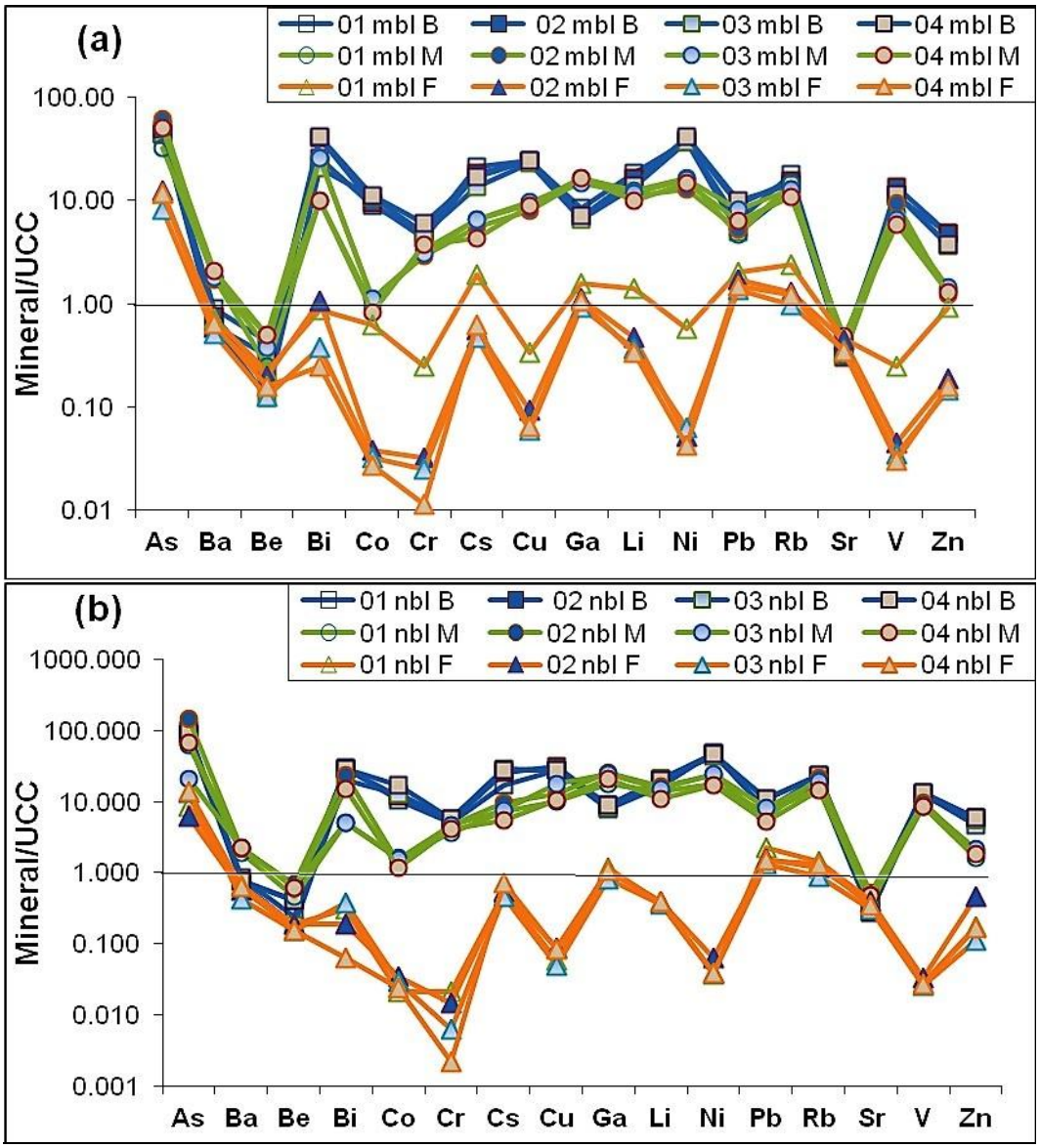

Figure 5.7 UCC normalized distribution patterns for trace elements of Biotite (B), Muscovite (M) and Feldspar (F) minerals in (a) mica-rich and (b) normal bedload sediments

5.2.2 River Sediments

Trace element concentrations in sediments result from the influence of provenance (Rollinson, 1993). Figure 5.8 displays UCC normalized distribution patterns for trace elements of mica-rich and normal bedload sediments in Gomati River. Bedload sediments are enriched in trace elements - As, Cs, Ga, Li, Rb, and Se. Arsenic concentration is very high in all the sediments samples of Gomati River Basin. Singh et al. (2010) concluded that river sediments must act as source of As in the groundwater of the Ganga Plain. Raju (2012) also found high arsenic

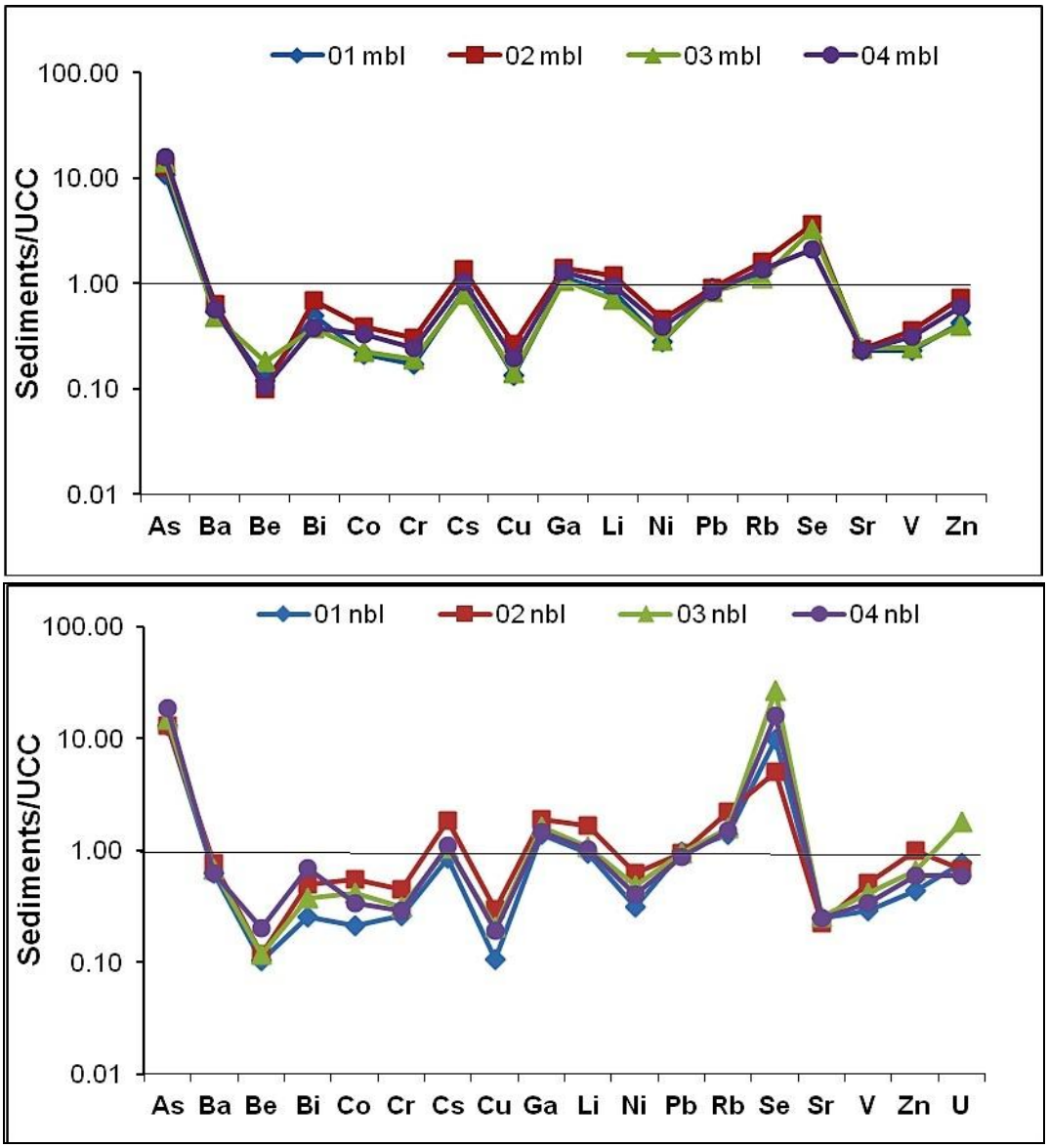

Figure 5.8 UCC normalized distribution patterns of trace elements in mica-rich and normal bedload sediments in Gomati River.

concentration within the newer alluvium deposited during middle Holocene to Recent in the Middle Ganga Plain. Raju et al. (2014) also evaluate the vulnerability of groundwater underlying the alluvium in Middle Ganga Plain for management and protection of groundwater resources.

5.3 Rare earth elements (REEs)

REEs are a group of elements whose chemical properties gradually change with their decreasing ionic radii from La to Lu causing slightly different behavior for light REEs and heavy REEs. The Rare Earth Elements (REEs) patterns have been exclusively used in deciphering history of the sediments. The REEs, due to their group behavior are immobile in water and faithfully

preserved the source compositions (McLennan et al., 1989). Table 5.1, 5.2 and Table 5.3 present the inter-correlation coefficient matrix of rare earths for Gomati river bedload sediments, Biotite and Feldspar minerals respectively. Analysis of the correlation matrix of rare earths for bedload sediments clearly indicates that bonds between various rare earths are stronger. The strong correlations between REE indicate common source of REE in the river sediments. Correlation matrix of rare earths for Biotite in bedload sediments displays the stronger bonds. Like Biotite, Muscovite also shows stronger bonds between rare earths (correlation coefficients are all superior to 0.72). Correlation matrix of rare earth for feldspar shows good correlation between LREEs (La to Sm). Correlation between LREEs and HREEs is poor. REEs of bedload sediments also have strong correlation with P_2O_5 and MnO. All REE coprecipitate in the presence of phosphate ions (PO_4^{3-}) due to close similarties in ionic radii and chemical properties. All REE can form strong dissolved complexes with phosphate ions and can adsorb onto the surface coating of Mn-oxyhydroxides.

Table 5.1 Inter-correlation coefficient matrix for rare earths in normal and mica-rich bedload sediments (n=8)

	La	Ce	Pr	Nd	Sm	Eu	Gd	Dy	Ho	Er	Yb	Lu
La	1.00											
Ce	1.00	1.00										
Pr	1.00	1.00	1.00									
Nd	1.00	1.00	1.00	1.00								
Sm	1.00	1.00	1.00	1.00	1.00							
Eu	0.99	0.99	0.99	0.99	0.99	1.00						
Gd	1.00	1.00	1.00	1.00	1.00	0.99	1.00					
Dy	0.98	0.98	0.98	0.98	0.99	0.98	0.99	1.00				
Ho	0.97	0.96	0.97	0.97	0.97	0.97	0.98	1.00	1.00			
Er	0.96	0.96	0.96	0.96	0.97	0.97	0.97	0.99	1.00	1.00		
Yb	0.92	0.92	0.92	0.92	0.92	0.94	0.94	0.96	0.98	0.99	1.00	
Lu	0.92	0.92	0.92	0.92	0.93	0.94	0.94	0.96	0.98	0.99	1.00	1.00

Table 5.2 Inter-correlation coefficient matrix for rare earths in Biotite of normal and mica-rich bedload sediments (n=8)

	La	Ce	Pr	Nd	Sm	Eu	Gd	Dy	Ho	Er	Yb	Lu
La	1.00											
Ce	1.00	1.00										
Pr	1.00	1.00	1.00									
Nd	1.00	1.00	1.00	1.00								
Sm	1.00	1.00	1.00	1.00	1.00							
Eu	0.99	0.99	0.99	0.99	0.99	1.00						
Gd	1.00	1.00	1.00	1.00	1.00	1.00	1.00					
Dy	0.98	0.98	0.98	0.98	0.98	0.99	0.98	1.00				
Ho	0.95	0.95	0.95	0.95	0.95	0.97	0.96	0.99	1.00			
Er	0.93	0.93	0.93	0.93	0.93	0.95	0.94	0.98	1.00	1.00		
Yb	0.86	0.86	0.86	0.86	0.86	0.90	0.87	0.94	0.97	0.99	1.00	
Lu	0.85	0.85	0.85	0.84	0.85	0.88	0.86	0.93	0.97	0.98	1.00	1.00

Table 5.3 Inter-correlation coefficient matrix for rare earths in Feldspar of normal and mica-rich bedload sediments (n=8)

	La	Ce	Pr	Nd	Sm	Eu	Gd	Dy	Ho	Er	Yb	Lu
La	1.00											
Ce	1.00	1.00										
Pr	1.00	1.00	1.00									
Nd	0.99	1.00	1.00	1.00								
Sm	0.96	0.97	0.98	0.99	1.00							
Eu	0.92	0.92	0.91	0.90	0.86	1.00						
Gd	0.96	0.97	0.98	0.98	1.00	0.87	1.00					
Dy	0.46	0.48	0.51	0.54	0.66	0.42	0.68	1.00				
Ho	0.44	0.46	0.49	0.53	0.64	0.43	0.66	0.99	1.00			
Er	0.47	0.49	0.51	0.55	0.65	0.46	0.68	0.99	0.99	1.00		
Yb	0.31	0.33	0.36	0.39	0.51	0.32	0.54	0.96	0.97	0.98	1.00	
Lu	0.39	0.41	0.43	0.47	0.58	0.41	0.60	0.96	0.97	0.99	0.99	1.00

REEs in Biotite are higher than Muscovite and Feldspar in Gomati River Sediments. REEs are more fractionated in Feldspar and less fractionated in Biotite. Total REE is highest in all the minerals of mica-rich sediments than normal sediments. Pair diagrams of LREEs and HREEs display the clear separation between biotite, muscovite and feldspar minerals where biotite shows enrichement in HREEs and feldspar show depletion in HREEs (Figure 5.9). All fractionation ratios of REEs are notably higher in feldspar than muscovite and biotite. Furthermore, plots of $(La/Yb)_{UCC}$ vs $(Gd/Yb)_{UCC,}$ $(Gd/Lu)_{UCC}$ vs $(La/Lu)_{UCC,}$ and $(La/Yb)_{UCC}$ vs $(La/Sm)_{UCC}$ reveal that in each case biotite consistently group in the lower range of values for either one or for all ratios (Figure 5.10).

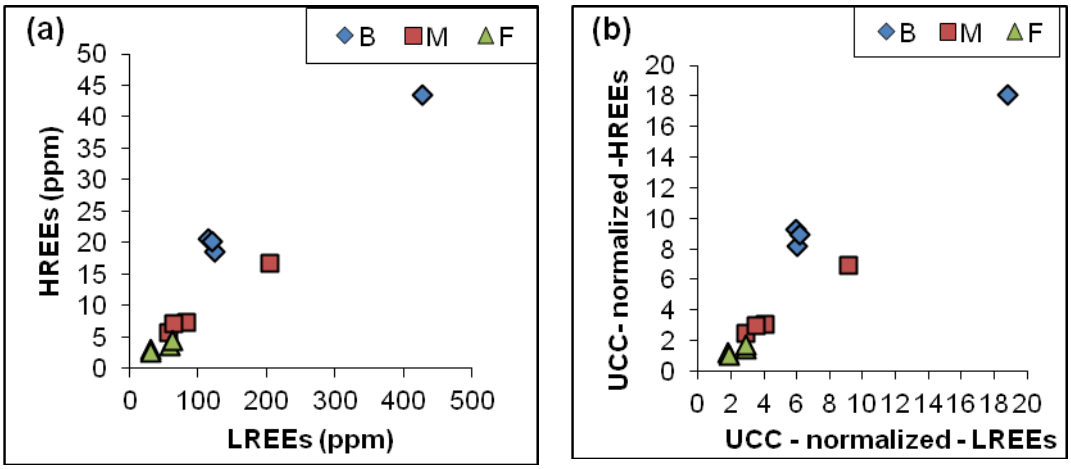

Figure 5.9 Relationship between **(a)** HREE and LREE contents, and **(b)** UCC normalized HREEs and LREEs contents for Biotite, Muscovite and Feldspar in normal bedload sediments

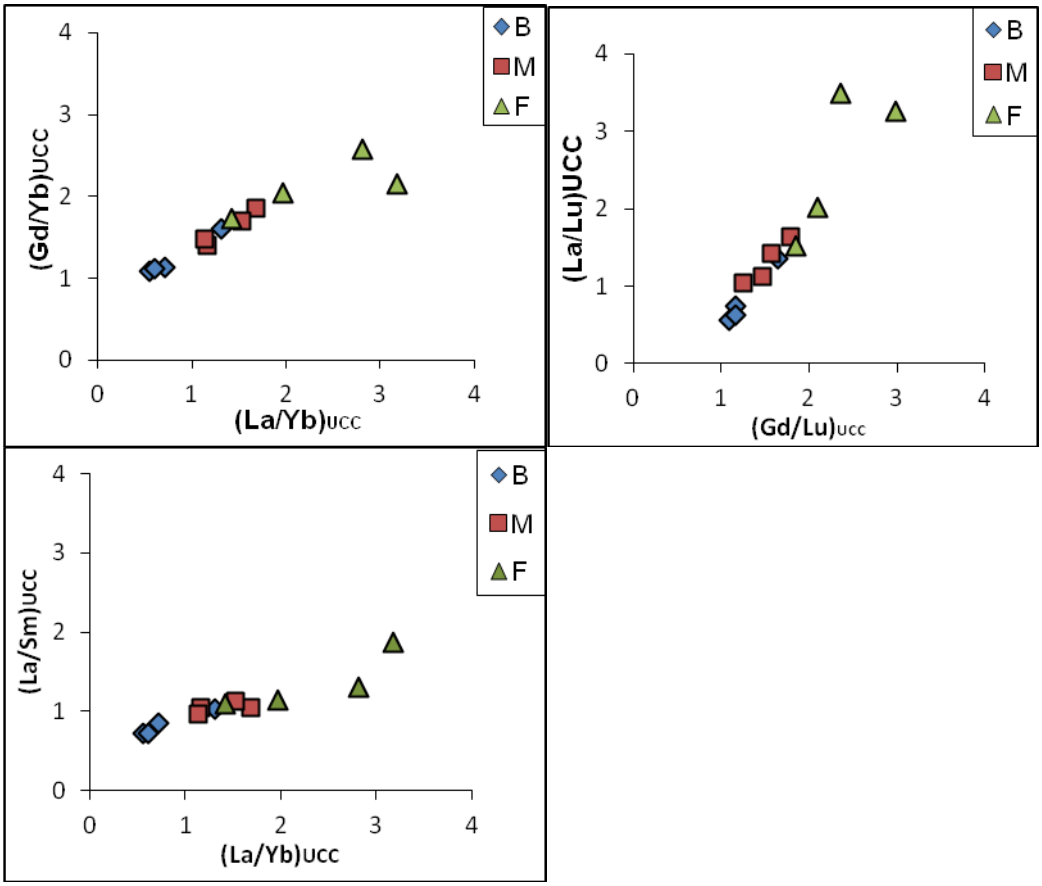

Figure 5.10 Relationship between selected REE fractionation ratios for discriminating Biotite (B), Muscovite (M) and Feldspar (F) in normal bedload sediments

LREEs and HREEs are noted in minerals- Biotite, Muscovite, Feldspar and sediments- normal and mica-rich bedload and plotted with location (figure 5.11 a,b,c,d,e). In Biotite and Muscovite, Naimeserayan area shows higher REEs whereas in Feldspar, Sultanpur area shows higher REEs. In normal bedload sediments, Sultanpur area shows higher REEs whereas in mica-rich bedload sediments, both Sultanpur and Chandwak area shows higher REEs. Figure 5.11(f) displays the comparison in the distribution of LREEs and HREEs of Yamuna, Chambal Rengarajan et al., 2004), Ganga (Chakrapani, 2005) and Gomati river sediments. Ganga river sediments show high HREEs and LREEs. Yamuna and Gomati river sediments show nearly equal concentrations of REEs whereas Chambal river sediments show low REEs among four river sediments.

5.3.1 Control of REE abundance

In all samples of the Gomati River Sediments, REE content are coherent and overlapping except one (03nbl – Sultanpur). The elevated REE content in the normal bedload sediments at Sultanpur indicates the significant input of higher proportion clastic components with the high REE concentrations. Due to tectonic upliftment accompanied by high erosion rate from alluvial deposits along the escarpments of the middle Gomati River Valley at Sultanpur, the active channel receives very fine-grained sediments and locally increases the silt-clay content (Thakur et al., 2009). Thus, the high REE values near Sultanpur are due to high proportion of fine-grained (silt) fraction in the Gomati River Sediment.

The REE properties of river sediments dependent on river water composition. The HREE enrichment in river sediments is generally associated with either high pH values of river water or the presence of heavy minerals. The Gomati River water has slightly alkaline (pH=8.0 to 8.9). The absence of HREE enrichment in the Gomati River Bedload sediments suggests that the role of heavy minerals is not important in the REE geochemistry. Epidote is the common heavy mineral present in the Gomati River sediments with marked enrichment of LREE over HREE (Grauch, 1989). Therefore, the characteristic of LREE enrichment in the Gomati River sediments indicates no controlling factor by heavy minerals in the REE geochemistry. In general, LREE preferentially adsorb on sediment surface, while HREE preferentially remain in river water. Therefore, river sediments display LREE enrichment relative to HREE (Sholkovitz et al., 2000) and is similar to that reported other major rivers in the world.

Detrital biotite is present in the normal as well as mica-rich bedload sediments and has higher REE values than muscovite and feldspar. The chemical weathering of biotite exerts important control on its REE pattern. The large temperature range (4 to 44°C) and monsoon climate (average precipitation 1000 mm/yr) result in very intense chemical weathering of mica-rich alluvial deposits at sub-surface of the alluvial plain of the Gomati River Basin. This intense chemical weathering annually generate dissolved elemental concentration in the river water one to three orders of magnitude higher than the average value of the world's river water (Jigyasu et al., 2014). It has been documented that dissolution and deposition of elements during chemical weathering go together at mineral-water interface (Langmuir, 1997).

The present study suggests that least weathering resistance and high REE containing biotite may act as REE source and exert a considerable influence on REE concentrations in the Gomati River Sediments.

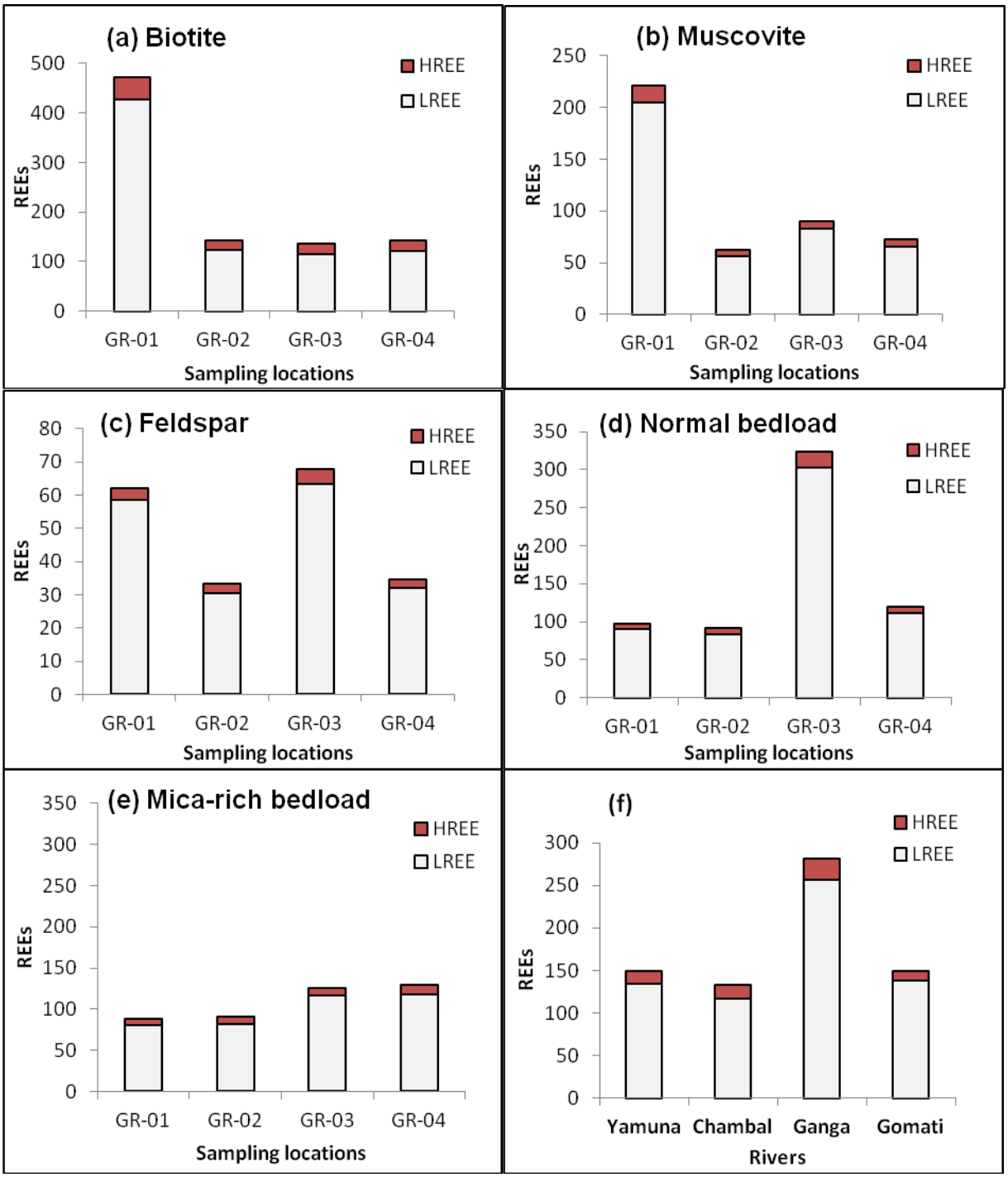

Figure 5.11 Bar diagram of LREEs and HREEs in (a) biotite, (b) Muscovite, (c) Feldspar minerals and (d) normal and (e) mica-rich bedload sediments of Naimeserayan (GR-01), Haidergarh (GR-02), Sultanpur (GR-03) and Chandwak (GR-04) area. (f) LREEs and HREEs in Yamuna, Chambal, Ganga and Gomati river sediments.

5.3.2 Ce, Gd and Eu anomalies

Ce is the most abundant of total REE composition in the Gomati River bedload sediments and their associated minerals but Ce did not show anomaly. A significant Ce anomaly was observed in temperate, arctic and other high latitude rivers whereas rivers of the tropical region do not show Ce anomaly due to sediment/mineral dissolution favoured by constant high temperature and intense rainfall condition (Sultan et al., 2009). The positive Gd-anomaly has been observed in all bedload sediments along with all biotite samples indicating the common chemical weathering process related to the both type of sediments.

River sediments derived from the Himalayan region are charecterized by having strong negative Eu anomaly (Chakrapani, 2005; Singh, 2009). Chondrite-normalised REE patterns of the Gomati River Sediments is coherent with the Ganga River Sediments (the Himalaya and the upper Ganga Alluvial Plain regions), except consistent Eu-anomaly. The significant negative Eu anomaly of the Ganga River Sediments is changed to a weak Eu-anomaly in the Gomati River Sediments. This anomalous behaviour of Eu is important in evaluating the geochemical processes of the Gomati River Basin as it is produced by the weathering processes of the Himalayan derived sediments of the Ganga Alluvial Plain. This transition in Eu-anomaly point out to the preferential dissolution of Eu bearing mineral may be Ca-feldspar of the Gomati River Sediments.

Feldspar minerals are enriched in Eu relative to other REEs because Eu^{2+} substitutes into Ca, Na and K sites during their crystallization and growth. The K-feldspar contains dominant feldspar (85 %) in the sand fraction of the Gomati River bedload sediments (Kumar & Singh, 1978). Positive Eu-anomalies in sediments attributed to preferential weathering of feldspar minerals have commonly been reported. In the Gomati River bedload sediments, this attributed to significant contribution of weathering of Ca feldspar mineral. Ca-feldspar is one of the least weathering resistance mineral present in the Gomati River sediments. Its weathering resistance is the 4 to 5 orders of magnitude lower than muscovite, K-feldspar and Na-plagioclase. Ca-feldspar also has its weathering resistance the two orders of magnitude lower than biotite (Langmuir, 1997).

5.3.3 REE mobility and Fractionation parameters

The PASS normalized REE enrichment factor of the Gomati River Sediments is significantly lower with respect to the Ganga River Sediments (figure 5.12). It reveals that REE are depleted during chemical weathering processes of the Gomati River Basin under humid sub-tropical

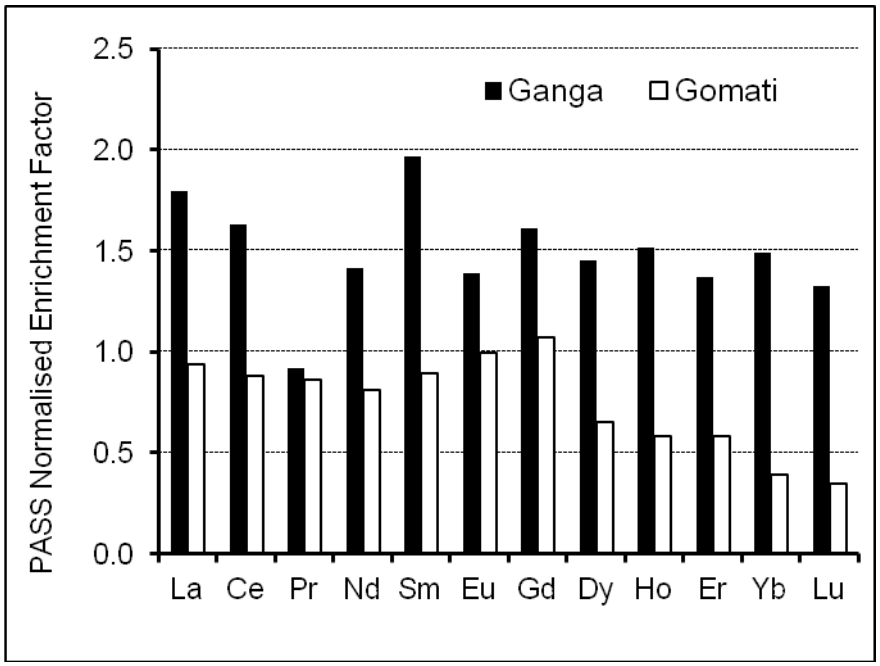

Figure 5.12 PASS normalized enrichment factor of REE in sediments of the Ganga River and the Gomati River. The characteristic observation is the enrichment factor of the Gomati River sediments is lower than the Ganga River sediments.

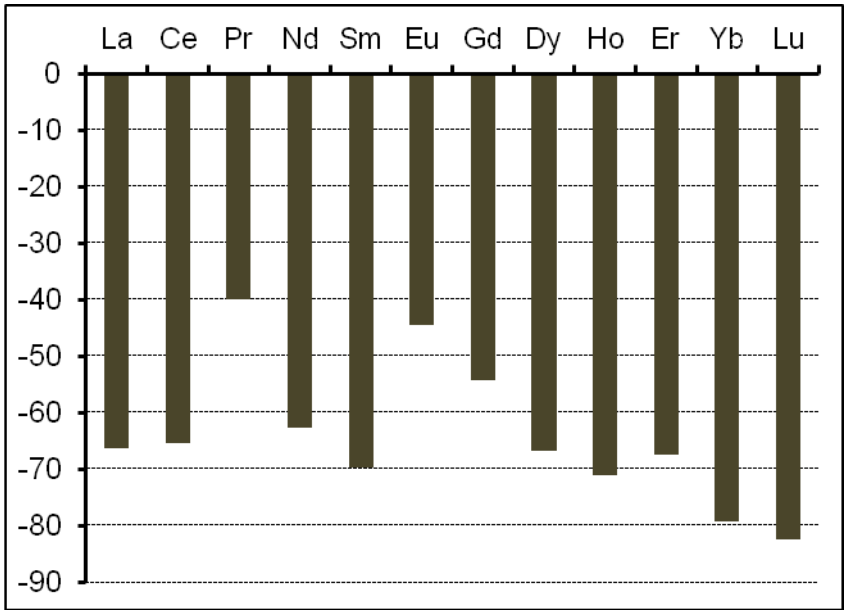

Figure 5.13 REE mobility calculated as mass change (in wt. %) as in the Gomati River Basin (Ganga Alluvial Plain).

climatic condition. It was established that Zr is relatively the most immobile trace elements during weathering of the Gomati River Basin (Jigyasu et al., 2015). The REE mobility as mass change was calculated and displayed in figure 5.13. Nearly 40 to 80 % decrease of mass change explaining

the REE loss from the parent material (the Ganga River Sediments) during the chemical weathering. Europium has been released to a slightly lower extend than the other neighbouring REE. HREE losses show increasing trend towards Lu and were controlled by their chemical properties.

The discrimination plot of fractionation parameters $(Gd/Yb)_{UCC}$ and $(La/Yb)_{UCC}$ for the bedload sediments and their associated feldspar, biotite and muscovite show a linear arrangement (figure 5.14). This linear arrangement displays weathering resistance ranged from minimum in muscovite of 01nblM -Naimeserayan to maximum in biotite of 04mblB – Chandwak of the river basin and reveals that chemical weathering exert important control over the REE composition of bedload sediments and their common silicate minerals.

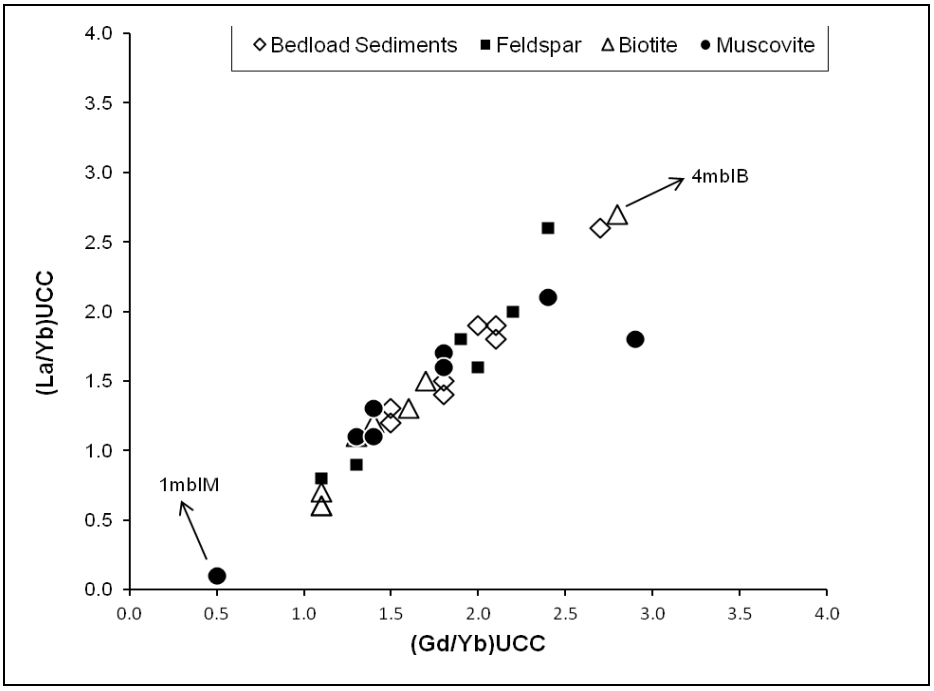

Figure 5.14 Discrimination plot of $(Gd/Yb)_{UCC}$ vs. $(La/Yb)_{UCC}$ for bedload sediments and their associated feldspar, biotite and muscovite minerals of the Gomati River. Note the chemical weathering direction along the linear arrangement from least (muscovite from upper part (1-Naimeserayan) to maximum biotite from distal part (4-Chandwak) of the river basin.

5.4 Inter-elemental Relationship

Correlation coefficient is a useful statistical consideration for investigating the association and source of elements. The correlation coefficient matrices of the major and trace elements in the minerals - Biotite, Muscovite, Feldspar and Gomati River bedload sediments are presented in Table 5.4, 5.5, 5.6, 5.7 respectively. The significant correlations of major and trace elements in

Table 5.4 Correlation coefficient among chemical parameters for biotite mineral of Gomati River. High correlation coefficient values are in bold.

	Al_2O_3	CaO	FeO(t)	K_2O	MgO	MnO	Na_2O	P_2O_5	TiO_2	As	Ba	Co	Cr	Cu	Li	Ni	Rb	Sr	V	Zn
Al_2O_3	1																			
CaO	-0.71	1																		
FeO(t)	0.88	-0.70	1																	
K_2O	0.85	**-0.93**	0.86	1																
MgO	**0.92**	-0.73	**0.92**	0.89	1															
MnO	-0.42	0.74	-0.21	-0.66	-0.36	1														
Na_2O	-0.15	0.07	-0.16	-0.07	0.09	0.09	1													
P_2O_5	0.59	-0.32	0.71	0.60	0.66	-0.21	-0.10	1												
TiO_2	0.69	-0.51	0.84	0.76	0.75	-0.31	0	**0.94**	1											
As	0.78	-0.53	**0.90**	0.73	0.82	-0.19	-0.21	0.89	**0.92**	1										
Ba	0.56	-0.32	0.26	0.23	0.23	-0.27	-0.44	0.01	0.04	0.26	1									
Co	0.57	-0.57	0.81	0.72	0.80	-0.09	0.39	0.63	0.66	0.71	-0.20	1								
Cr	0.49	-0.15	0.58	0.47	0.67	0.05	0.29	0.65	0.63	0.51	-0.37	0.69	1							
Cu	0.84	-0.64	0.83	0.80	0.84	-0.44	-0.39	0.75	0.87	0.88	0.34	0.50	0.47	1						
Li	0.86	**-0.92**	0.81	**0.93**	0.78	-0.65	-0.35	0.42	0.64	0.65	0.49	0.48	0.23	0.80	1					
Ni	0.70	-0.38	0.73	0.62	0.70	-0.29	-0.23	**0.95**	**0.91**	**0.93**	0.24	0.52	0.51	0.86	0.52	1				
Rb	**0.91**	-0.88	**0.91**	**0.97**	0.89	-0.55	-0.23	0.57	0.76	0.76	0.36	0.65	0.45	0.84	**0.97**	0.62	1			
Sr	0.20	-0.07	0.13	0.14	0.32	0.14	0.78	-0.11	-0.18	-0.13	-0.19	0.44	0.52	-0.22	-0.03	-0.23	0.09	1		
V	0.27	-0.55	0.44	0.57	0.30	-0.51	-0.01	0.60	0.59	0.51	0.00	0.51	0.10	0.30	0.44	0.49	0.47	-0.16	1	
Zn	0.86	**-0.94**	0.82	**0.93**	0.83	-0.65	-0.21	0.48	0.64	0.73	0.50	0.56	0.19	0.81	**0.95**	0.60	**0.93**	-0.05	0.49	1

Table 5.5 Correlation coefficient among chemical parameters for muscovite mineral of Gomati River. High correlation coefficient values are in bold.

	Al_2O_3	CaO	FeO(t)	K_2O	MgO	MnO	Na_2O	P_2O_5	TiO_2	As	Ba	Co	Cr	Cu	Li	Ni	Rb	Sr	V	Zn
Al_2O_3	1																			
CaO	-0.06	1																		
FeO(t)	0.28	0.59	1																	
K_2O	0.11	0.66	0.88	1																
MgO	-0.06	0.79	0.85	**0.93**	1															
MnO	0.40	0.12	0.75	0.38	0.43	1														
Na_2O	0.10	0.27	0.26	-0.02	0.20	0.47	1													
P_2O_5	-0.26	0.74	0.78	**0.90**	**0.93**	0.30	-0.05	1												
TiO_2	-0.06	0.63	0.86	**0.97**	**0.92**	0.38	-0.03	**0.93**	1											
As	0.08	0.41	0.45	0.49	0.49	0.18	-0.05	0.53	0.39	1										
Ba	-0.51	0.48	0.37	0.70	0.69	-0.16	-0.41	0.83	0.78	0.24	1									
Co	0.05	0.67	0.85	0.65	0.72	0.68	0.27	0.72	0.71	0.19	0.34	1								
Cr	-0.23	0.55	0.67	**0.90**	0.84	0.15	-0.28	**0.91**	**0.95**	0.31	**0.93**	0.56	1							
Cu	-0.07	0.60	0.69	0.82	0.76	0.21	0.03	0.75	0.88	-0.03	0.71	0.66	0.85	1						
Li	0.28	0.57	**0.99**	0.88	0.84	0.72	0.30	0.75	0.87	0.39	0.37	0.81	0.68	0.74	1					
Ni	-0.04	0.59	0.86	**0.94**	0.89	0.41	0.10	0.87	**0.98**	0.28	0.70	0.70	0.89	**0.92**	**0.90**	1				
Rb	0.15	0.67	**0.95**	**0.96**	**0.96**	0.56	0.22	0.86	**0.94**	0.50	0.56	0.73	0.80	0.77	**0.95**	**0.93**	1			
Sr	-0.23	0.58	0.19	0.53	0.43	-0.45	-0.48	0.61	0.51	0.53	0.69	0.15	0.61	0.42	0.19	0.41	0.35	1		
V	0.38	0.78	0.71	0.65	0.77	0.50	0.35	0.58	0.54	0.46	0.21	0.64	0.41	0.40	0.67	0.49	0.74	0.18	1	
Zn	-0.27	0.75	0.77	0.89	**0.93**	0.29	0.09	**0.94**	**0.95**	0.27	0.81	0.75	**0.91**	**0.90**	0.78	**0.94**	0.87	0.49	0.55	1

Biotite, Muscovite, Feldspar and sediments are presented in figure 5.15, 5.16, 5.17, and 5.18 respectively. These correlations are (Al with Fe), (Cr with Fe), (Al with Ni), (Rb with Fe), (Fe with Co), (Al with Rb), (Ba with Cr), (Ba with Li), in the Gomati River sediments. MgO shows strong correlation coefficient with with Al_2O_3, K_2O, FeO, moderate correlation coefficient with CaO in Biotite. In sediments K shows high correlation coefficient with Al, indicating the common mineral

sources in mica minerals and Mg shows strong correlation coefficient with Al, K, Ca, and Fe, indicating the common mineral sources in plagioclase and mica minerals.

Table 5.6 Correlation coefficient among chemical parameters for Feldspar mineral of Gomati River. High correlation coefficient values are in bold.

	Al_2O_3	CaO	FeO(t)	K_2O	MgO	MnO	Na_2O	P_2O_5	TiO_2	As	Ba	Co	Cr	Cu	Li	Ni	Rb	Sr	V	Zn
Al_2O_3	1																			
CaO	-0.37	1																		
FeO(t)	0.82	-0.19	1																	
K_2O	**0.90**	-0.51	0.67	1																
MgO	0.79	-0.12	**0.99**	0.61	1															
MnO	0.82	-0.21	**1.00**	0.68	**0.99**	1														
Na_2O	**0.94**	-0.42	0.63	0.81	0.61	0.63	1													
P_2O_5	0.07	0.11	0.37	-0.02	0.40	0.38	-0.09	1												
TiO_2	-0.52	**0.98**	-0.38	-0.62	-0.31	-0.40	-0.53	0.01	1											
As	-0.02	-0.31	0.13	0.05	0.14	0.13	-0.05	-0.13	-0.32	1										
Ba	0.77	-0.39	0.55	**0.95**	0.48	0.55	0.65	-0.12	-0.47	0.00	1									
Co	0.82	-0.19	**1.00**	0.67	**0.99**	**1.00**	0.63	0.37	-0.38	0.13	0.54	1								
Cr	0.85	-0.14	**0.99**	0.69	**0.99**	**0.99**	0.67	0.39	-0.33	0.08	0.56	**0.99**	1							
Cu	0.87	-0.21	**0.99**	0.72	**0.98**	**0.99**	0.70	0.24	-0.40	0.13	0.60	**0.99**	**0.98**	1						
Li	0.86	-0.20	**1.00**	0.70	**0.99**	**0.99**	0.69	0.34	-0.39	0.14	0.57	**1.00**	**0.99**	**0.99**	1					
Ni	0.82	-0.16	**1.00**	0.66	**0.99**	**1.00**	0.63	0.37	-0.36	0.09	0.54	**1.00**	**0.99**	**0.99**	**0.99**	1				
Rb	**0.94**	-0.39	**0.91**	**0.91**	0.88	**0.92**	0.78	0.20	-0.55	0.10	0.82	**0.91**	**0.92**	**0.94**	**0.93**	**0.91**	1			
Sr	**0.91**	-0.10	0.61	0.78	0.60	0.60	**0.92**	0.05	-0.23	-0.21	0.67	0.61	0.67	0.67	0.67	0.61	0.75	1		
V	0.84	-0.17	**1.00**	0.68	**1.00**	**1.00**	0.66	0.35	-0.36	0.12	0.55	**1.00**	**1.00**	**0.99**	**1.00**	**1.00**	**0.92**	0.64	1	
Zn	0.85	-0.23	**0.92**	0.68	**0.90**	**0.92**	0.72	0.18	-0.40	-0.14	0.55	**0.92**	**0.91**	**0.94**	**0.92**	**0.93**	0.87	0.67	**0.92**	1

Table 5.7 Correlation coefficient among chemical parameters for sediments of Gomati River. High correlation coefficient values are in bold.

	Al_2O_3	CaO	FeO(t)	K_2O	MgO	MnO	Na_2O	P_2O_5	TiO_2	As	Ba	Co	Cr	Cu	Li	Ni	Rb	Sr	V	Zn
Al_2O_3	1																			
CaO	0.81	1																		
FeO(t)	**0.91**	**0.93**	1																	
K_2O	0.73	0.61	0.82	1																
MgO	0.84	0.87	**0.97**	0.89	1															
MnO	0.67	0.74	0.71	0.36	0.59	1														
Na_2O	-0.73	-0.76	-0.87	-0.75	**-0.92**	-0.35	1													
P_2O_5	0.32	0.45	0.26	-0.21	0.07	0.80	0.12	1												
TiO_2	0.25	0.13	0.27	0.55	0.32	-0.30	-0.37	-0.51	1											
As	0.01	0.33	0.05	-0.21	0.02	-0.10	-0.11	0.10	-0.14	1										
Ba	**0.98**	0.75	0.86	0.71	0.80	0.62	-0.70	0.27	0.22	0.03	1									
Co	**0.90**	**0.96**	**0.99**	0.78	**0.96**	0.70	-0.86	0.29	0.26	0.14	0.85	1								
Cr	**0.97**	0.83	**0.93**	0.79	**0.91**	0.59	-0.84	0.17	0.25	0.11	**0.95**	**0.93**	1							
Cu	0.74	0.88	**0.94**	0.85	**0.97**	0.60	-0.87	0.09	0.28	0.08	0.70	**0.94**	0.82	1						
Li	**0.94**	0.77	**0.94**	**0.90**	**0.94**	0.53	-0.86	0.04	0.41	-0.07	**0.93**	**0.91**	**0.96**	0.86	1					
Ni	**0.94**	**0.93**	**0.99**	0.80	**0.96**	0.69	-0.87	0.26	0.27	0.12	**0.90**	**0.99**	**0.96**	**0.91**	**0.95**	1				
Rb	**0.96**	0.79	**0.94**	0.87	**0.93**	0.56	-0.84	0.10	0.40	-0.03	**0.95**	**0.92**	**0.98**	0.84	**0.99**	**0.96**	1			
Sr	-0.16	-0.09	-0.31	-0.60	-0.42	0.23	0.50	0.58	-0.84	0.42	-0.11	-0.27	-0.20	-0.40	0	-0.26	-0.36	1		
V	**0.97**	**0.92**	**0.98**	0.74	**0.92**	0.73	-0.82	0.34	0.19	0.11	**0.93**	**0.97**	**0.97**	0.86	**0.93**	**0.99**	**0.95**	-0.17	1	
Zn	**0.90**	0.89	**0.99**	0.87	**0.99**	0.60	**-0.91**	0.11	0.36	0.05	0.86	**0.98**	**0.94**	**0.95**	**0.97**	**0.98**	**0.96**	-0.40	**0.95**	1

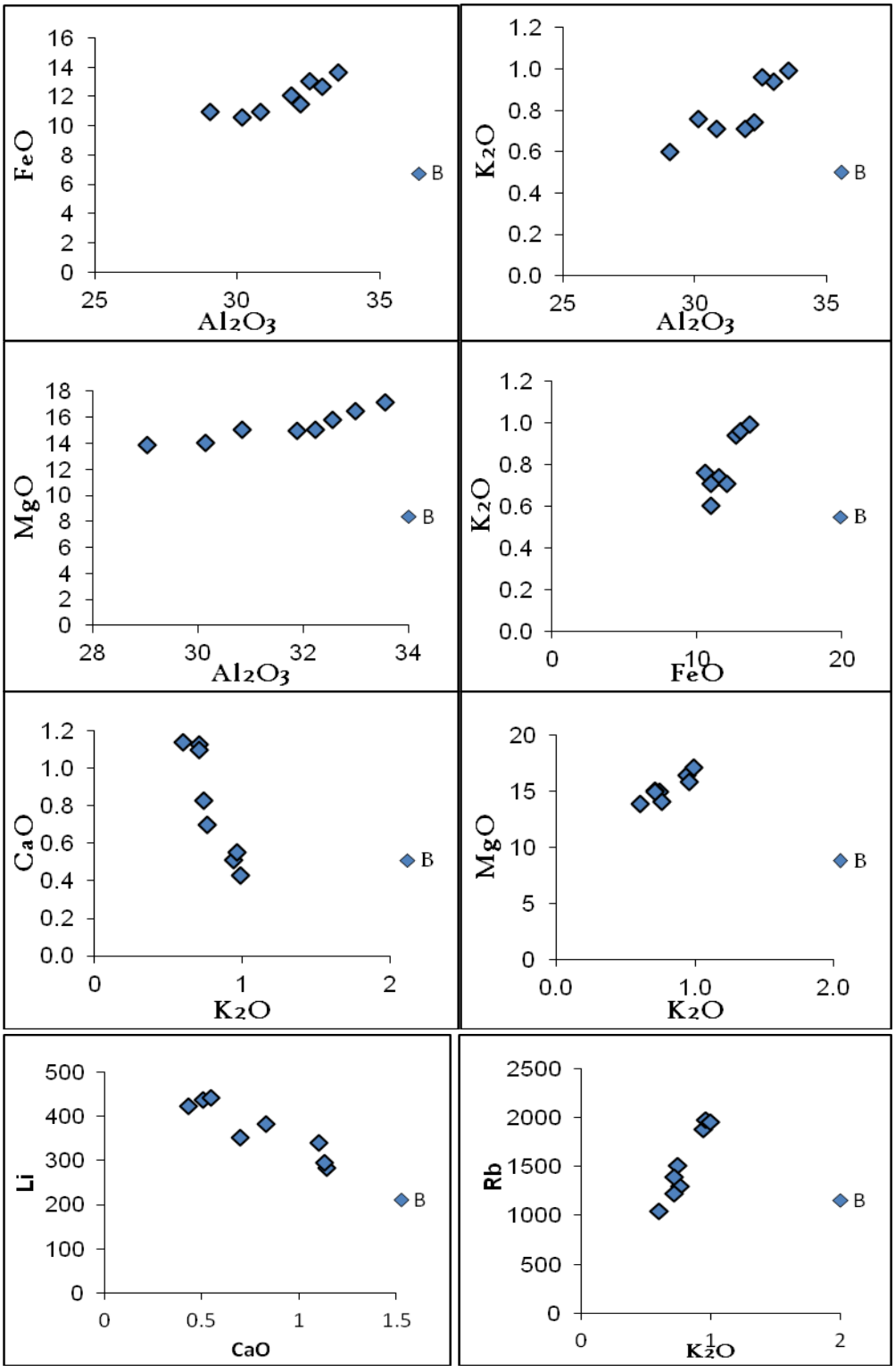

Figure 5.15 Bivariate plots showing the inter-elements relationship between major and trace elements in Biotite (B) of Gomati River sediments.

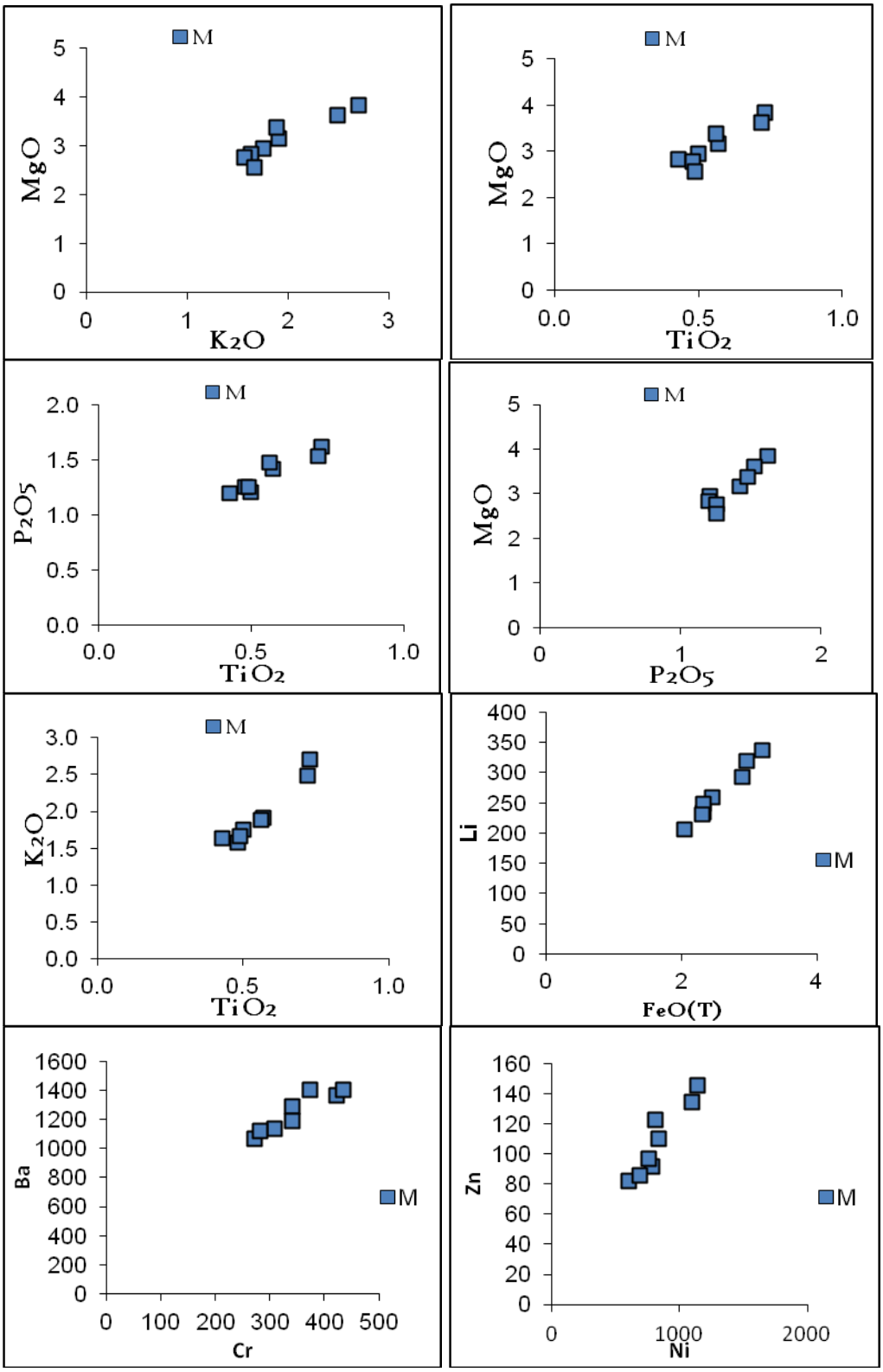

Figure 5.16 Bivariate plots showing the inter-elements relationship between major and trace elements in Muscovite (M) of Gomati River sediments.

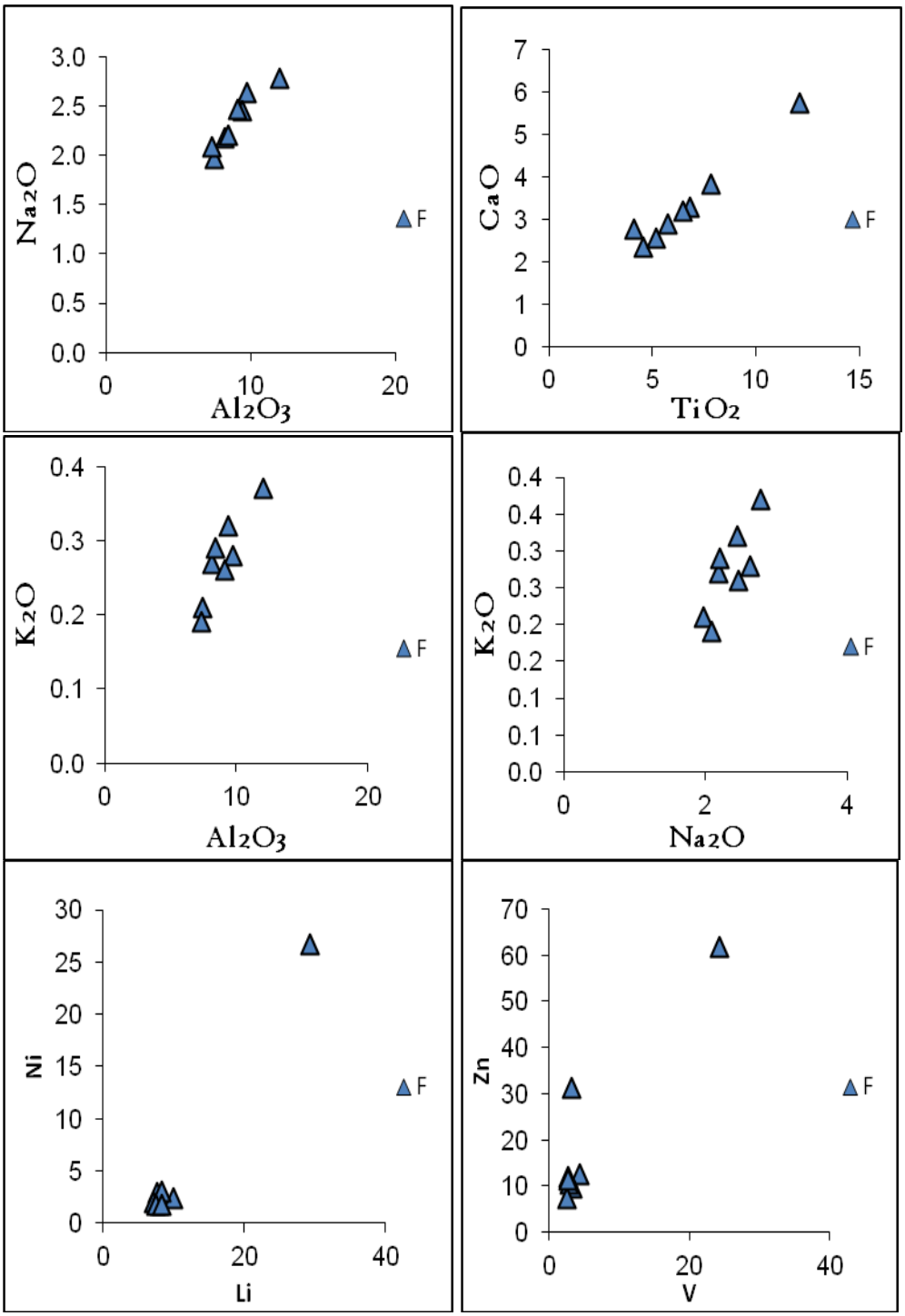

Figure 5.17 Bivariate plots showing the inter-elements relationship between major and trace elements in Feldspar (F) of Gomati River sediments.

Some important variation diagrams showing the inter-elements relationship between major-major (K_2O-Al_2O_3, K_2O-$FeO_{(t)}$, K_2O-P_2O_5), major-trace ($FeO_{(t)}$-As, $FeO_{(t)}$-Cr, K_2O-Sr) and trace-trace (V- Zn, Rb -Sr, Ba -Li) elements in minerals - Biotite, Muscovite, Feldspar and bedload

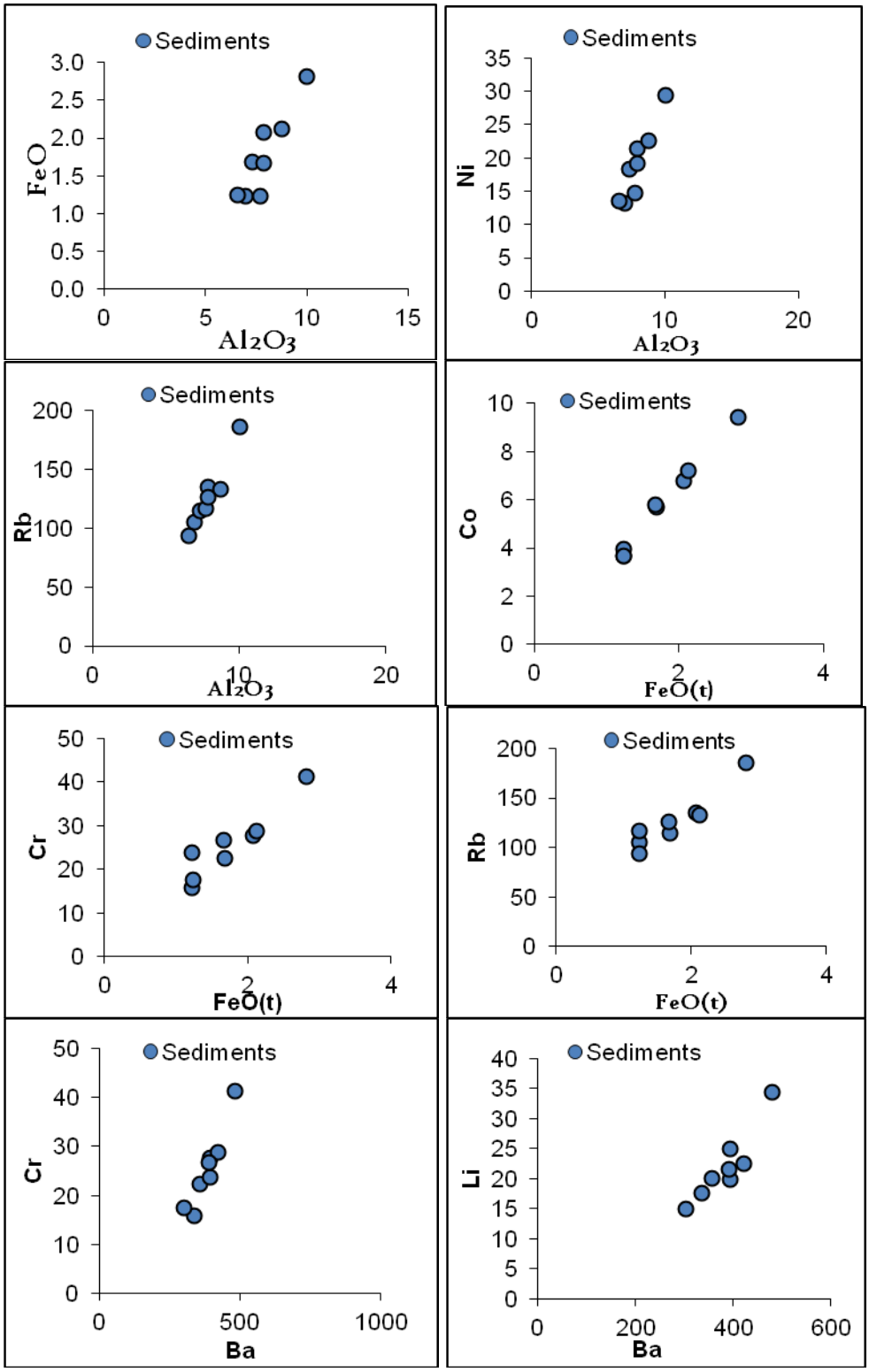

Figure 5.18 Bivariate plots showing the inter-elements relationship between major and trace elements of Gomati River bedload sediments.

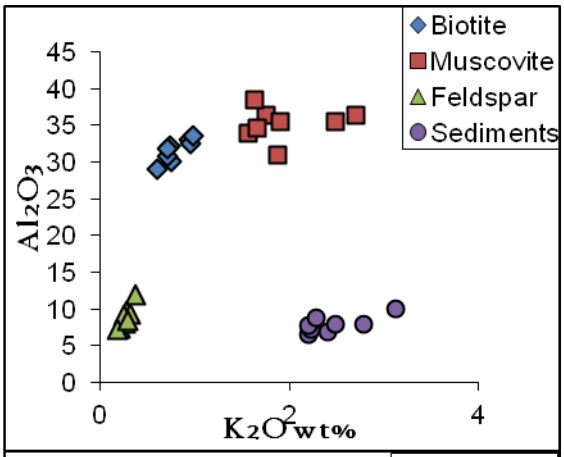
Biotite
Muscovite
Feldspar
Sediments
Al2O3
K2O wt%

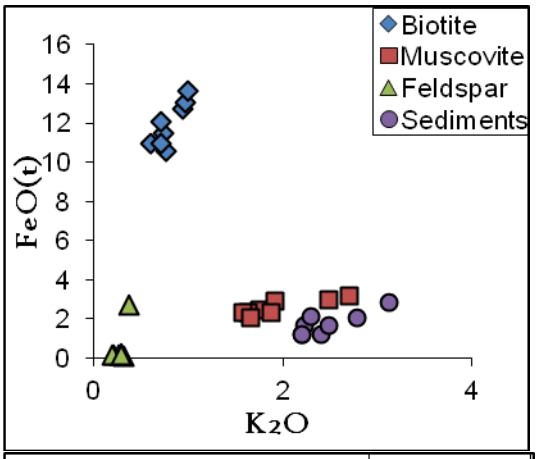
Biotite
Muscovite
Feldspar
Sediments
FeO(t)
K2O

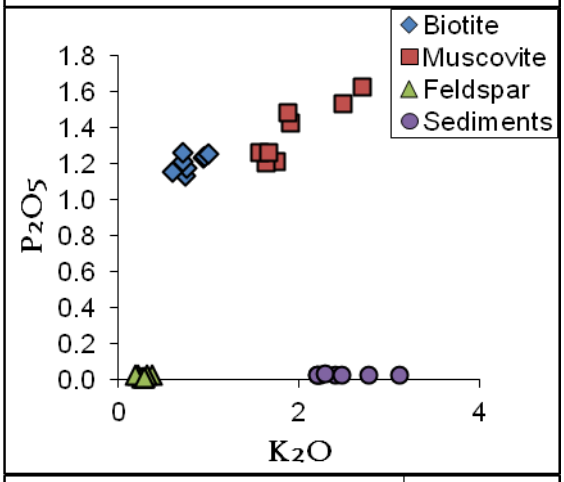
Biotite
Muscovite
Feldspar
Sediments
P2O5
K2O

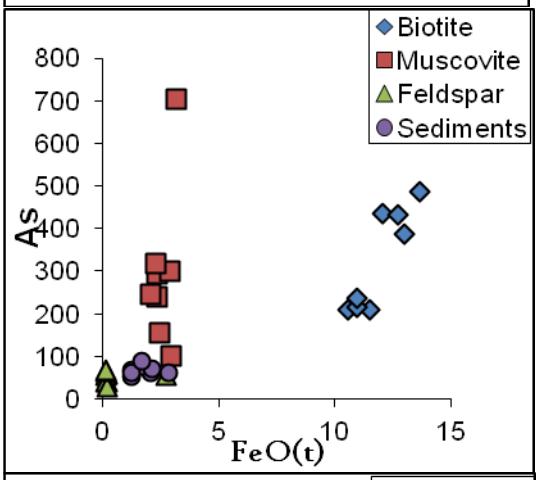
Biotite
Muscovite
Feldspar
Sediments
As
FeO(t)

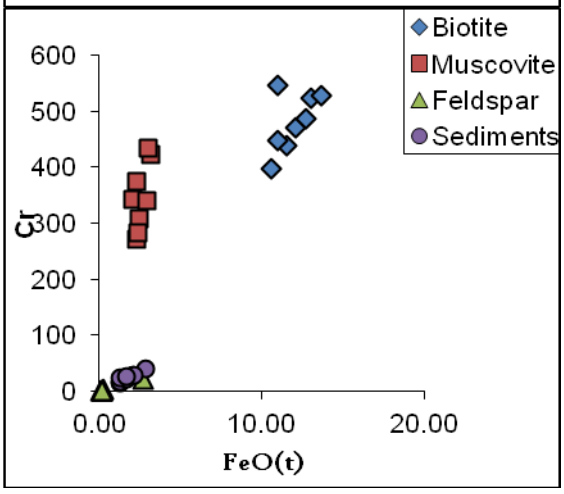
Biotite
Muscovite
Feldspar
Sediments
Cr
FeO(t)

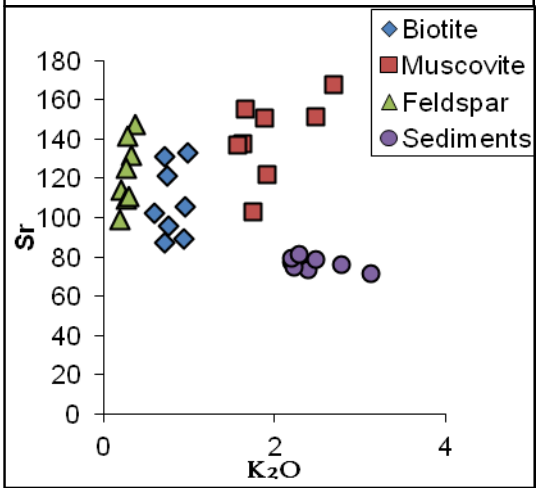
Biotite
Muscovite
Feldspar
Sediments
Sr
K2O

……conti

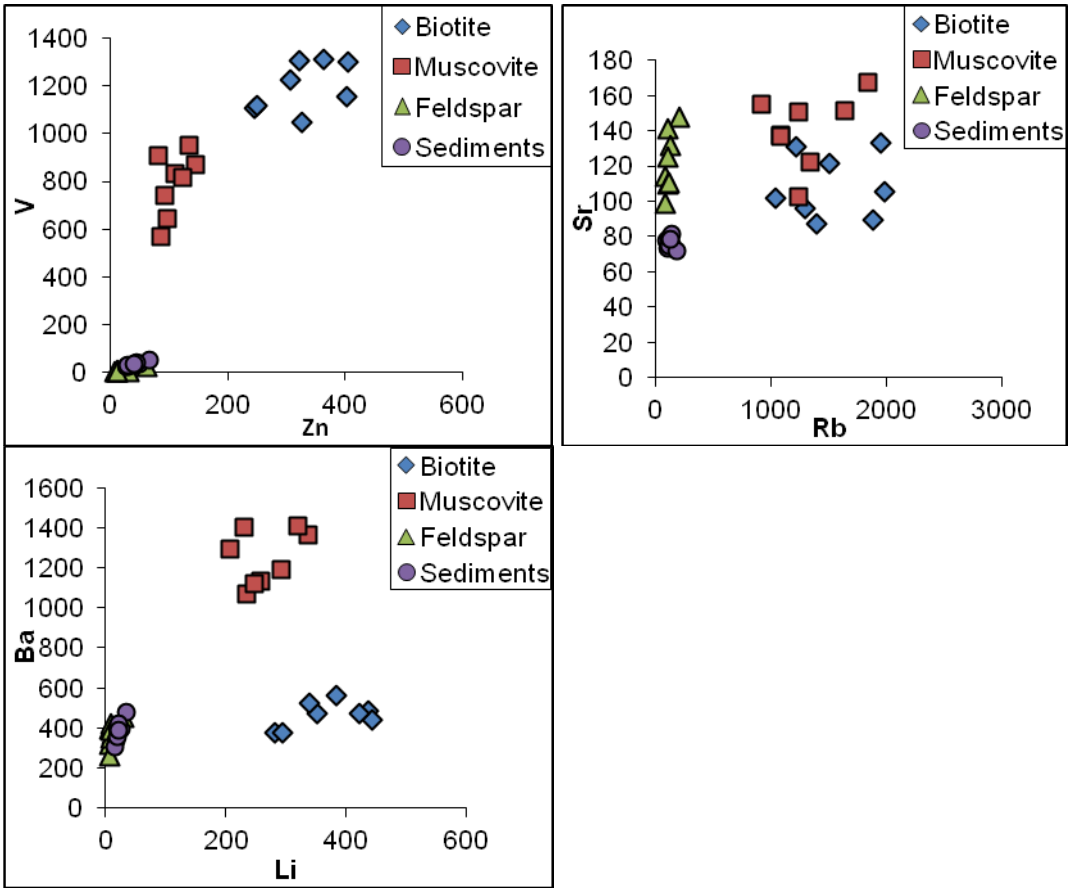

Figure 5.19 Some Bivariate plots showing the inter-elements relationship between major-major (K_2O-Al_2O_3, K_2O-$FeO_{(t)}$, K_2O-P_2O_5), major-trace ($FeO_{(t)}$-As, $FeO_{(t)}$-Cr, K_2O-Sr) and trace-trace (V-Zn, Rb-Sr, Ba-Li) elements of Gomati River bedload sediments.

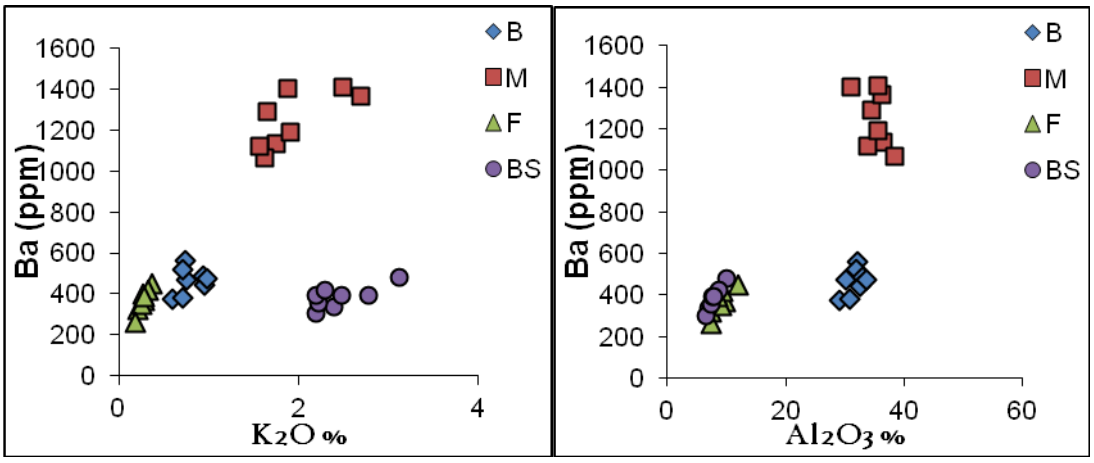

Figure 5.20 Variation of Ba versus (a) K_2O and (b) Al_2O_3 in Gomati River bedload sediments (BS) and associated minerals- Biotite (B), Muscovite (M) and Feldspar (F).

sediments of Gomati River are plotted in figure 5.19. Variation of Ba versus K_2O and Al_2O_3 in minerals- Biotite, Muscovite, Feldspar and bedload sediments of Gomati River are plotted in figure 5.20. Significant positive correlation of Ba with K_2O and Al_2O_3 favours its association with K-aluminosilicates.

Normal bedload sediments are compared with alluvial sediments of Ganga Plain. Major elements of Bedload sediments are highly enriched in CaO. Major elements of Gomati river bedload sediments shows similar pattern to alluvial sediments (Kuvar, 2012) of Behta Nala section near Lucknow (figure 5.21). Ca is the most variable element and enriched in all sediment samples which also denotes that carbonate weathering dominates in Ganga Alluvial Plain.

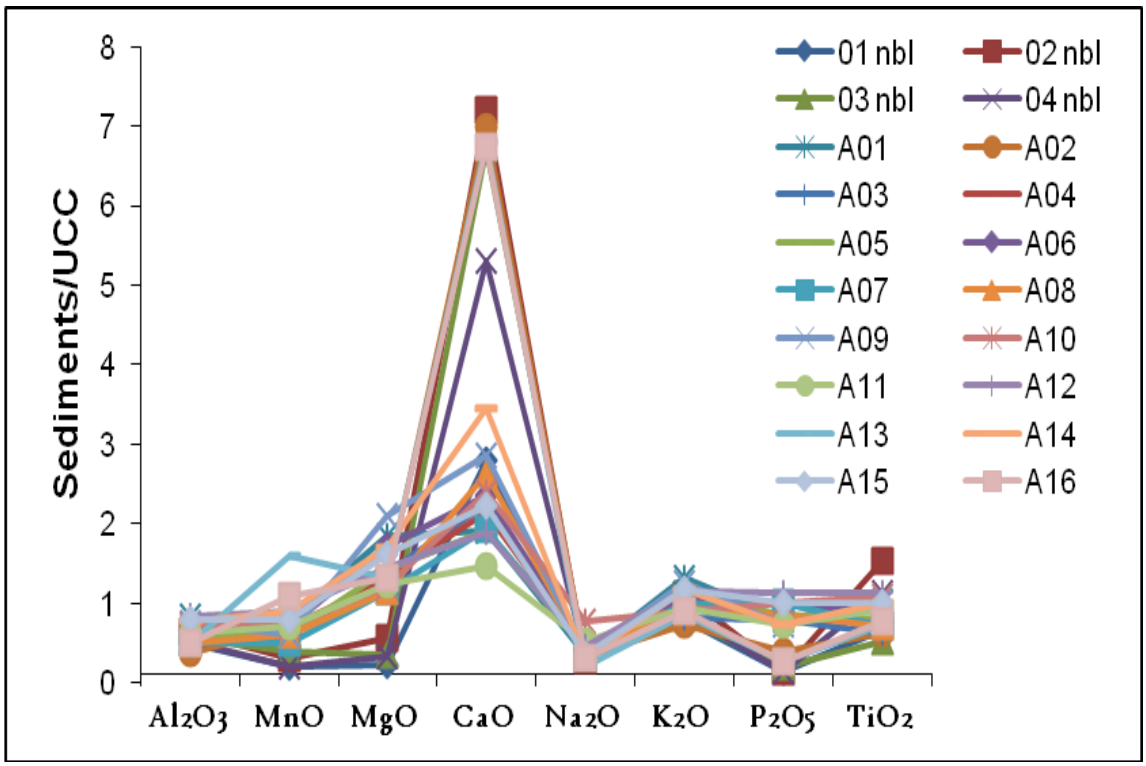

Figure 5.21 Major element oxide conc. of alluvial sediments (A01-A16) and Gomati river sediments (01 nbl- 04 nbl) normalized to UCC.

Normal bedload sediments are compared with probable source rocks- Higher Himalayan rocks, Lesser Himalayan rocks. Higher Himalayan rocks- Biotite Leucogranites, Tourmaline Leucogranites and metasediments shows different patterns with bedload sediments (figure 5.22). Metasediments show higher values of all major elements except CaO than bedload sediments. Both leucogranites shows similar patterns with enriched Al_2O_3, Na_2O and K_2O values, depletion in MgO and similar values for MnO compared to bedload sediments. REEs of

metasediments and bedload sediments shows similar pattern except for Yb and Lu. Among Higher Himalayan rocks metasediments show similarity with bedload sediments. This indicates that bedload sediments have been derived from metasediments and the pattern indicate that it is very unlikely that the bedload sediments have been derived from Biotite leucogranite or Tourmaline leucogranite. Lesser Himalayan rocks- Pellites shows enrichment of Al_2O_3, MnO, MgO, K_2O, P_2O_5 and similar values of Na_2O (figure 5.23). Quartzite show depletion of elements relative to bedload sediments. REEs in Pellites have high concentration than bedload sediments and Quartzites have lower concentrations than bedload sediments. This also indicates the source being Pellite not Quartzite.

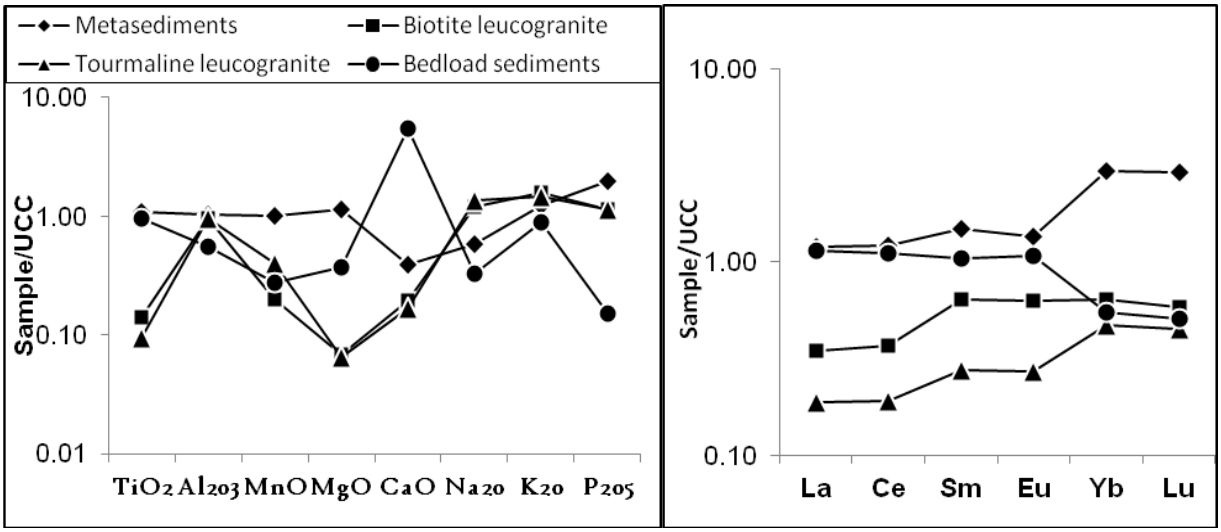

Figure 5.22. UCC normalized patterns for major elements and REEs of bedload sediments of Gomati river. For comparison average of samples from Higher Himalayan rocks (Ayres and Harris, 1997) are also plotted.

5.5 Silicate Minerals

Common silicate minerals present in parent and weathered materials of the Ganga Alluvial Plain are quartz, muscovite, plagioclase and biotite. Langmuir (1997) reported the lifetime span (in years) of common silicate minerals such as quartz, muscovite, K-feldspar, Na-plagioclase, hornblende, biotite and Ca-plagioclase (figure 5.24). It clearly indicates that biotite and Ca-plagioclase are the most weatherable silicate minerals.

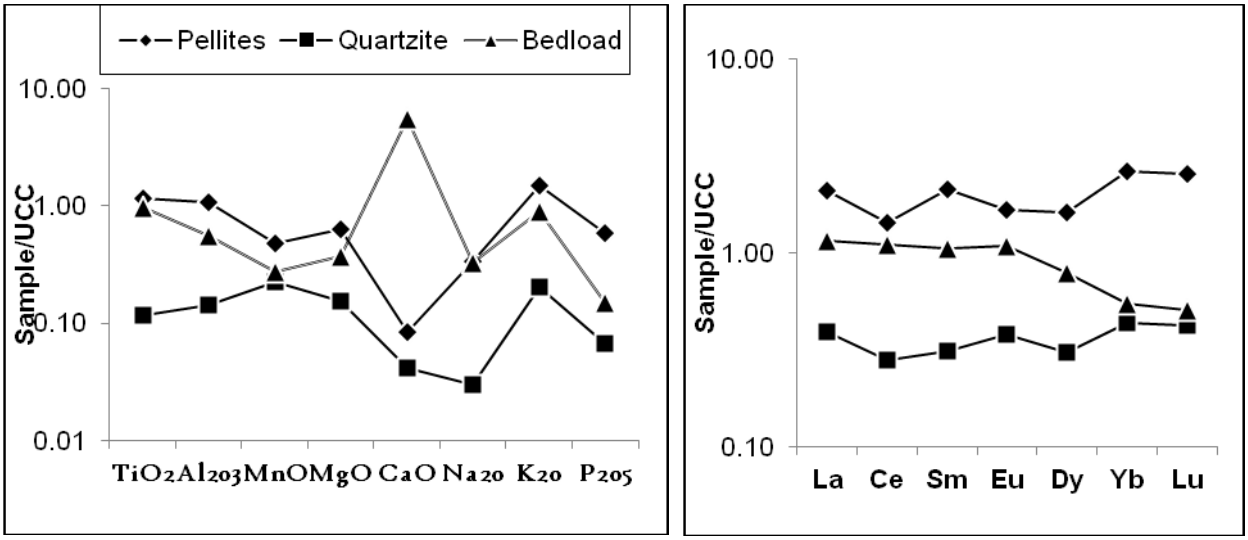

Figure 5.23. UCC normalized patterns for major elements and REEs of bedload sediments of Gomati river. For comparison average of samples from Lesser Himalayan rocks (Rashid, 2002) are also plotted.

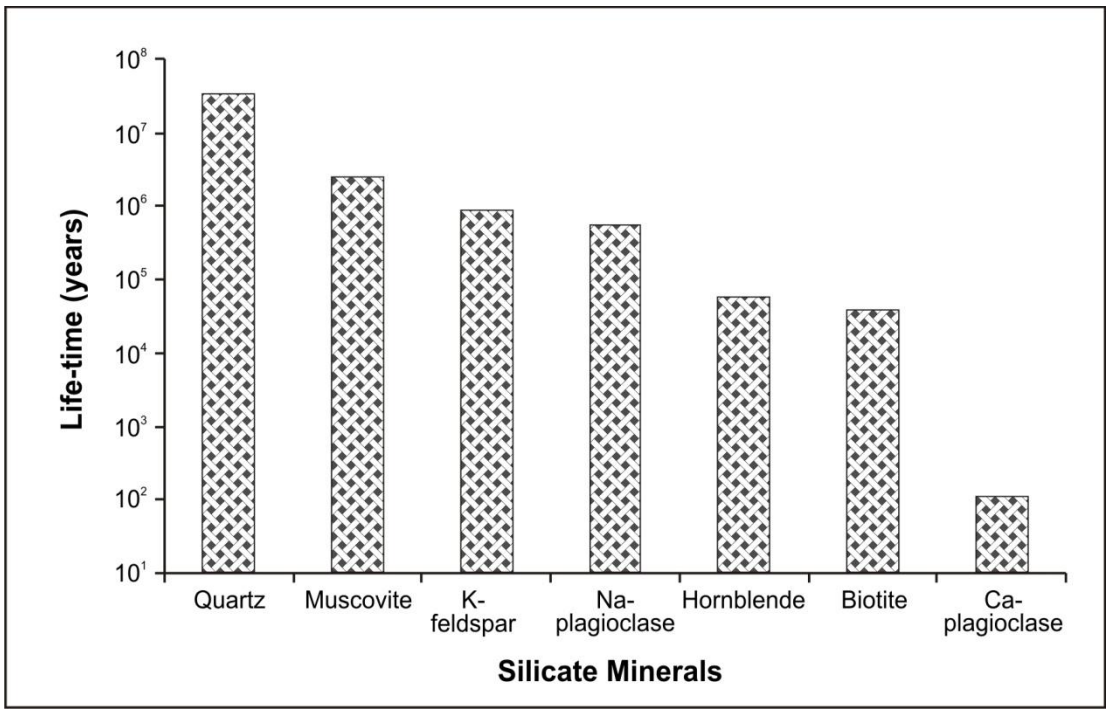

Figure 5.24 Theoretical mean lifetimes (in years) of a 1 mm diameter cube of common silicate minerals at pH = 5 and 25 ºC. Minerals are arranged in order from least weatherable to most weatherable (Langmuir, 1997)

The mica mineral is composed of t-o-t layering. Mica consists of octahedral (o-layer) sheet sandwich between two identical tetrahedral (t-layer) sheets. The strength of binding within a sheet is much stronger than bonding between layers (Perkins, 2009). The tetrahedral sheets are occupied by Si, Fe, B, Be and Al, whereas octahedral sheets are usually inhabited by

Fe, Mg, Ti, Al, Mn, Cr, V, Mg and other cations. The interlayer site is typically resided by K, Na, Rb, Ca and Ba (Tischendorf et al., 2007). The common formula for mica is $K(Al,Mg,Fe)_{2-3}(AlSi_3O_{10})(OH)_2$, where as K^+ cation placed an interlayer between the tretrahedral layers. The apices of the tetrahedral are occupied by Fe^{2+}, Mg^{2+}, or Al^{3+} and Al^{3+} which are commonly substitutes for some Si^{4+}. Based on the compositions of these ions, micas are found in three end association; muscovite [$KAl_2(AlSi_3O_{10})(OH_2)$], annite [$(KFe_3(AlSi_3O_{10})(OH)_2$] and phlogopite [$KMg_3(AlSi_3O_{10})(OH)_2$]. The phlogopite refers to Mg-rich biotite and annite refers to Fe-rich biotite whereas they are also known as brown and Black micas, respectively. The minerals muscovite refers as white mica as compared with biotite (Tischendorf et al., 2007).

Biotite [$K(Mg,Fe)_3(AlSi_3O_{10})(OH)_2$] is distinguished by its association, nature and dark colour. The two t-o-t layers of biotite are linked by K^+ ions, which occupy large sites between them. Octahedral sites are occupied by the Fe with Mg, which make solid solution between the two principal biotite end members i.e. annite and phlogopite. Third octahedral sites are vacant due to coupled substitutions of Al for replacement of three Mg and Fe. Mn, Ti, and a number of alkalis and alkaline earth elements may also be present. Other important mica mineral is muscovite. Muscovite is common dioctahedral mica with wide variety of elemental substitutions. It is identical to that of biotite except that Al has replaced two out of every three Fe and Mg. Other alkalis and alkaline earth elements may also replace K, F replaces some OH and Li replace some Al. The weathering rate of biotite is three orders of magnitude higher than muscovite (Langmuir 1997).

Several trace elements can be incorporated in octahedral sites of the phyllo-structure in mica minerals. For the incorporation with Al, the trace elements must have ionic radii in the range of ±15% of Al (Goldshmidt, 1945). In this range, elements Cr, Mn, Cu, Fe, Se, Ti, Ni, Mo, Co, V and As are incorporated with Al in VI-fold coordination. During the chemical weathering processes, trace elements exchange may be involved in release and deposit of similar element simultaneously from the t-o-t layer of mica minerals (Mason, 1966; Velde and Meunier, 2008; Kabata-Pendias, 2011).Weathering of biotite may release significant concentrations of elements like Si, Fe and Al from the tetrahedral sheet (-t layer), Ti, Al, Fe, Mn, Cr, V, and Mg from the octahedral sheet (-o layer) and K, Na, Rb, Ca, Ba from the interlayer (Tischendorf et al., 2007).

5.5.1 Microanalysis of biotite

The interaction between minerals and water play an important role in the geochemical processes of elemental mobility. The study of chemical weathering processes of minerals in natural system is essential to estimate the release of various elements into solution. In the previous chapter, biotite mineral collected from bedload sediments of the Gomati River (GR-01 and GR-04) were studied with the help of EDX analysis and results were presented in Figures 4.6 and 4.7. The margins of biotite grain show depletion of Mg, Al, K, and Ti elements indicating effect of weathering. The loss of these elements in biotite mineral weathering leads to the significant gain of these elements in the dissolved load of the Gomati River (Jigyasu et al., 2014). The scanning results prominently show that the margins of biotite grain display a distinctive tonal change due to the physical and chemical alteration. All the grains show prominent difference in the chemical composition of the core and the margin. Quantitatively, the margins of grain show variability in the relative concentration of various elements. It has been documented that dissolution and deposition processes of elements during weathering go together and concentration of elements in weathered part depends upon flushing into moving water (Putnis et al., 2013). The atomic percent of Al, Fe, Mg, K and Ti at the core of biotite grain are 8.74%, 5.99%, 5.23%, 3.42% and 0.66% and decreases to 6.58%, 3.85%, 4.72%, 2.34% and 0.45% at the margin, respectively. Thus, it is believed that along the margins of the biotite grain, silicate structure is broken during the chemical weathering to remove these elements into their dissolved phase.

5.6 Sr isotopic ratio

$^{87}Sr/^{86}Sr$ ratio is a very useful indicator of water rock interaction. In sedimentary rocks, the distribution of Sr is affected by both strong adsorption of Sr on clay minerals, extensive substitution of Sr for Ca in carbonate minerals as well as amount of detrital feldspars. The present day Ganga–Brahmaputra (G-B) waters are characterized by high $^{87}Sr/^{86}Sr$ ratio and moderately high Sr concentration which has led to the suggestion that the G–B rivers play a key role in the Sr isotope evolution of seawater during the Cenozoic (Veizer, 1989; Edmond, 1992; Krishnaswami et al., 1992; Raymo and Ruddiman, 1992; Richter et al., 1992). The steady increase in marine $^{87}Sr/^{86}Sr$ ratio since the Cenozoic led to further hypothesize that seawater Sr evolution during this period was a result of enhanced silicate weathering resulting from rapid uplift of the Himalaya (Raymo and Ruddiman, 1992; Richter et al., 1992). For proper understanding of Sr flux of Ganga plain system, a systematic study of Sr flux through time has

been attempted in the cross- section within Ganga alluvial plain. One study is from a section of the GAP- Ramnagar cliff, Varanasi (Baskey, 2009) where sediment flux is both from peninsular india as well as for the Himalaya. Another study is from cliff section on the right margin of Behta nadi near lucknow (Geethumol, 2008) where only the Himalayan derived sediments are present The Ganga River separates the northern plains forming Himalayan sediments from the southern plains built up by sediments derived from peninsular India. At Varanasi the Ganga River carries a mixed sediment load derived both from Himalaya and peninsular craton. Shukla and Raju (2008) also suggested that Peninsula could have supplied sediments to the Ganga Plain. The Ramnagar cliff section (20m high) is on the eastern bank of the Ganga channel. It has two distinct types of sedimentary packages namely A and B and 5 different events. These packages are physically as well as lithologically different. Sr isotopic ratio values of the package A and package B do not show marked differences (figure 5.25a), therefore it is evident that source of sediments for package A (only southern Indian craton source) and package B (mainly Himalaya flux also with southern Indian cratonic source) Sr isotopic ratios. Package A, indicating drier climate, shows overall increase in the Sr ratio. Package A also have influx of the sediment for southern part i. e. Indian craton. Package B

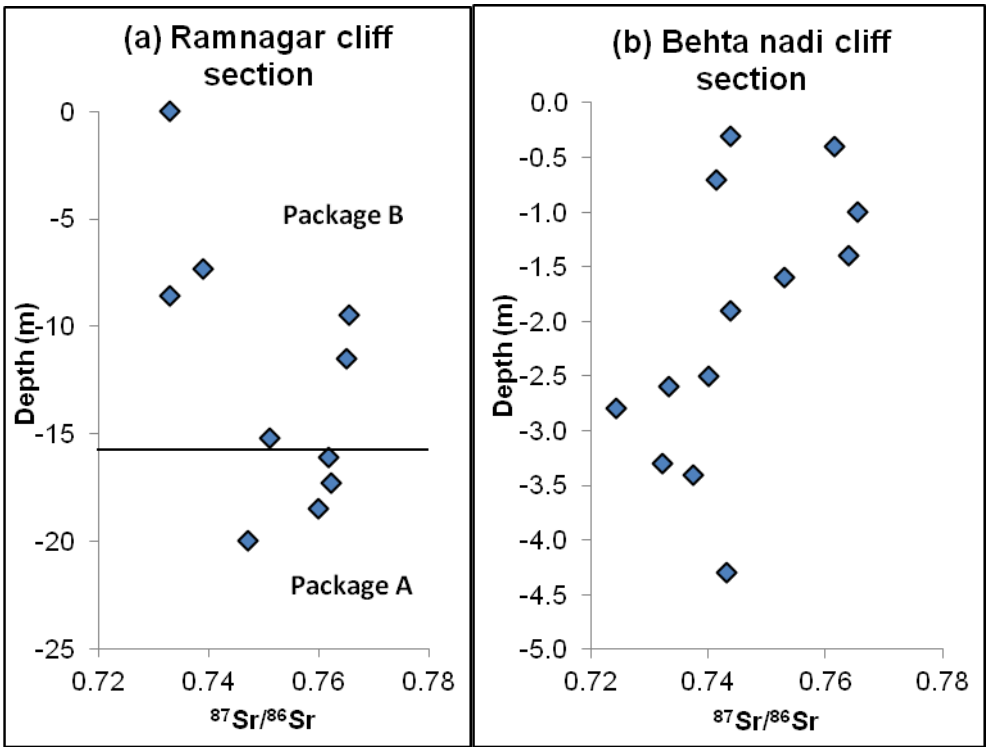

Figure 5.25 Variations in Sr isotope compositions of the sediments from the (a) Ramnagar cliff section and (b) cliff section near Behta nadi with depth.

have 3 events and they indicate wetter climate with a dry spell corresponding to LGM (Last Glacial Maxima) at around 18 ka, at that time sea level was about 130 m lower than present. This event is followed by very wet climate known as monsoon (between 9 ka and 6 ka). If we look carefully to the data for Ramnagar cliff we see a marked correlation between climate and Sr isotopic ratios. This data clearly indicate the influence of climate over Sr isotopic concentration. The data from lithofacies section of Behta nadi, a tributary of Gomati River shows that Sr isotopic values are increasing from bottom to top of the facies (figure 5.25b).

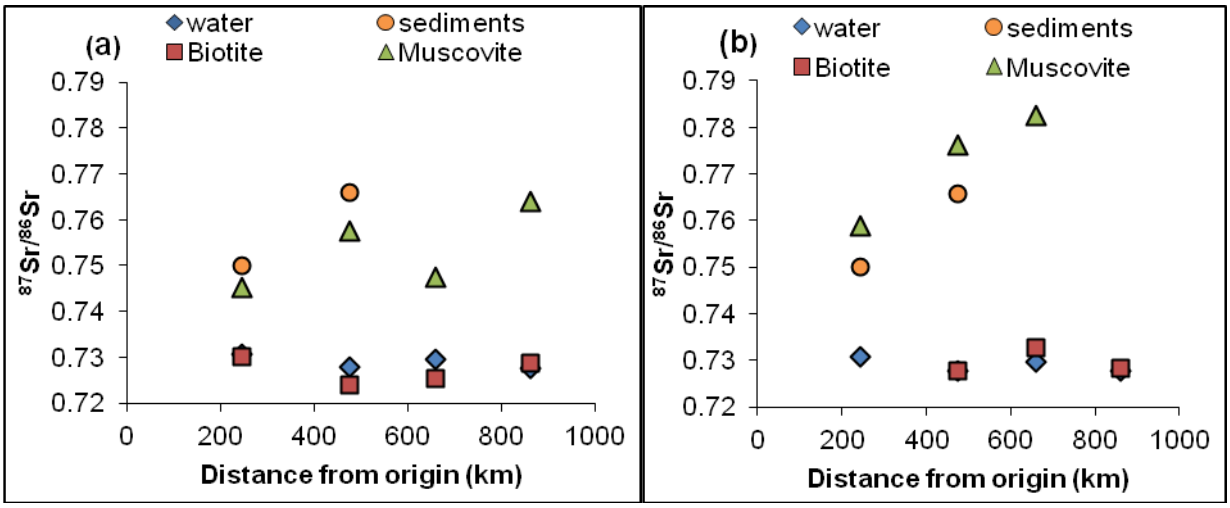

Figure 5.26 variations in $^{87}Sr/^{86}Sr$ ratio of minerals –biotite, muscovite, water (Paliwal, 2007) and sediments of (a) mica-rich bedload (b) normal bedload of Gomati River.

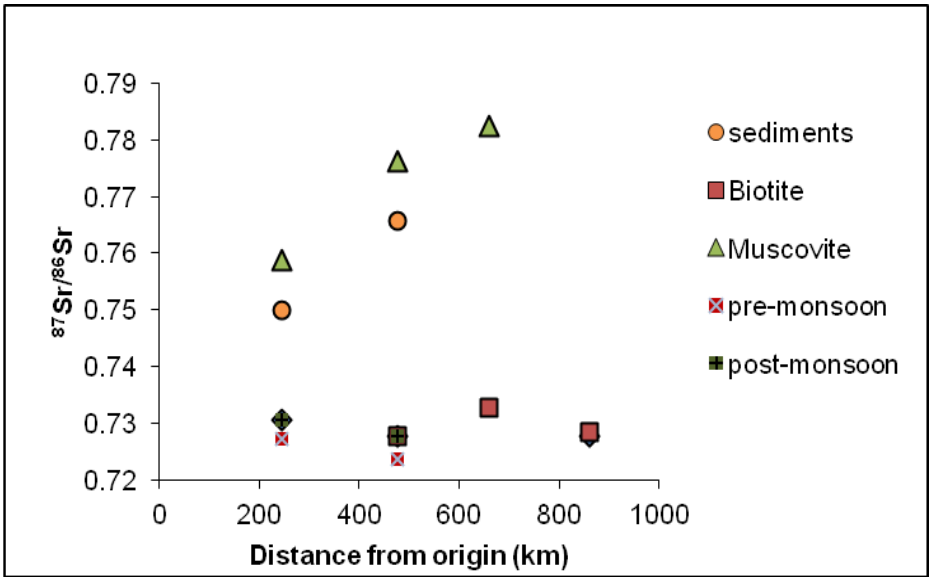

Figure 5.27 Marked variations in $^{87}Sr/^{86}Sr$ ratio of the Gomati River water in pre-monsoon and post-monsoon seasons (Singh et al., 2010) along with Biotite, muscovite of normal bedload and sediments.

Sr values are lower for the older strata and younger rocks indicate increase in strontium values. Himalayan rivers are considered as main potential source of steady increase of marine Sr isotopic budget during the past ~40 Ma. From above observations it is concluded that Ganga Alluvial Plain plays a very important role in recycling of the sediments from the Himalaya through its tributaries and the increased Sr flux to the Bay of Bengal.

Figure 5.26 displays that Sr ratio show very little change in downstream direction in Gomati River. Water and biotite have lower values of Sr ratio whereas muscovite and sediments show higher Sr ratios. In figure 5.27 pre-monsoon and post- monsoon water data (Singh et al., 2010) is plotted along with sediments, biotite and muscovite. Elevated $^{87}Sr/^{86}Sr$ ratios of the Gomati River during post-monsoon season compare to pre-monsoon data indicates that the interaction within the GAP sediments increased the Sr-influx after monsoon season. It has also been established that GAP plays an important role in contribution of Sr-influx to the Ocean.

Chapter 6 Conclusions

In the present study, the distribution of bedload sediments along with associated silicate minerals- biotite, muscovite and feldspar was focused to understand the mobility of major, trace and rare earth elements in Ganga plain. The systematic geochemical study of the Gomati river basin was carried out. The conclusions of present study are:

1. The decreasing order of major and trace element concentration in common silicate minerals was biotite > muscovite > feldspar. Biotite show enrichment in Al_2O_3, P_2O_5, FeO, MgO, MnO,TiO_2 and depletion in Na_2O, K_2O, CaO relative to UCC. Muscovite show enrichment in Al_2O_3, P_2O_5, and depletion in Na_2O, K_2O, FeO, MnO, CaO. Except for CaO, and TiO_2, all other major elements are depleted in Feldspar relative to UCC. Bedload Sediments are enriched in CaO and TiO_2 and depleted in Al_2O_3, $FeO_{(T)}$,MgO ,MnO, Na_2O, P_2O_5 relative to UCC. The high concentration of K_2O with compare to Na_2O may indicate the presence of potassic feldspar. Biotite show enrichment in As, Co, Cs, Cr, Cu, Ga, Li, Ni, Pb, Rb, V and Zn. Muscovite show enrichment in As, Ba, Co, Cs, Cr, Cu, Ga, Li, Ni, Pb, Rb, V and Zn. Feldspar show enrichment in As and other trace elements are depleted. Bedload sediments are enriched in As, Cs, Ga, Li, Rb, and Se.
2. The REE study further clarify the weathering processes of the Gomati River Basin and minerals (biotite, muscovite and feldspar) weathering. In the normal bedload sediments, Ce is the most abundant of the ΣREE compositions. The order of average concentrations of REE was as follows (in decreasing order): Ce > La > Nd > Pr > Sm > Gd > Dy > Er > Yb > Eu > Ho > Lu. The ΣREE, LREE and HREE concentrations were 92.1-323.1, 83.7-302.1 and 7.8-21.0 ppm, respectively. The content of LREE accounted for more than 90% of the ΣREE content. Mica-rich sediments have higher ΣREE than normal bedload sediments. The degree of LREE fractionation was slightly lower than that of HREE fractionation. Influenced by the tectonic induced weathering activity in the middle segment of the Gomati River, relatively high ΣREE, LREE and HREE enrichment were recorded in the Gomati River Sediments. The absence of HREE enrichment suggests that the influence of heavy minerals on REE geochemistry is insignificant. The decreasing order of ΣREE concentration in common silicate minerals was biotite > muscovite > feldspar. Weathering influences the spatial variability in ΣREE content in biotite of the bedload sediments. The ΣREE concentrations in biotite of the normal bedload sediments decrease from 471 ppm to 142 ppm with downstream suggesting the release of REE through the intensive chemical weathering of easily weatherable biotite. On the other hand, total REE concentration in

biotite of the mica-rich bedload sediments increased markedly with downstream from 375 ppm to 1445 ppm due to secondary deposition on the mineral's surface. Chondrite-normalised REE patterns of the river sediments show strong LREE enrichment, relatively flat HREE, weak positive Gd anomaly and absence of prominent negative Eu-anomaly. Positive Eu-anomaly was shown by feldspar and muscovite, whereas negative Eu-anomaly by biotite. Biotite differs from feldspar and muscovite in REE enrichment and positive Gd-anomaly.

3. Higher Himalayan rock- Metasediments and Lesser Himalayan Rock- Pellites can be source rock for bedload sediments of Gomati River Basin as these rocks shows similar patterns with bedload sediments.

4. In SEM- EDX analysis of biotite mineral grains, the grains show prominent difference in the chemical composition of the core and the margin. Quantitatively, the margins of grain show variability in the relative concentration of various elements. The atomic percent of Al, Fe, Mg, K and Ti at the core of biotite grain decreases at the margin indicating effect of weathering. Along the margins of the biotite grain, silicate structure is broken during the chemical weathering to remove these elements into their dissolved phase.The loss of these elements in biotite mineral weathering leads to the significant gain of these elements in the dissolved load of the Gomati River.

5. The $^{87}Sr/^{86}Sr$ ratio of Biotite ranges from 0.72391 to 0.73278. The Sr isotopic ratio of Muscovite range from 0.74733 to 0.78256. Biotite has lower $^{87}Sr/^{86}Sr$ and lower Sr content in sediments of Gomati River Basin. The Sr isotopic ratio is increasing from Biotite to Muscovite to sediments in Gomati River Basin. Water and biotite have lower values of Sr ratio while muscovite and sediments have higher Sr ratios. Lower values of Sr may be due to relative increase in carbonate weathering or due to dilution of Sr concentration due to increase in water discharge.

6. Sr isotopic data from Ramnagar cliff section indicate the influence of climate over Sr isotopic concentration. Sedimentary package A indicates drier climate and shows overall increase in the Sr ratio whereas sedimentary package B has 3 events of different climates and shows first increase then decrease in Sr ratio. In Behta nadi cliff section, Sr isotopic values are lower for older rocks and higher for younger rocks. It concludes that Sr ratio is increasing within the Ganga Alluvial Plain through recycling of sediments and Ganga Alluvial Plain is the main reason for increased Sr flux in Gomati River and Bay of Bengal.

References

Abbas N. and Subramaniam V. (1984) Erosion sediment transport in the Ganges river basin (India). Journal of hydrology 69:173-182.

Aiuppa A., Allard P., Alessandro W. D., Michel A., Parello F., Treuil M. and Valenza M. (2000) Mobility and fluxes of major, minor and trace metals during basalt weathering and groundwater transport at Mt. Etna volcano (Sicily). Geochemica et Cosmochimica Acta, 64: 1827–2000.

Antonina A. N., Shazili N A. M., Kamaruzzaman B.Y., et al (2013) Geochemistry of the Rare Earth Elements (REE) Distribution in Terengganu Coastal Waters: A Study Case from Redang Island Marine Sediment. Open J Mar Sci 03:154–159.

Ayres M. and Harris N. (1997) REE fractionation and Nd isotope disequilibrium during crustal anatexis: constraints from Himalayan leucogranites. Chemical Geology 139: 249–269.

Banfield J. F. and Eggleton R. A. (1988) Transmission electron microscope study of Biotite weathering. Clays Clay Miner. 36: 47–60.

Barrett T. J., Fralick P. W., Jarvis I. (1988) Rare-earth-element geochemistry of some Archean iron formations north of Lake Superior, Ontario. Canadian Journal of Earth Sciences, 25(4): 570-580

Baskey R. S. (2009) Strontium Isotopic Study of Ramnagar cliff along Ganga River, M.Sc. dissertation thesis. Department of Earth Sciences, Indian Institute of Technology Roorkee.

Bau M. (1999) Scavenging of dissolved yttrium and rare earths by precipitating iron oxyhydroxide: Experimental evidence for Ce oxidation, Y-Ho fractionation, and lanthanide tetrad effect. Geochim Cosmochim Acta 63:67–77.

Benincasa E., Brigatti M. F., Poppi L., & Barredo F. B. (2003). Crystal chemistry of dioctahedral micas from peraluminous granites. European Journal of Mineralogy 15(3):543-550.

Bickle M. J., Harris N. B. W., Bunbury J., Chapman H. J., Fairchild I. J., Ahmad T. (2001) Controls on the $^{87}Sr/^{86}Sr$ of carbonates in the Garwal Himalaya, headwaters of the Ganges. J Geol 109:737– 753.

Bickle M. J., Bunbury J., Champman H. J., Harris N. B. W., Fairchild I. J., Ahmad T. (2003) Fluxes of Sr into the headwaters of the Ganges. Geochem Cosmochem Acta 67:2567–2584.

Birck J. M. (1986) Precision K–Rb–Sr isotopic analysis: application to Rb– Sr chronology. Chemical Geology 56:73–83.

Blum J. D., Erel Y., Brown K. (1993) $^{87}Sr/^{86}$ Sr ratios of Sierra Nevada stream waters: Implications for relative mineral weathering rates. Geochimica et Cosmochimica Acta 57 (21):5019-5025.

Blum J.D., Erel Y. (1997) Rb-Sr isotope systematic of a granitic soil chronosequence: The importance of biotite weathering. Geochimica et Cosmochimica Acta, 61:3193-3204.

Blum J. D., Gazis C.A., Jacobson A.D. and Chamberlain C.P. (1998) Carbonate versus silicate weathering in the Raikhot watershed within the High Himalayan Crystalline Series Geology 26:411–414.

Botes P.J., Stadenvan J.F. (2005) Investigation of trace element mobility in river sediments using ICP-OES. Water SA 31:183-191.

Canfield D. E. (1997) The geochemistry of river particulates from the continental USA: major elements. Geochimica et Cosmochimica Acta 61: 3349-3365.

Chakrapani G. J. (2005) Major and trace element geochemistry in upper Ganga River in the Himalayas, India. Environmental Geology 48:189-201.

Corteel C., Dini A., Deyhle A. (2005) Element and isotope mobility during water rock interaction processes. Physics and Chemistry of the Earth 30: 993-996.

Dalai T. K., Krishnaswami S., & Kumar A. (2003) Sr and 87Sr/86 Sr in the Yamuna River System in the Himalaya: Sources, fluxes, and controls on sr isotope composition. Geochimica et Cosmochimica Acta 67(16):2931–2948.

Dalai T. K., Rengarajan R., & Patel P. P. (2004) Sediment geochemistry of the Yamuna River System in the Himalaya: Implications to weathering and transport. Geochemical journal 38(5):441-453.

Das A., Krishnaswami S. (2006) Barium in Deccan Basalt Rivers: Its Abundance, Relative Mobility and Flux. Aquatic Geochemistry 12: 221–238.

Das A., Krishnaswami S. (2007) Elemental geochemistry of river sediments from the Deccan Traps, India: Implications to sources of elements and their mobility during basalt–water interaction. Chemical Geology 242:232-254.

Deer W. A., Howie R. A. and Zussman J. (1966) An introduction to the Rock-forming minerals. Longman, England. 52: p528.

Deer W. A., Howie R. A., & Zussman J. (1978) Rock-forming Minerals.: Single-chain Silicates. V. 2A. Wiley.

Delvigne, J., Bisdom E. B. A., Sleeman J., & Stoops G. (1979) Olivines, their pseudomorphs and secondary products (No. 151). Stiboka.

Derry L.A., France-Lanord C. (1996) Neogene Himalayan weathering history and river 87Sr/86Sr: Impact on the marine Sr record. Earth Planet Sci Lett 142:59–76.

Dickin A. P. (1995) Radiogenic isotope geology, Cambridge University Press, Great Britain.

Dong H., Peacor D. R. and Murphy S. F. (1998) TEM study of progressive alteration of igneous biotite to kaolinite throughout a weathered soil. Geochim. Cosmochim. Acta 62: 1881–1887.

Edmond J. M. (1992) Himalayan tectonic,weathering processes and strontium isotope record in marine limestone. Science 258:1594-1597.

English N. B., Quade J., DeCelles P. G., & Garzione C. N. (2000) Geologic control of Sr and major element chemistry in Himalayan Rivers, Nepal. Geochimica et Cosmochimica Acta 64(15): 2549–2566.

Feldman S. B., Zelazny L. W. and Baker J. C. (1991) High-elevation forest soils of the southern Appalachians: I. Distribution of parent materials and soil-landscape relationships. Soil Science Society of America Journal 55: 1629–1637.

Foley N.K., De Vivo B., Salminen R. (2013) Rare earth elements: The role of geology, exploration, and analytical geochemistry in ensuring diverse sources of supply and a globally sustainable resource. J Geochemical Explor 133:1–5.

Fralick P.W., Kronberg B.I. (1997) Geochemical discrimination of clastic sedimentary rock sources. Sedimentary Geology 113: 111-124.

Gaillardet J., Viers J. and Dupré B. (2003) Trace Elements in River Waters. In Treatise on geochemistry (ed: James I. D.) 5:225–272.

Galy A., & France-Lanord C. (1999) Weathering processes in the Ganges-Brahmaputra basin and the riverine alkalinity budget. Chemical Geology 159:31–60.

Galy A., & France-Lanord C. (2001) Higher erosion rates in the Himalaya: geochemical constraints on riverine fluxes. Geology 29(1):23–26.

Garbarino J. R., Kanagy L. K. and Cree M. E. (2006) Determination of Elements in Natural-Water, Biota, Sediment, and Soil Samples Using Collision/Reaction Cell Inductively Coupled Plasma–Mass Spectrometry. U.S. Geological Survey Techniques and Methods, book 5, sec. B, chap. 1, 88p.

Garcon M., Chauvel C., France-Lanord C., Limonta M., & Garzanti E. (2014) Which minerals control the Nd-Hf-Sr-Pb isotopic compositions of river sediments? Chemical Geology 364:42–55.

Geethumol K. G. (2008) Analysis of Sr Isotope from the Gomati River Basin, M.Sc dissertation thesis. Department of Earth Sciences, Indian Institute of Technology Roorkee

Girty G. H. (1991) A note on the composition of plutoniclastic sand produced in different climatic belts: short note. Journal of Sedimentary Research 61(3).

Goldshmidt V. M. (1945) The geochemical background of minor element distribution. Soil Science 60:1–7.

Goldstein S. J., Jacobsen S. B. (1988) Nd and Sr isotopic systematics of river water suspended material: implications for crustal evolution. Earth Planet. Sci. Lett 87: 249–265.

Goldstein S. J., Jacobsen S. B. (1988) Rare earth elements in river waters. Earth Planet Sci Lett 89:35–47.

Goldstein J., Newbury D. E., Joy D. C., Lyman C. E., Echlin P., Lifshin E., Sawyer L. and Michael J. R. (2003) Scanning Electron Microscopy and X-ray Microanalysis. Characterization & Evaluation of Materials XIX, 690p.

Grauch R I. (1989) Rare earth elements in metamorphic rocks, In Geochemistry and Mineralogy of Rare Earth Elements. Review in Mineralogy, Edited by Lipin B R, Mckay G A, 21: 147.

Gupta L. P., Subramanian V. (1994) Environmental geochemistry of the River Gomati: A Tributary of the Ganges River. Environmental Geology 24: 235-243.

Harris N. (1995) Significance of weathering Himalayan metasedimentary rocks and leucogranites for the Sr isotopic evolution of seawater during the early Miocene. Geology 23(9):795-798.

Henderson P, editor. (1984) Rare earth elements geochemistry. In:Development in geochemistry. New York: Elsevier Science Publishers 139.

Holser W. T. (1997) Evaluation of the application of rare-earth elements to paleoceanography. Palaeogeogr Palaeoclimatol Palaeoecol 132:309–323.

Hu Z., Haneklaus S., Sparovek G., Schnug E. (2006) Rare Earth Elements in Soils. Commun Soil Sci Plant Anal 37:1381-1420.

Jacobson A. D., Blum J. D., Walter L.M. (2002) Reconciling the elemental and Sr isotope composition of Himalayan weathering fluxes: Insights from the carbonate geochemistry of stream waters. Geochim Cosmochim Acta 66:3417–3429.

Jain A. K., Ahmad T., Singh S., Ghosh S. K., Patel R. C., Kumar R., Agarwal K. K., Perumal J., Islam R. And Bhargava O. N. (2012) Evolution of the Himalaya. Proc Indian natn Sci Acad 78 (3):259-275.

Jigyasu D. K., Kuvar R., Shahina, Singh P., Singh S., Singh I. B., & Singh M. (2014) Chemical weathering of biotite in the Ganga Alluvial Plain. Current Science 106(11): 1484–1486.

Jigyasu D. K., Kuvar R., Srivastava N., Singh S., Singh I. B., Singh M. (2015) High Mobility of Aluminium in Gomati River Basin: Implication to Human Health. Current Science 108(3): 434.

Johannesson K. H., Xiaoping Z. (1997) Geochemistry of the rare earth elements in natural terrestrial waters: A review of what is currently known. Chinese J Geochemistry 16:20–42.

Kabata-Pendias A. (2011) Trace elements in soils and plants (4th Ed.). CRC Press Taylor & Francis Group, Boca Raton, 534p.

Karim A., Veizer J. (2000) Weathering processes in Indus River Basin: implication from riverine carbon, sulfur, oxygen and strontium isotope. Chemical Geology 170:153-177.

Krishnaswami S., Trivedi J. R., Sarin M. M., Ramesh R., Sharma K. K. (1992) Strontium isotopes and Rubidium in the Ganga–Brahmaputra river system: weathering in the Himalaya, fluxes to the Bay of Bangal and contributions to the evolution of oceanic 87Sr/86Sr. Earth Planet Sci Lett 109:243–253.

Krishnaswami S., Singh S. K. and Dalai T. K. (1999) Silicate weathering in the Himalayas: Role in contributing to major ions and radiogenic Sr to the Bay of Bengal. In: Ocean Science, trends and future directions (ed.B.L.K.Somayajulu) 23-51.Indian National Science Academy and Akademi Book International, New Delhi.

Kronberg B. I., Nesbitt H. W. and Fyfe W. S. (1987). Mobilities of alkalis, alkaline earths and halogens during weathering. Chemical Geology 60: 41–49.

Kumar S., Singh I. B. (1978) Sedimentological Study of Gomati River Sediments, Uttar Pradesh, India. Example of a river in Alluvial Plain. Senckenbergiana marit 10:145-211.

Kumar R., Suresh N., Sangode S. J., Kumaravel V. (2007) Evolution of the Quaternary alluvial fan system in the Himalayan foreland basin: Implications for tectonic and climatic decoupling. Quat Int 159:6–20.

Kuvar R. (2014) Mobility of alkali and alkaline earth elements during weathering of the Ganga Plain, northern India. Unpublished Ph. D. Thesis.

Land M. and Öhlander B. (2000) Chemical weathering rates, erosion rates and mobility of major and trace elements in a boreal granite till. Aquatic Geochemistry 6: 435–460.

Langmuir D. (1997) Aqueous Environmental Geochemistry. Prentice-Hall, Inc. Upper Saddle River, New Jersey, 590p.

Leech M. L., Klemperer S. L., Singh S. and Jain A. K. (2004) Early, steep subduction of India beneath Asia required by timing of UHP metamorphism. In AGU Fall Meeting Abstracts.

Leech M. L., Singh S., Jain A. K., Klemperer S. L. & Manickavasagam R. M. (2005) The onset of India–Asia continental collision: early, steep subduction required by the timing of UHP metamorphism in the western Himalaya. Earth and Planetary Science Letters 234(1):83-97.

Li C., Kang S., Zhang Q., Wang F. (2009) Rare earth elements in the surface sediments of the Yarlung Tsangbo (Upper Brahmaputra River) sediments, southern Tibetan Plateau. Quat Int 208:151–157.

Li C. S., Shi X. F., Kao S. J., Liu Y. G., Lyu H. H., Zou J. J., Liu S. F., Qiao S. Q. (2013) Rare earth elements in fine-grained sediments of major rivers from the high-standing island of Taiwan. Journal of Asian Earth Sciences 69:39–47.

Li D. F., Yong H., Zhang C. L., Fralick P., Hollings P. , Mi M., Lu W. J., Han J. S., Wang C. M., Fang J. (2016) Geochemistry of fine-grained clastic rocks in the Mesoproterozoic Kawabulake Group: implications for provenance and the tectonic model of the Eastern Tianshan, Xinjiang, NW China. Int J Earth Sci (Geol Rundsch).

Loughnan F. C. (1969) Chemical weathering of the silicate minerals.

Martin J. M. & Whitfield M. (1983) The significance of the river input of chemical elements to the ocean. In Trace metals in sea water (pp. 265-296). Springer US.

Mason B. (1966) Principles of geochemistry. John Wiley and Sons, New York, 329p.

McLennan S. M. (1989) Rare earth elements in sedimentary rocks; influence of provenance and sedimentary processes. Reviews in Mineralogy and Geochemistry 21(1): 169-200.

McLennan S. M. (1995) Sediments and soils; chemistry and abundances, in: Rock Physics and Phase Relations: A Handbook of Physics Constants (ed. T. J. Ahrens). American Geophysical Union Reference Shelf 3: 8–19.

Middleburg J. J., Cornelis H., Weijden V. D. and Woittiez J. R. W. (1988) Chemical processes affecting the mobility of major, minor and trace elements during weathering of granite rocks. Chemical Geology 68: 253–273.

Mongelli G., Cullers R.L., Dinelli E., Rottura A. (1998) Elemental mobility during the weathering of exposed lower crust: the Kinzigitic paragneisses from the Serre, Calabria, Southern Italy. Terra nova 10:190-195.

Moors E., Harding R., Biemans H., Collins D., Froebrich J., Gosain A., Groot A., Haerter J., Kumar P., Shrestha M. L., Ludwig F., Mishra A., Sarthi P. P., Rees G., C. Terwisscha van

Scheltinga, Tomar S., Siderius C., Stoffel M., Werners S. (2009) Water Resources of the Ganga Basin under a Changing Climate: interaction between Glaciers and Monsoon in the Himalaya. Proceedings of the 37th IAH Congress, 6-12.

Nagell R. H. (1962) Geology of the Serra do Navio manganese district, Brazil. Economic Geology 57(4):481-498.

Nier A. O. (1940) A mass spectrometer for routine isotope abundance measurements. Review of Scientific Instruments 11(7):212-216.

Nesbitt H.W., Markovics G., Price R.C.(1980). Chemical processes affecting alkalis and alkaline earths during continental weathering. Geochimica et Cosmochimica Acta 44: 1659-1666.

Nesbitt H.W., Young G.M. (1982). Early Proterozoic climates and plate motions inferred from major element chemistry of lutites. Nature 299:715-717.

Nesbitt H.W., MacRae N. D., Kronberg B. I. (1990) Amazon deep-sea fan muds: light REE enriched products of extreme chemical weathering. Earth and Planetary Science Letters 100:118–123.

Norra S., Lanka-Panditha M., Kramar U., Stüben D. (2006) Mineralogical and geochemical patterns of urban surface soils, the example of Pforzheim, Germany. Applied Geochemistry 21:2064–2081

Paliwal V. P. (2007) Strontium Isotopic studies in Gomati River, M.Sc dissertation thesis. Department of Earth Sciences, Indian Institute of Technology Roorkee.

Palmer M.R., Edmond J.M. (1989) The strontium isotope budget of modern ocean. Geochim Cosmochim Acta 92:11–26.

Palmer M.R., Edmond J.M. (1992) Control over the Strontium isotope composition of the river water. Geochim Cosmochim Acta 56:2099–2111.

Patel R. C., Singh S, Asokan A., Manickavasagam R. M., and Jain A. K. (1993), Extensional tectonics in the Himalayan orogen, Zanskar, NW India, in Himalayan Tectonics, edited by P. J. Treloar and M. P. Searle, Spec. Publ. Geol. Soc. 74:445 – 459.

Patino L. C., Velbel M. A., Price J. R. and Wade J. A. (2003) Trace element mobility during spheroidal weathering of basalts and andesites in Hawaii and Guatemala. Chemical Geology 202: 343–364.

Perkins D.(2009) Mineralogy. (2nd Ed.) PHL Learning Private Limited, New Delhi, 473p.

Price J. R. and Velbel M. A. (2014) Rates of biotite weathering, and clay mineral transformation and neoformation, determined from watershed geochemical mass-balance methods for the Coweeta hydrologic laboratory, Southern Blue Ridge Mountains, North Carolina, USA. Aquatic Geochemistry 20:203–224.

Putnis C. V. and Ruiz-Agudo E. (2013) The mineral–water interface: where minerals react with the environment. Elements 9:177–182.

Rai S. K., Singh S. K., & Krishnaswami S. (2010) Chemical weathering in the plain and peninsular sub-basins of the Ganga: Impact on major ion chemistry and elemental fluxes. Geochimica et Cosmochimica Acta 74(8):2340–2355.

Raju N. J. (2012) Arsenic Exposure through Groundwater in the Middle Ganga Plain in the Varanasi Environs, India: A Future Threat. Journal Geological Society of India 79:302-314.

Raju N. J., Ram P., Gossel W (2014) Evaluation of Groundwater Vulnerability in the Lower Varuna Catchment Area, Uttar Pradesh, India using AVI Concept. Journal Geological Society of India, 83:273-278.

Ramesh R., Ramanathan A.L., Ramesh S. et al (2000) Distribution of rare earth elements and heavy metals in the surficial sediments of the Himalayan river system. Geochemical J 34:295–319.

Rao K. L. (1975) India's Water Health. Orient Longman Limited, New Delhi, 267p.

Rao K.L. (1979) India's water wealth: Its assessment, uses and projections. Orient Longman Limited, New Delhi, 267p.

Rashid S. A. (2002) Geochemical characteristics of Mesoproterozoic clastic sedimentary rocks from the Chakrata Formation, Lesser Himalaya: implications for crustal evolution and weathering history in the Himalaya. Journal of Asian Earth Sciences 21: 283–293.

Raymo M. E. & Ruddiman W. F. (1992) Tectonic forcing of late Cenozoic climate. Nature 359(6391):117-122.

Rees H. G. & Collins D. N. (2006) Regional differences in response of flow in glacier-fed Himalayan Rivers to climatic warming. Hydrol. Processes 20:2157-2169.

Rengarajan R., Sarin M. M. (2004) Distribution of rare earth elements in the Yamuna and the Chambal rivers, India. Geochem J 38:551–569.

Richter F. M., Rowley D. B. & DePaolo D. J. (1992) Sr isotope evolution of seawater: the role of tectonics. Earth and Planetary Science Letters 109:11–23.

Rollinson H. R. (1993) Using Geochemical Data: Evolution, Presentation, Interpretation. Longman Scientific and Technical, London 352 pp.

Ross G. R., Guevara S. R., Arribere M. A. (1995) Rare earth geochemistry in sediments of the Upper Manso River Basin, Rio Negro, Argentina. Earth Planet Sci Lett 133:47–57.

Rudnick R. L., Gao S. (2003) Composition of the Continental Crust. In: Rudnick, R.L. (Ed.), The Crust. In: Holland, H.D., Turekian, K.K. (Eds.), Treatise on Geochemistry 3:1-64 Elsevier-Pergamon, Oxford.

Sarin M. M., Krishnaswami S., Dilli K., Somayajulu B. L. K. & Moore W. S. (1989) Major ion chemistry of the Ganga-Brahmaputra river system: Weathering processes and fluxes to the Bay of Bengal. Geochimica et cosmochimica acta 53(5):997-1009.

Schäfer J., Norra S., Klein D., Blanc G. (2009) Mobility of trace metals associated with urban particles exposed to natural waters of various salinities from the Gironde Estuary, France. J Soils Sediments 9:374–392.

Schleicher N. J., Norra S., Chai F., Chen Y., Wang S., Cen K., Yu Y., Stüben D. (2011) Temporal variability of trace metal mobility of urban particulate matter from Beijing–A contribution to health impact assessments of aerosols. Atmospheric Environment 45(39), 7248-7265

Shand P., Darbyshire D. P. F., Love A. J. & Edmunds W. M. (2009) Sr isotopes in natural waters: Applications to source characterisation and water–rock interaction in contrasting landscapes. Applied Geochemistry 24(4):574-586.

Sholkovitz E.R. (1995) The aquatic chemistry of rare earth elements in rivers and estuaries. Aquat Geochemistry 1:1–34.

Sholkovitz E. R., Szymczak R. (2000) The estuarine chemistry of rare earth elements: comparison of the Amazon, Fly, Sepik and the Gulf of Papua Systems. Earth and Planetary Science Letters 179:299.

Shukla U. K. and Raju N. J. (2008) Migration of the Ganga River and its implication on hydro-geological potential of Varanasi area, U.P., India. J. Earth Syst. Sci. 117(4):489–498.

Singh D. S. (2009) Rivers of Ganga Plain: Boon / Bane. E-Journal Earth Science India, pp 1-10

Singh D. S., Awasthi A., and Nishat (2010) Impact of Climate Change on the Rivers of Ganga Plain. International Journal of Rural Development and Management Studies, 4 (1): 1-8.

Singh I. B. (1996) Geological evolution of Ganga plain- an overview. Journal of the Paleontological Society of India.

Singh I. B., Srivastava P., Sharma S., Sharma M., Singh D. S., Rajagopalan, G., & Shukla, U. K. (1999) Upland Interfluve (Doab) Deposition: Alternative Model to Muddy Overbank Deposits. Facies 40: 197–210.

Singh, I. B. (2004) Late Quaternary History of the Ganga Plain, J. Geol. Soc. India 64: 431–454.

Singh I. B., Singh S. & Singh M. (2008) Weathering in the Ganga Alluvial Plain: Geochemical signatures linking of the Himalayan source and the Bay of Bengal sink. 23rd Himalayan-Karakoram-Tibet Workshop.

Singh M., Sharma M., & Tobschall H. J. (2005) Weathering of the Ganga alluvial plain, northern India: Implications from fluvial geochemistry of the Gomati River. Applied Geochemistry 20:1–21

Singh M., Singh I. B., & Muller G. (2007) Sediment characteristics and transportation dynamics of the Ganga River. Geomorphology 86:144–175.

Singh M., Singh A. K., Srivastava N., Singh S., & Chowdhary A. K. (2010) Arsenic mobility in fluvial environment of the Ganga Plain, northern India. Environmental Earth Sciences 59(8):1703-1715.

Singh M., Kumar S., Kumar B., Singh S. and Singh I. B. (2013) Investigation on the hydrodynamics of Ganga alluvial plain using environmental isotopes: a case study of the Gomati river basin, Northern India. Hydrogeology Journal 21(3):687-700.

Singh P., Rajamani V. (2001) REE geochemistry of recent clastic sediments from the Kaveri floodplains, Southern India: Implication to source area weathering and sedimentary processes. Geochim Cosmochim Acta 65:3093–3108.

Singh P. (2009) Major, trace and REE geochemistry of the Ganga River sediments: Influence of provenance and sedimentary processes. Chem Geol 266:251–264.

Singh P. (2010) Geochemistry and provenance of stream sediments of the Ganga River and its major tributaries in the Himalayan region, India. Chemical Geology 269:220–236.

Singh P. (2011) Weathering and Chemical Variability in Ganga Plain Sediments. Geological Processes and Climatic Change 257-268

Singh S., Singh M., Choudhary A. K., Saxena A., Singh I. B., & Jain, A. K. (2010) Sr isotopic signature of the Ganga Alluvial Plain and its implication to Sr flux of the Ganga River System. International Journal of Earth Sciences 99:1991–1997.

Song Y. H., Choi M. S. (2009) REE Geochemistry of fine-grained sediments from major rivers around the Yellow Sea. Chemical Geology 266:328-342

Sultan K., Shazili N. A. (2009) Rare earth elements in tropical surface water, soil and sediments of the Terengganu River Basin, Malaysia. J Rare Earths 27:1072–1078.

Sun S. S., McDonough W. F. (1989) Chemical and isotopic systematics of oceanic basalts: implications for mantle composition and processes. Geol Soc London, Spec Publ 42:313–345

Suttner L. J., Basu A., & Mack G. H. (1981) Climate and the origin of quartz arenites. Journal of Sedimentary Research 51(4).

Suttner L. J. & Dutta P. K. (1986) Alluvial sandstone composition and paleoclimate, I. Framework mineralogy. Journal of Sedimentary Research 56(3).

Taylor S. R., Mclennan S. M. (1985) The continental crust: Its composition and evolution. Blackwell, London, 301p.

Taylor, S. R., & McLennan, S. M. (1988). The significance of the rare earths in geochemistry and cosmochemistry. Handbook on the physics and chemistry of rare earths, 11, 485-578.

Thakur A. (2008) Morphology and basin characteristics of the Gomati River, the Ganga Plain, India. Unpublished Ph. D. Thesis, 125p.

Thakur A., Singh M., Singh I. B. (2009) Fluvial Incision of the Gomati River in the Ganga Plain, India: its Implications. Himalayan Geology 30(2):43.

Tischendorf G., Förster H.-J., & Gottesmann B. (2001) Minor- and trace-element composition of trioctahedral micas: a review. Mineralogical Magazine. 65: 249–276.

Tischendorf G., Förster H.-J., Gottesmann B., and Rieder M. (2007) True and brittle micas: composition and solid-solution series. Mineralogical Magazine, 71: 285–320.

Tripathy, G. R., Goswami, V., Singh, S. K., & Chakrapani, G. J. (2010) Temporal variations in Sr and 87Sr/86Sr of the Ganga headwaters: Estimates of dissolved Sr flux to the mainstream. Hydrological Processes 24:1159–1171

Tripathi J. K., Bock B., Rajamani V. and Eisenhauer A. (2004) Ca and Sr dynamics in the Indo-Gangetic plains: Different sources and mobilization processes in northwestern India. Current Science 87(10):1453-1458.

Tripathi, J. K., Ghazanfari, P., Rajamani, V., & Tandon, S. K. (2007) Geochemistry of sediments of the Ganges alluvial plains: Evidence of large-scale sediment recycling. Quaternary International 159:119–130.

Tripathi J. K., Bock B., Rajamani V. (2013) Nd and Sr isotope characteristics of Quaternary Indo-Gangetic plain sediments: Source distinctiveness in different geographic regions and its geological significance. Chemical Geology 344: 12–22.

Tyler G. (2004) Rare earth elements in soil and plant systems - A review. Plant Soil 267:191–206.

Veizer J. (1989) Strontium isotopes in seawater through time. Annual Review of Earth and Planetary Sciences 17(1):141-167.

Velde B. B. & Meunier A. (2008) The origin of clay minerals in soils and weathered rocks. Springer Science & Business Media.

Vital H., Stattegger K., Garbe-Schonberg C. D. (1999) Composition and trace-element geochemistry of detrital clay and heavy-mineral suites of the lowermost Amazon River: a provenance study. Journal of Sedimentary Research 69: 563–575.

Vital H., & Stattegger K. (2000) Major and trace elements of stream sediments from the lowermost Amazon River. Chemical Geology 168:151–168.

Vuba S., Farnaaz S., Sagar N., Ahmad S. M. (2013) Geochemical and mineralogical characteristics of recent clastic sediments from lower Godavari River: Implications of source rock weathering. Journal of the Geological Society of India 82:217–226.

Weijden C.H. van der., Weijden R.D. van der. (1995) Mobility of major, minor and some redox-sensitive trace elements and rare-earth elements during weathering of four granitoids in central Portugal. Chemical Geology 125(3-4):149-167.

White A. F., Blum A. E., Bullen T. D., Vivit D. V., Schulz M., and Fitzpatrick J. (1999) The effect of temperature on experimental and natural chemical weathering rates of granitoid rocks. Geochimica et Cosmochimica Acta 63:3277–329.

Wilson M.J. (2004) Weathering of primary rock forming minerals: processes, products and rates. Clay Minerals 39:233-266.

Wronkiewicz D. J. & Condie, K. C. (1987) Geochemistry of Archean shales from the Witwatersrand Supergroup, South Africa: source-area weathering and provenance. Geochimica et Cosmochimica Acta 51(9):2401-2416.

Yingjun M., Congqiang L. (1999) Trace element geochemistry during chemical weathering – As exemplified by the weathered crust of granite, Longnan, Jiangxi. Chinese Science Bulletin 44:2260-2263.

Zhu W., Kennedy M., De Leer E. W. B. et al (1997) Distribution and modelling of rare earth elements in Chinese river sediments. Science of the total environment 204:233–243.

Publications

Jigyasu D. K., Kuvar R., Shahina, **Singh P**., Singh S., Singh I. B., & Singh M. (2014) Chemical weathering of biotite in the Ganga Alluvial Plain. Current Science 106(11): 1484–1486.

Singh P., Singh S, Jigyasu D. K., Singh I. B., & Singh M. (2017) Rare Earth Elements in Gomati River Sediments and their associated Silicate Minerals: Implications of Biotite Weathering Process in Humid Sub-tropical Climate. Geochemical Journal (under review)